NIST

United States Department of Commerce
Technology Administration
National Institute of Standards and Technology

NISTIR 5013

ELECTROMECHANICAL PROPERTIES OF SUPERCONDUCTORS FOR DOE FUSION APPLICATIONS

J.W. Ekin
S.L. Bray
C.L. Lutgen
W.L. Bahn

NISTIR 5013

ELECTROMECHANICAL PROPERTIES OF SUPERCONDUCTORS FOR DOE FUSION APPLICATIONS

J.W. Ekin
S.L. Bray
C.L. Lutgen
W.L. Bahn

Electromagnetic Technology Division
Electronics and Electrical Engineering Laboratory
National Institute of Standards and Technology
Boulder, Colorado 80303-3328

January 1994

CONTENTS

Appendices:

Electromechanical Properties of
Superconductors for DOE Fusion Applications

J. W. Ekin, S. L. Bray, C. L. Lutgen, and W. L. Bahn

Electromagnetic Technology Division
Electronics and Electrical Engineering Laboratory
National Institute of Standards and Technology
Boulder, Colorado 80303

The electrical performance of many superconducting materials is strongly dependent on mechanical load. This report presents electromechanical data on a broad range of high-magnetic-field superconductors. The conductors that were studied fall into three general categories: candidate conductors, experimental conductors, and reference conductors. Research on candidate conductors for fusion applications provides screening data for superconductor selection as well as engineering data for magnet design and performance analysis. The effect of axial tensile strain on critical-current density was measured for several Nb_3Sn candidate conductors including the US-DPC (United States Demonstration Poloidal Coil) cable strand and an ITER (International Thermonuclear Experimental Reactor) candidate conductor. Also, data are presented on promising experimental superconductors that have strong potential for fusion applications. Axial strain measurements were made on a V_3Ga tape conductor that has good performance at magnetic fields up to 20 T. Axial strain data are also presented for three experimental Nb_3Sn conductors that contain dispersion hardened copper reinforcement for increased tensile strength. Finally, electromechanical characteristics were measured for three different Nb_3Sn reference conductors from the first and second VAMAS (Versailles Project on Advanced Materials and Standards) international Nb_3Sn critical-current round robins. Published papers containing key results, including the first measurement of the transverse stress effect in Nb_3Sn, the effect of stress concentration at cable-strand crossovers, and electromechanical characteristics of Nb_3Al, are included throughout the report.

Key words: axial stress effect; electromechanical; fusion; Nb_3Al; Nb_3Sn; stress effect; superconductor; transverse stress effect; V_3Ga

Executive Summary

This report presents the results of work done for the U. S. Department of Energy, Office of Fusion Energy, during the period 1986-1993, under interagency agreement No. DE-AI01-84ER52113.

Within the windings of an energized superconducting magnet, the Lorentz force can produce large stresses that increase with magnet size and field. These stresses can significantly degrade the performance of the magnet through a reduction in the superconductor's critical-current density (J_c). There are two dominant stress components, a tensile stress that is aligned with the wire's longitudinal axis (axial stress) and a compressive stress that is perpendicular to its axis (transverse stress).

Presently, the most common conductor material used in high-field (>10 T) superconducting magnet designs is Nb_3Sn. The J_c of Nb_3Sn is highly sensitive to its stress state. Consequently, it is the internal stress state of the magnet windings, rather than the J_c of the unstressed superconductor, that determines the design limits for large high-field magnets. Electromechanical measurements of Nb_3Sn candidate conductors for ITER (International Thermonuclear Experimental Reactor) provide screening data for superconductor selection as well as engineering data for magnet design and performance analysis. Data are presented on several Nb_3Sn candidate conductors.

As new magnet designs call for larger coils and higher fields, stresses must be limited by structural reinforcement of the magnet windings. Control of the stress, which accumulates radially within the windings, requires distributed reinforcement. Aside from complicating the design and increasing the cost of the magnet, additional internal reinforcement limits the superconductor packing fraction and, thus, reduces the magnetic field. At present, the determining factors of the amount of reinforcement are not just structural, but dominated by the stress sensitivity of Nb_3Sn. Consequently, a superconductor less sensitive to stress than the existing high-field conductors, but comparable in J_c, could significantly extend the present magnet design limits. Data are presented on five experimental conductors that have strong potential for fusion applications with lowered stress sensitivity—V_3Ga, Nb_3Al, and Nb_3Sn superconductors with dispersion hardened copper.

The consistency of interlaboratory J_c measurements of Nb_3Sn superconductors is typically much lower than for NbTi. This is largely due to stress effects, which are much smaller for NbTi. Since measurement inconsistency implies uncertainty in the engineering data for these conductors, it directly impacts DOE magnet designs. In response to this situation, two studies on J_c measurements of Nb_3Sn, the first and second VAMAS (Versailles Project on Advanced Materials and Standards) international Nb_3Sn critical-current round robins, have been conducted. NIST participated in both of these studies, providing electromechanical data on the superconductors. The results of these measurements are presented in the Appendices.

The report has three main sections: Electromechanical Characteristics of Nb_3Sn Superconductors, Electromechanical Characteristics of Experimental High-Field Superconductors, and the Appendices. Within each main section, the data are presented in two formats: published papers, which present comprehensive results, and unpublished data on specific conductors.

The first section contains papers reporting seminal measurements of the transverse stress effect in Nb_3Sn, a comparison of transverse stress effects in bronze-process and internal-tin Nb_3Sn conductors, and the effect of concentrated transverse stress at cable-strand crossover points. Key results from these publications show that the effect of transverse stress on the J_c of Nb_3Sn is much greater than that of axial stress, that anisotropy in stress sensitivity is not a peculiarity associated with a specific Nb_3Sn processing method, and that transverse stress data from measurements of single wires subjected to uniform stress are applicable in modeling the concentrated stress at strand crossover points in superconducting cables. Also, complete sets of axial stress data are presented for the US-DPC (United States Demonstration Poloidal Coil) Nb_3Sn cable strand, the LLNL (Lawrence Livermore National Laboratory) cable-test strand, and an ITER (International Thermonuclear Experimental Reactor) candidate conductor.

The section on experimental superconductors includes a paper on stress effects in Nb_3Al, where this superconducting compound was shown to be significantly less sensitive to both axial and transverse stress than Nb_3Sn. Like Nb_3Sn, the Nb_3Al conductor was more sensitive to transverse stress than axial stress. This demonstrates that the anisotropy, which was first observed in Nb_3Sn, is not associated with a particular processing method or even a particular material, but is much more general. Axial stress data are also presented for a V_3Ga tape conductor that has good performance at magnetic fields up to 20 T and for three experimental Nb_3Sn conductors that contain dispersion hardened copper reinforcement for increased tensile strength.

In addition to the VAMAS publications and data, the Appendices contain an excerpt from the Concise Encyclopedia of Magnetic & Superconducting Materials entitled "Superconductor Specification" and a paper on the development of an internal-tin Nb_3Sn conductor for fusion applications, which is processed using hot isostatic pressure (HIP) to double its intrinsic irreversible strain limit.

Unless otherwise noted, the critical-current measurement accuracy is ±2%. Axial strains were determined within ±0.02%, and transverse loads were determined within ± 1%.

Effect of transverse compressive stress on the critical current and upper critical field of Nb₃Sn

J. W. Ekin

Electromagnetic Technology Division, National Bureau of Standards, Boulder, Colorado 80303

A large reversible degradation of the critical current of multifilamentary Nb₃Sn superconductors has been observed when uniaxial compressive stress is applied transverse to the conductor axis at 4 K. In bronze-process multifilamentary Nb₃Sn, the onset of significant degradation occurs at about 50 MPa. In an applied field of 10 T, the magnitude of the effect is about seven times larger for transverse stress than for stress applied along the conductor axis. The transverse stress effect increases with magnetic field and is associated with a reversible degradation of the upper critical field. The intrinsic effect of transverse stress on the upper critical field is about ten times greater than for axial stress. Although axial stresses on the Nb₃Sn filaments are greater than transverse stresses in most applications, the transverse stress effect will need to be considered in the internal design of large magnets because of the greater sensitivity of Nb₃Sn to transverse stress. It is shown that the transverse stress from the Lorentz force on the conductor is proportional to conductor thickness. This will place limits on conductor dimensions and the spacing between distributed reinforcement in large magnets. The effect may be particularly significant in cabled conductors where large transverse stress concentrations can occur at strand crossover points.

I. INTRODUCTION

A large data base has been obtained for the effect of *axial* tensile stress and strain on the critical current of A15 superconductors.[1] However, little is known about the effects of stress components other than the axial component. In practical superconducting magnets, however, the superconductor is subjected to three-dimensional stresses. Typically, the transverse component of stress is large and compressive. For example, in solenoidal magnets the transverse component arises from hoop stress which compresses the magnet winding radially, and in dipole magnets it arises from Lorentz force compression of the magnet windings at the midplane. This article reports the first measurements of the effect of *transverse* stress on the critical current and upper critical field of Nb₃Sn.[2]

II. EXPERIMENT

A. Apparatus

To obtain data on the electrical effects of the transverse component of stress, an apparatus was designed and built to simultaneously apply mutually perpendicular components of current, magnetic field, and transverse compressive stress to a single-strand superconductor in a 4-K liquid helium bath. Current was supplied by a 900-A battery supply, magnetic field by a 10-T split-pair magnet, and compressive stress by a servohydraulic testing system.

Considerable care was used to ensure drag-free stress application as well as uniform stress over the test section between the voltage taps. As shown in Fig. 1, the sample was compressed between two stainless-steel anvil heads. One of the anvil heads was fixed. The other was designed to pivot so

that it conforms to the flat surface of the first anvil head. This ensures that stress is applied uniformly along the sample length. The edges of the anvil heads were tapered and rounded in order to avoid any stress concentration where the sample enters and exits the pressure section. Voltage taps were soldered to the sample *within* the compressed region so that the electric field was measured only over the region where stress was uniformly applied to the test specimen.

B. Sample characteristics

These results were obtained on a Nb₃Sn strand material used to make internally-cooled cabled superconductors for several large magnet systems. Sample characteristics are given in Table I. Two types of samples of the same bronze-process starting material were tested, one with a round cross section of diameter 0.69 mm, the other flattened before reaction to a rectangular shape 0.38 × 0.76 mm². The samples were composed of 2869 filaments, each about 3.8 μm in di-
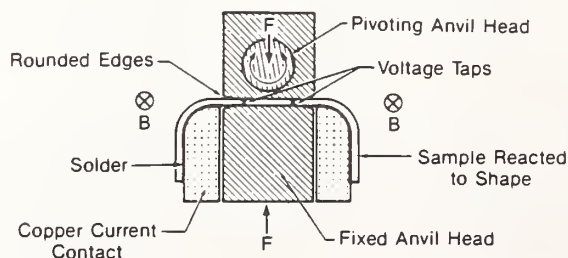

FIG. 1. Schematic view of transverse stress test apparatus showing mutually perpendicular magnetic field, current, and stress. Anvil edges are tapered and rounded to avoid stress concentration. Voltage taps are attached to the side of the sample within the uniform compression region.

4

FIG. 3. Comparison of critical-current degradation in multifilamentary Nb₃Sn for transverse and axial compressive stress in magnetic fields of 8 and 10 T. Transverse stress degradation is shown for both (a) round and (b) flat samples. Negative values of stress represent compression, positive values represent tension.

load chain (from matrix to filament, to matrix, to filament, etc.). Fortunately, the axial strain intrinsic to the Nb₃Sn filaments can be measured[3–5] and this can be used to calculate the axial stress in the Nb₃Sn filaments. This was done assuming a Nb₃Sn elastic modulus[6] of 165 GPa to generate the axial stress curve in Fig. 3(a). (Conversely, all of the results could be given in terms of strain by dividing the reported stresses by the modulus of Nb₃Sn.)

Figure 3(a) shows the difference in the magnitudes of the transverse and axial stress effects. For transverse stress, the degradation is a little less than 10% at 10 T under a transverse pressure of 50 MPa and rises to nearly 30% degradation at a transverse pressure of 100 MPa. For axial stress, on the other hand, the degradation was less than 2%

up to about 200 MPa. Looking at the data in Fig. 3(a) over a wide range shows that the stress which causes a given amount of critical-current degradation at 10 T is generally about seven times less for transverse stress than for axial stress. This ratio will increase at higher magnetic fields because of the effect of the upper critical field, as discussed below.

The critical-current degradation was *reversible* in character. Upon unloading the sample, the critical current recovered toward its nondegraded value. The recovery was not total, probably because the Nb₃Sn filaments were kept in partial compression by the plastically deformed soft matrix material.

B. Critical current: Flat sample

Figure 3(b) shows the critical current of a piece of the same conductor which was flattened to a rectangular cross section 0.38×0.76 mm prior to reacting. Preflattening the conductor eliminates any ambiguities associated with a change in the contact area for the round sample. Figure 3(b) shows that the decrease with transverse stress is nearly the same as for the round sample at degradation levels up to about 30%. This indicates that the copper matrix does indeed distribute the stress relatively uniformly into the filament region, and that the effective stress described above is a good approximation to the average stress experienced by the Nb₃Sn filaments.

Figure 3(b) also shows that the transverse stress effect in the flat sample has a small peak in critical current as a function of transverse stress. The data in Fig. 3(b) have been plotted with the transverse stress curves shifted so the peak occurs at the abscissa zero. This peak is not present in the results for the round sample. We postulate that this effect in the flattened sample is due to anisotropic precompression from thermal contraction of the matrix material. Each filament has a slightly flattened cross section prior to reaction, with an average aspect ratio of slightly less than 2:1, as shown in Fig. 2. After cooldown from reacting the Nb₃Sn, this results in less thermal compression by the bronze matrix along the shorter axis marked y in Fig. 2 than along the longer x axis. A finite element calculation by Fukumoto *et al.*[7] showed this effect quite clearly for *in situ* conductors, which have highly aspected filament cross sectional shapes prior to reaction. Thus, the Nb₃Sn filaments in the flat sample are under more thermal precompression along their width than along their narrow dimension.

The effect of this anisotropic precompression on the critical current can be understood in terms of distortional strain. Distortional strain produces a much greater degradation of the critical current of a superconductor than hydrostatic strain.[8] One method for combining the effect of different strain components ϵ_x, ϵ_y, and ϵ_z along the three major axes is to use the geometric average strain $\langle \epsilon \rangle$[5,8]:

$$\langle \epsilon \rangle = 2^{1/2}(1 + \nu)^{-1}[(\epsilon_x - \epsilon_y)^2 + (\epsilon_y - \epsilon_z)^2 + (\epsilon_z - \epsilon_x)^2]^{1/2}, \quad (1)$$

where ν is Poisson's ratio. This represents the distortional strain state of the material. Anisotropic thermal precompression along the x and y transverse axes of the flat

sample leads to a compressive prestrain along the y axis which is less than along the x axis, i.e., a finite value for the first term in Eq. (1). As external transverse pressure is applied along the y axis, the initial effect is to remove the distortional strain between the x and y axes, reducing the difference between ϵ_x and ϵ_y in the first term of Eq. (1). This reduces the distortional geometric average strain and thus increases the critical current. As more transverse stress is applied, the critical current eventually passes through a peak and starts to decrease. This is because the strain along the y axis exceeds that along the x axis, thereby increasing the distortional strain. For the round sample, on the other hand, the precompression from thermal contraction in the transverse direction is isotropic and thus, the symmetry breaking application of transverse stress along the x axis immediately leads to crystal distortion and a monotonically decreasing critical current. These results are a strong indication that a distortional strain expression such as Eq. (1) can be used for combining multi-axial strains in analyzing strain degradation of the critical current in practical superconductor applications.

If this is true, the results for the round and flat samples can be compared with each other by defining the zero transverse stress state for the flat sample as being where the peak in the critical current occurs. This procedure has been followed in Fig. 3(b) and for the results on the upper critical field in Sec. IV.

Figures 3(a) and 3(b) also show the scaling of the transverse stress effect with magnetic field B. The effect was significantly greater at 10 T than at 8 T in both the round and flat samples. For example, at 100 MPa transverse compression, the critical-current degradation increased from 20% at 8 T to 29% at 10 T. The increase of the degradation with magnetic field suggests that the transverse stress effect is associated with a reversible degradation of the upper critical field.

C. Upper critical field

The effective upper critical field B_{c2}^* ($\equiv \mu_0 H_{c2}^*$) was determined as a function of stress by extrapolating the J_c vs B data to high fields for each transverse stress level. Instead of using the Kramer extrapolation, which is inaccurate for many conductors, the extrapolation was carried out using
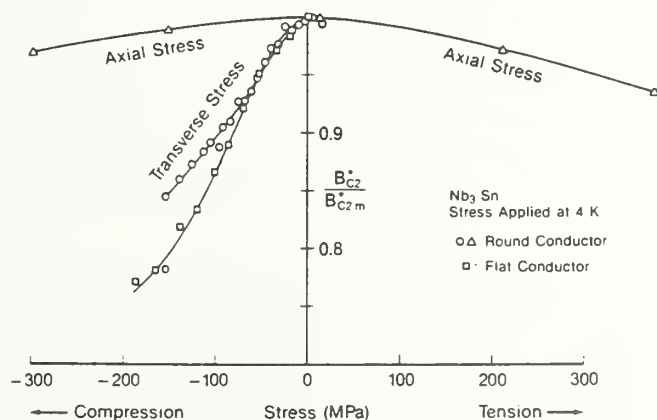
FIG. 4. Intrinsic effect of transverse and axial stress on the upper critical field of Nb$_3$Sn.

the strain scaling law[3] (SSL) and the actual shape of the $J_c(B)$ curve measured for this conductor up to fields of 19 T. Because of the universality of the strain scaling law for many different materials having widely varying strain sensitivities and shapes of the Lorentz-force curve, we believe its validity for transverse stress to be a good assumption. Using a general form for the shape of the field-dependent pinning force curve, the SSL for the Lorentz force F in the elastic regime (where applied stress σ is proportional to strain) can be expressed as[3]

$$F \equiv J_c(\sigma,B)$$
$$= K(\sigma)[B/B_{c2}^*(\sigma)]^p\{1 - [B/B_{c2}^*(\sigma)]\}^q. \quad (2)$$

where $K(\sigma)$ is a stress-dependent factor proportional to the maximum Lorentz force, and p and q are parameters that are *independent* of transverse stress. P and q were determined from zero-stress J_c vs B data measured at magnetic fields from 8 to 19 T and found to have the values of 0.89 and 2.0, respectively.

Using the strain scaling relation given in Eq. (2) and the measured shape of the high-field $J_c(B)$ data for this conductor, values of $B_{c2}^*(\sigma)$ were determined from the $J_c(\sigma,B)$ data of Fig. 3 and are plotted in Fig. 4. Again, the striking result is the large effect of transverse stress on this intrinsic parameter. The effect is much larger than for axial stress. The transverse stress that gives rise to a given level of B_{c2}^* degradation is generally about ten times less than the axial stress. For example, the degradation in the upper critical field reaches 5% at about 45 MPa of transverse stress, compared with 430 MPa of axial stress within the Nb$_3$Sn filaments. Thus, the intrinsic sensitivity of the upper critical field to transverse compressive stress is significantly greater than for axial stress.

IV. DISCUSSION

The relatively large magnitude of the transverse stress effect compared with the axial stress effect is striking. The effect is much larger than the error limits on the value of the elastic modulus used to compare axial and transverse stress results. The difference in sensitivity of the critical current appears to be intrinsic, as evidenced by the reversibility of the effect and by the large difference in sensitivity (about an order of magnitude) observed for the upper critical field.

One possible explanation for the difference between the magnitudes of the axial and transverse effects may be a preferred crystal growth orientation in the Nb$_3$Sn reaction layer. The growth pattern in multifilamentary samples is radial within each filament, which would define an anisotropy between axial and transverse properties. Togano and Tachigawa[9] have reported a very strong (100) [011] texture in Nb$_3$Sn and V$_3$Ga tapes. Further micrographic characterization of multifilamentary conductors might help clarify this.

The observation of a small peak in the J_c vs stress curve for the flat sample, compared with the absence of such a peak for the round sample, is significant in light of its consistency with the three-dimensional treatment of strain expressed by Eq. (1). If this, or an expression modified to account for the observed anisotropy in stress sensitivity, could be proven quantitatively accurate, it would represent an important

7

simplification in the engineering analysis of three-dimensional strain effects in magnet design. The extensive body of data that already exists for axial stress effects could be applied to three-dimensional analyses.

Equation (1) also shows that when both axial tensile and transverse compressive strains are present, they will combine to create a greater distortional state in the material (i.e., greater $\langle\epsilon\rangle$). Axial tension will produce a positive ϵ_z and transverse compression a negative ϵ_y, enhancing $\langle\epsilon\rangle$ through the last term in Eq. (1). This situation is the usual case for the three-dimensional stress state in most magnets. For example, in a solenoid, the Lorentz force generates axial tension through hoop stress and transverse compression through radial pressure. Thus, the effects reported here for transverse compression will in general add to (not compensate) the effects of axial tension.

V. APPLICATION

First, it should be noted that the large sensitivity of the critical current and upper critical field of Nb_3Sn to transverse stress does not necessarily mean that transverse stress will be a significantly worse design problem than axial stress. The transverse stress effect is about an order of magnitude greater than the axial effect, but its relative importance is tempered by the fact that axial stresses in the Nb_3Sn filaments can, in practice, accumulate to much higher values than transverse stresses. This is because the axial stress on the conductor is concentrated in the Nb_3Sn filaments with the majority of the conductor cross section (the soft copper and bronze) not bearing much of the load. Also, for the axial case, the stress is not transmitted to the Nb_3Sn filaments through a soft matrix material, which limits the stress for the transverse case.

The axial stress also scales with winding radius. For example, in a simple solenoid, the hoop stress on the overall conductor $\sigma_\parallel$ will be given by

$$\sigma_\parallel = JBR, \qquad (3)$$

where J is the overall current density in the conductor, B is the magnetic field, and R is the radius of the winding. The intrinsic stress experienced by the Nb_3Sn filaments will be significantly greater than the overall stress given by Eq. (3), however. The exact enhancement depends on the volume ratio of superconductor in the conductor and the mechanical properties of the nonsuperconducting material. The important point is that axial stress scales with the winding radius and can become significant in large applications.

Transverse stress $\sigma_\perp$, on the other hand, scales with the thickness of the conductor t (or accumulated winding thickness between distributed reinforcements), in the direction perpendicular to both the current and field (which would be in the radial direction for a solenoid):

$$\sigma_\perp = JBt. \qquad (4)$$

Thus, transverse stress is dependent on conductor size and shape, not directly on overall magnet size as for axial stress.

Transverse stress effects will become important mainly as applications call for larger conductors needed to limit inductance and keep induced quench voltages low in large magnet applications. The transverse stress effect will place limits on both the conductor dimensions and on the radial spacing between distributed reinforcement in the magnet.

As an example of the application of these results, consider the transverse stress degradation of the critical current at 10 T, given by the data in Fig. 3. The decrease in critical current becomes significant (i.e., exceeds 10%) at about 50 MPa. Substituting this value for $\sigma_\perp$ in Eq. (4) and assuming a current density of 10^9 A/m² at 10 T leads to a limit on the radial thickness of the conductor of about 5 mm. This is a worst-case situation with no shared support of the Lorentz force from hoop stress, for example. Other values can be substituted for the parameters in Eq. (4) to determine limits on unsupported conductor thicknesses for specific applications.

In cabled conductors, stress concentrations at strand crossover points could aggravate the transverse stress effects reported here, because the stress is no longer uniformly applied to the conductor, but is concentrated at the crossover points. Since the critical current of the conductor is a weak link problem, the effect could be significant in the design of cabled conductors. The stress state *inside* cabled conductors may be as important as what happens outside the conductor, i.e., the internal stress design of large conductors needs to be considered along with the overall conductor stress.

VI. CONCLUSION

These data show that there is a relatively large effect of transverse stress on the critical current of Nb_3Sn multifilamentary conductors. The onset of significant (10%) transverse stress degradation occurs at about 50 MPa. The magnitude of the effect is significantly larger than for stress applied along the conductor axis. At 10 T, for example, comparable degradation of the critical current is observed at transverse stress levels seven times smaller than for axial stress.

The effect on the critical current has been shown to be associated with a reversible transverse stress degradation of the upper critical field. The intrinsic sensitivity of the upper critical field to transverse compressive stress is significantly greater than for axial stress. The stress that gives rise to a given level of B_{c2}^* degradation is generally about ten times less for transverse stress than for axial stress. The transverse stress effect on B_{c2}^* will be the dominating factor in determining the degradation of the critical current at high fields; the relative degradation of J_c will increase as the magnetic field approaches the upper critical field.

Based on the universality of the axial strain effect[1,3] and the intrinsic effect of transverse stress on the upper critical field, we believe the effect of transverse stress is a general effect and will be operable not only in Nb_3Sn conductors, but also other A-15 superconductors such as V_3Ga, Nb_3Al, and Nb_3Ge.

The geometric average strain expressed by Eq. (1) gives a consistent account of the presence of a peak in the flat samples and the absence of such a peak in the round samples. This, or a modified representation of the distortional strain state, could be an important simplification in the engineering analysis of three-dimensional strain effects in magnet design.

As magnet systems are scaled to larger size, the transverse stress effect will have an impact on their design. The

8

transverse stress scales with the thickness of the conductor as described in Eq. (4). This places a limit on the dimensions of the conductor and conductor stacking without support in the direction mutually perpendicular to field and current. It will also affect the *internal* stress design of cabled conductors," since stress concentration at strand crossover points can significantly enhance the effect.

ACKNOWLEDGMENTS

[1]See, for example, the references given in J. W. Ekin, Adv. Cryog. Eng. 30, 823 (1984).

[2]This article is based on data presented by the author at the U. S. Dept. of Energy Workshop on N_3Sn, Cambridge, MA, August 4–5, 1986.

[3]J. W. Ekin, Cryogenics 20, 611 (1980).

[4]G. Rupp, IEEE Trans. Magn. **MAG-13**, 1565 (1977).

[5]R. M. Scanlan, R. W. Hoard, D. N. Cornish, and J. P. Zbasnik, in *Filamentary A15 Superconductors*, edited by M. Suenaga and A. F. Clark (Plenum, New York, 1980), p. 221.

[6]D. S. Easton, D. M. Kroeger, W. Specking, and C. C. Koch, J. Appl. Phys. **51**, 2748 (1980).

[7]M. Fukumoto, K. Katagiri, T. Okada, and K. Yasohama, in *Proceedings of the International Symposium on Flux Pinning and Electromagnetic Properties in Superconductors*, edited by T. Matsushita, K. Yamafuji, and F. Irie (Matsukuma, Fukuoka, Japan, 1986), p. 278.

[8]D. O. Welch, Adv. Cryo. Eng. **26**, 48 (1980).

[9]K. Togano and K. Tachikawa, J. Appl. Phys. **50**, 3495 (1979).

TRANSVERSE STRESS EFFECT ON MULTIFILAMENTARY Nb$_3$Sn SUPERCONDUCTOR*

J. W. Ekin

Electromagnetic Technology Division
National Bureau of Standards
Boulder, CO 80303

ABSTRACT

A large reversible degradation of the critical current of multifilamentary Nb$_3$Sn superconductors has been observed under the application of uniaxial compressive stress applied transverse to the conductor axis at 4 K. In bronze-process multifilamentary Nb$_3$Sn, the onset of significant degradation occurs at about 50 MPa. The intrinsic effect of _transverse_ stress on the upper critical field is about ten times greater than for _axial_ stress. Although transverse stress on the Nb$_3$Sn filaments is less than axial stress in most applications, it will need to be considered in the internal stress design of large magnets because of the greater sensitivity of Nb$_3$Sn to transverse stress. The effect scales with conductor thickness and this will place limits on conductor dimensions and the spacing between distributed reinforcement in large magnets.

INTRODUCTION

The effects of _axial_ stress on the critical current of practical multifilamentary Nb$_3$Sn superconductors were first measured about a decade ago.[1-3] A large amount of data has been accumulated on this component of stress since then.[4] In practical superconducting magnets, however, the superconductor is subjected to three-dimensional stresses. Typically the _transverse_ component of stress is large and compressive. The first data on the effect of transverse compressive stress on the critical current of Nb$_3$Sn were reported last year.[5] The effect has subsequently been observed by the group at Karlsruhe.[6]

In this paper we summarize the main properties of the transverse stress effect given in Ref. 5, and consider the application to large magnet design. The effect of the transverse component of stress on the critical current is significantly greater than the axial component, about seven time greater at 10 T. The effect has its origin in an intrinsic reversible degradation of the upper critical field. The effect of transverse stress on the upper critical field is about an order of magnitude greater than for axial stress.

10
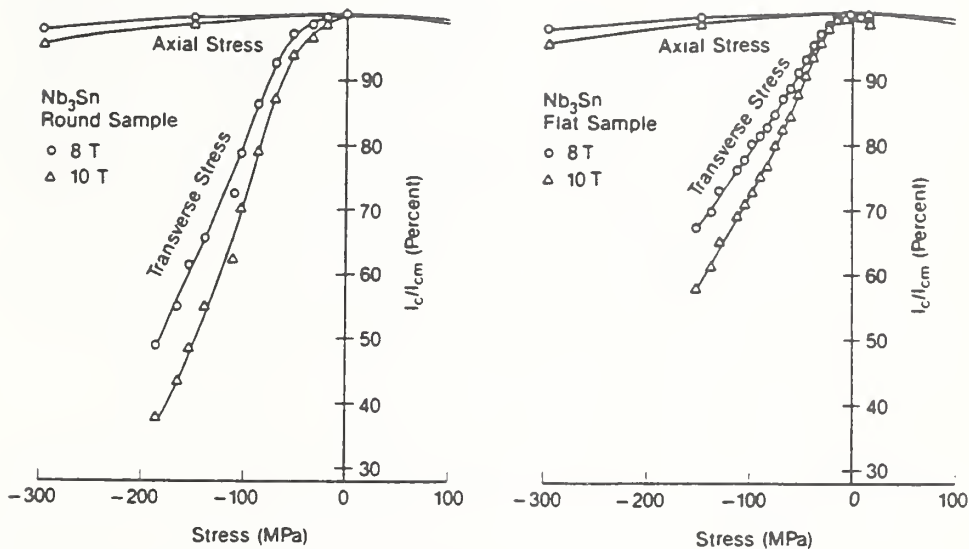
Fig. 1. Comparison of critical current degradation in multifilamentary Nb₃Sn for transverse and axial compressive stress in magnetic fields of 8 and 10 T. Transverse stress degradation is shown for both round (a) and flat (b) samples. Negative values of stress represent compression, positive values represent tension (after Ref. 5).

The transverse stress effect scales with the thickness of the conductor. The main impact of the effect will be to place limits on both the conductor thickness and the radial spacing between distributed reinforcement in large superconducting magnet design.

RESULTS

Critical Current

Fig. 1a shows the critical current of a multifilamentary bronze-process Nb₃Sn conductor as a function of transverse compressive stress for applied fields of 8 and 10 T. The ordinate is the measured critical current normalized to the starting (zero-stress) value. The abscissa is the effective overall transverse stress obtained by dividing the applied load by the area of the sample. A projected area in the direction of the transverse load is used, consisting of the length (9.5 mm) over which compressive load is applied times the original sample diameter (0.70 mm).

In this test, the anvil heads were flat in order to apply uniaxial transverse load. The sample was round, however, so this simple method of estimating stress does not take into account the change in contact area between the anvil heads and the sample as the sample was compressed. However, the copper layer completely surrounded the Nb₃Sn filament region and was relatively thick, so it served to uniformly distribute the load into the filament region. Thus, the effective stress from the projected area represents reasonably well the approximate average stress experienced by the Nb₃Sn filaments within the composite. This has been confirmed by data on the preflattened conductor, described below.

Also shown in Fig. la for comparison are data on the critical current degradation from <u>axial</u> stress. These data were obtained from critical-current degradation measurements on another piece of the same conductor which was subjected to axial stress.[7] Under axial stress, the total axial force is known, but it is apportioned among the various composite materials because they all occupy parallel load-bearing paths. This is different from the transverse case where all the components of the composite experience approximately the same stress, which is transferred from one material to the next in a serial load chain (from matrix to filament, to matrix, to filament, etc.) Fortunately, the axial strain intrinsic to the Nb_3Sn filaments can be measured[8,9] and this can be used to calculate the axial stress in the Nb_3Sn filaments. This was done assuming a Nb_3Sn elastic modulus[10] of 165 GPa to generate the axial stress curve in Fig. 1. (Conversely, all of the results presented could be given in terms of strain by dividing the reported stress values by the modulus of Nb_3Sn.)

Note the difference in the magnitudes of the transverse and axial stress effects. For transverse stress, the degradation is a little less than 10% at 10 T under a transverse pressure of 50 MPa and rises to nearly 30% degradation at a transverse pressure of 100 MPa. For axial stress, on the other hand, the degradation is unmeasurable ($\leq$ 1%) up to about 200 MPa. Looking at the data in Fig. 1 over a wide range shows that the stress which causes a given amount of critical-current degradation at 10 T is generally about seven times less for transverse stress than for axial stress. This ratio will increase at higher magnetic fields because of the effect of the upper critical field, as discussed below.

The critical current degradation was <u>reversible</u>. Upon unloading the sample, the critical current recovered toward its non-degraded value. The recovery was not total, probably because the Nb_3Sn filaments were kept in partial compression by the plastically deformed soft matrix material.

Fig. 1b shows the critical current of a piece of the same conductor which was flattened to a rectangular cross section 0.38 mm x 0.76 mm prior to reacting. This eliminates any ambiguities associated with a change in the contact area for the round sample. Note in Fig. 1b that the decrease with transverse stress is nearly the same as for the round sample at degradation levels up to about 30%. This indicates that the copper matrix does indeed distribute the stress relatively uniformly into the filament region and that the effective stress described above is a reasonable approximation to the average stress experienced by the Nb_3Sn filaments.

The transverse stress effect in the flat sample shows a small peak in critical current as a function of transverse stress. The data in Fig. 1b has been plotted with the transverse stress curve shifted so the peak occurs at the abscissa zero. This peak is not present in the results for the round sample. We believe this effect in the flattened sample is due to anisotropic precompression from thermal contraction of the matrix material. Each filament has a slightly flattened cross section prior to reaction, with an average aspect ratio of slightly less than 2:1. After cooldown from reacting the Nb_3Sn, this results in less thermal compression by the bronze matrix along the narrow dimension of the filaments than along their width. A finite element calculation by Fukumoto et al.[11] showed this effect quite clearly for in-situ conductors, which have highly aspected filament cross sectional shapes prior to reaction.

As external transverse pressure is applied along the narrow dimension of the filaments, the initial effect is to remove the distortional strain in the filament, increasing the critical current. As more transverse stress is applied, the critical current eventually passes through a peak and starts to decrease. This is because the strain along the narrow dimension exceeds the
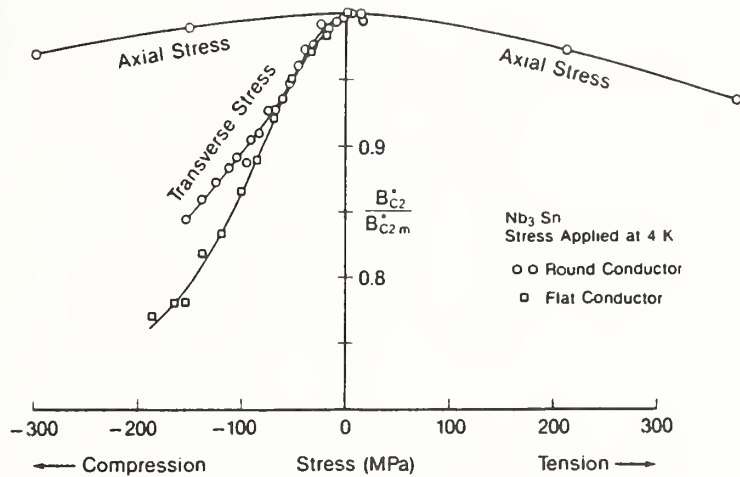
Fig. 2. Intrinsic effect of transverse and axial stress on the upper
critical field of Nb$_3$Sn (after Ref. 5).

precompression along the filament width, thus increasing the distortional
strain of the crystal structure. For the round sample, on the other hand,
the precompression from thermal contraction transverse to the filament is
isotropic and thus the symmetry breaking application of uniaxial transverse
stress immediately leads to crystal distortion and a monotonically
decreasing critical current.

Figs. 1a and 1b also show the scaling of the transverse stress effect
with magnetic field, B. The effect was significantly greater at 10 T than
at 8 T in both the round and flat samples. The increase of the degradation
with magnetic field suggests that the transverse stress effect has its
origin in a reversible degradation of the upper critical field.

Upper Critical Field

The effective upper critical field $B_{c2}*[\equiv\mu_0H_{c2}*]$ was determined as a
function of stress by extrapolating the J_c vs. B data to high fields for
each transverse stress level. This was done by using the zero-stress
J_c-vs.-B characteristic measured at magnetic fields from 8 T to 19 T and
then assuming that the strain scaling law holds for transverse stress (i.e.
that the shape of the Lorentz force curve remains the same and simply scales
with transverse stress, just as has been shown for axial stress).[7]

The results are shown in Fig. 2. Again, the striking result is the
large difference in the sensitivity of the superconductor properties to
transverse stress compared with axial stress. The stress that gives rise to
a given level of $B_{c2}*$ degradation is generally about ten times less for the
transverse direction than for the axial direction. For example, the
degradation in the upper critical field reaches 5% at an axial stress of 430
MPa within the Nb$_3$Sn filaments, compared with about 45 MPa of transverse
stress. Thus the intrinsic sensitivity of the upper critical field to
transverse compressive stress is significantly greater than for axial stress
and is the dominating factor in degrading the critical current at high
fields.

550

13

APPLICATION

First, it should be noted that the large sensitivity of the critical current and upper critical field of Nb_3Sn to transverse stress does not necessarily mean that transverse stress will be a significantly worse design problem than axial stress. The transverse stress effect is about an order of magnitude greater than the axial effect, but its relative importance is tempered by the fact that axial stresses in the Nb_3Sn filaments can, in practice, accumulate to much higher values than transverse stresses. This is because the axial stress on the conductor is concentrated in the Nb_3Sn filaments with the majority of the conductor cross section (the soft copper and bronze) not bearing much of the load. Also, for the axial case, the stress is not transmitted to the Nb_3Sn filaments through a soft matrix material, which limits the stress for the transverse case.

Axial stress scales with the winding radius and can become significant in large applications. Transverse stress, $\sigma_\perp$, on the other hand, scales with the thickness of the conductor, t, in the direction perpendicular to both the current and field (which would be the radial direction for a solenoid):

$$\sigma_\perp \sim JBt \qquad (1)$$

Consequently, transverse stress is dependent on conductor size and shape, not directly on overall magnet size as for axial stress.

Thus, transverse stress effects will become important mainly as applications call for larger conductors needed to limit inductance and keep induced quench voltages low in large magnet applications. The transverse stress effect will place limits on both the conductor dimensions and on the radial spacing between distributed reinforcement in the magnet.

As an example of the application of these results, consider the transverse stress degradation of the critical current at 10 T, given by the data in Fig. 1. The decrease in critical current becomes significant (i.e. exceeds 10%) at about 50 MPa. Substituting this value for $\sigma_\perp$ in Eq. (1) and assuming a current density of 10^9 A/m^2 at 10 T leads to a limit on the radial thickness of the conductor of about 5 mm. Other values can be substituted for the parameters in Eq. (1) to determine limits on unsupported conductor thicknesses for specific applications.

In cabled conductors, stress concentrations at strand crossover points could aggravate the transverse stress effects reported here, because the stress is no longer uniformly applied to the conductor but is concentrated at the crossover points. Since the critical current of the conductor is a weak link problem, the effect could be significant in the design of cabled conductors. The stress state inside cabled conductors may be as important as what happens outside the conductor, i.e. the internal stress design of large conductors needs to be considered along with the overall conductor stress.

CONCLUSION

The onset of significant (10%) transverse stress degradation in Nb_3Sn multifilamentary conductors occurs at about 50 MPa. The magnitude of the effect is significantly larger than for stress applied along the conductor axis. At 10 T, for example, comparable degradation of the critical current is observed at transverse stress levels seven times smaller than for axial stress.

The data indicate that the effect has its origin in a reversible degradation of the upper critical field. The intrinsic sensitivity of the upper critical field to transverse compressive stress is significantly greater than for axial stress. The stress that gives rise to a given level of B_{c2}^* degradation is generally about ten times less for transverse stress than for axial stress. Because of the intrinsic decrease in the upper critical field, the effect on the critical current will become increasingly greater at fields higher than those reported here.

We have also measured the effect of transverse stress on a multifilamentary jelly-roll conductor and obtained results similar to those reported here for a bronze-process Nb_3Sn conductor. Based on the universality of the axial strain effect,[7,4] we believe the effect of transverse stress is a general effect and will be operable not only in Nb_3Sn conductors, but also other A-15 superconductors such as V_3Ga, Nb_3Al, and Nb_3Ge.

As magnet systems are scaled to larger size, the transverse stress effect will have an impact on their design. The transverse stress scales with the thickness of the conductor as described in Eq. (1). This places a limit on the dimensions of the conductor and conductor stacking without support in the direction mutually perpendicular to field and current. It will also affect the internal stress design of cabled conductors, since stress concentration at strand crossover points can significantly enhance the effect.

REFERENCES

1.   J. W. Ekin, Appl. Phys. Lett. 29, 216 (1976).
2.   D. S. Easton and R. E. Schwall, Appl. Phys. Lett. 29, 319 (1976).
3.   J. L. McDougall, Proc. ICEC 6, IPC Science and Technology Press, 396 (1976).
4.   See, for example, the references given in J. W. Ekin, Adv. Cryog. Eng. 30, 823 (1984).
5.   J. W. Ekin, Jour. Appl. Physics, 1987, to be published; presented at the U.S. Dept. of Energy Workshop on Nb_3Sn, Cambridge, MA, August 4-5, 1986.
6.   W. Specking, W. Goldacker, and R. Flukiger, these conference proceedings.
7.   J. W. Ekin, Cryogenics 20, 611 (1980).
8.   G. Rupp, IEEE Trans. Mag. MAG-13, 1565 (1977).
9.   R. M. Scanlan, R. W. Hoard, D. N. Cornish, and J. P. Zbasnik, in Filamentary A15 Superconductors, edited by M. Suenaga and A. F. Clark, Plenum, NY (1980), p. 221.
10. D. S. Easton, D. M. Kroeger, W. Specking, and C. C. Koch, J. Appl. Phys. 51, 2748 (1980).
11. M. Fukumoto, K. Katagiri, and T. Okada, and K. Yasohama, in Proc. Int. Symp. on Flux Pinning and Electromagnetic Properties in Superconductors, edited by T. Matsushita, K. Yamafuji, and F. Irie, Matsukuma Press, Fukuoka, Japan (1986), p. 278.

552

Transverse Stress Effect on the Critical Current of Internal Tin and Bronze Process Nb_3Sn Superconductors

J. W. Ekin and S. L. Bray
National Institute of Standards and Technology, Boulder, CO

P. Danielson and D. Smathers
Teledyne Wah Chang, Albany, OR

R. L. Sabatini and M. Suenaga
Brookhaven National Lab., Upton, NY

The effect of transverse stress on the critical current density, J_c, has been shown to be significant in bronze process Nb_3Sn, with the onset of significant degradation at about 50 MPa.[1] In an applied field of 10 T, the magnitude of the effect is about seven times larger for transverse stress than for axial tensile stress. In a subsequent study,[2] similar results were observed in another bronze process Nb_3Sn conductor made by a different manufacturer.

Because axial tensile stress on typical magnet conductors is usually greater than transverse stress, the effect on J_c of the two types of stress will be comparable in importance in magnet engineering. The main effect of transverse stress will be to place limits on the conductor thickness in the direction of the Lorentz force. This can be particularly significant in cabled conductors where stress concentrations can occur at strand crossover points.

In bronze process wires, the magnitude of the effect has been observed to be the same for round strands as for flattened strands (round strands that were flattened prior to reaction) except that there is a small peak in the J_c vs. compression curve for the flattened sample due to anisotropic precompression of the filaments.[1]

The mechanism accounting for the transverse stress effect and its large magnitude compared with the axial tensile effect is still the subject of speculation. In an attempt to better understand the nature of the effect, we have undertaken a series of experiments to determine whether the transverse stress effect depends on the grain morphology of the Nb_3Sn reaction layer in the superconductor.

To do this, we have measured the effect in an internal tin conductor with excess tin, which yields a more equiaxed Nb_3Sn grain morphology than for bronze process Nb_3Sn, where the grains are more columnar.[3]

The results for the effect of transverse compression on the J_c of a round bronze process Nb_3Sn wire are shown in Fig. 1.[1] Fig. 2 shows the results for a round internal tin superconductor. A comparison of the two sets of results shows nearly the same transverse stress effect in each within the limits of error. The unloaded values of J_c recovered more for the bronze process Nb_3Sn than for the internal tin Nb_3Sn, probably because the yield strength of the matrix may have been greater for the bronze process wire, retaining more residual transverse stress on the Nb_3Sn filaments upon unloading.

However, the effect of transverse stress on J_c was nearly identical for the two conductors, indicating that the transverse stress effect is probably not dependent on grain morphology. The data also indicate that the effect is not highly sensitive to the conductor fabrication procedure, and hence these data are probably applicable to a wide variety of Nb_3Sn conductors for magnet engineering.
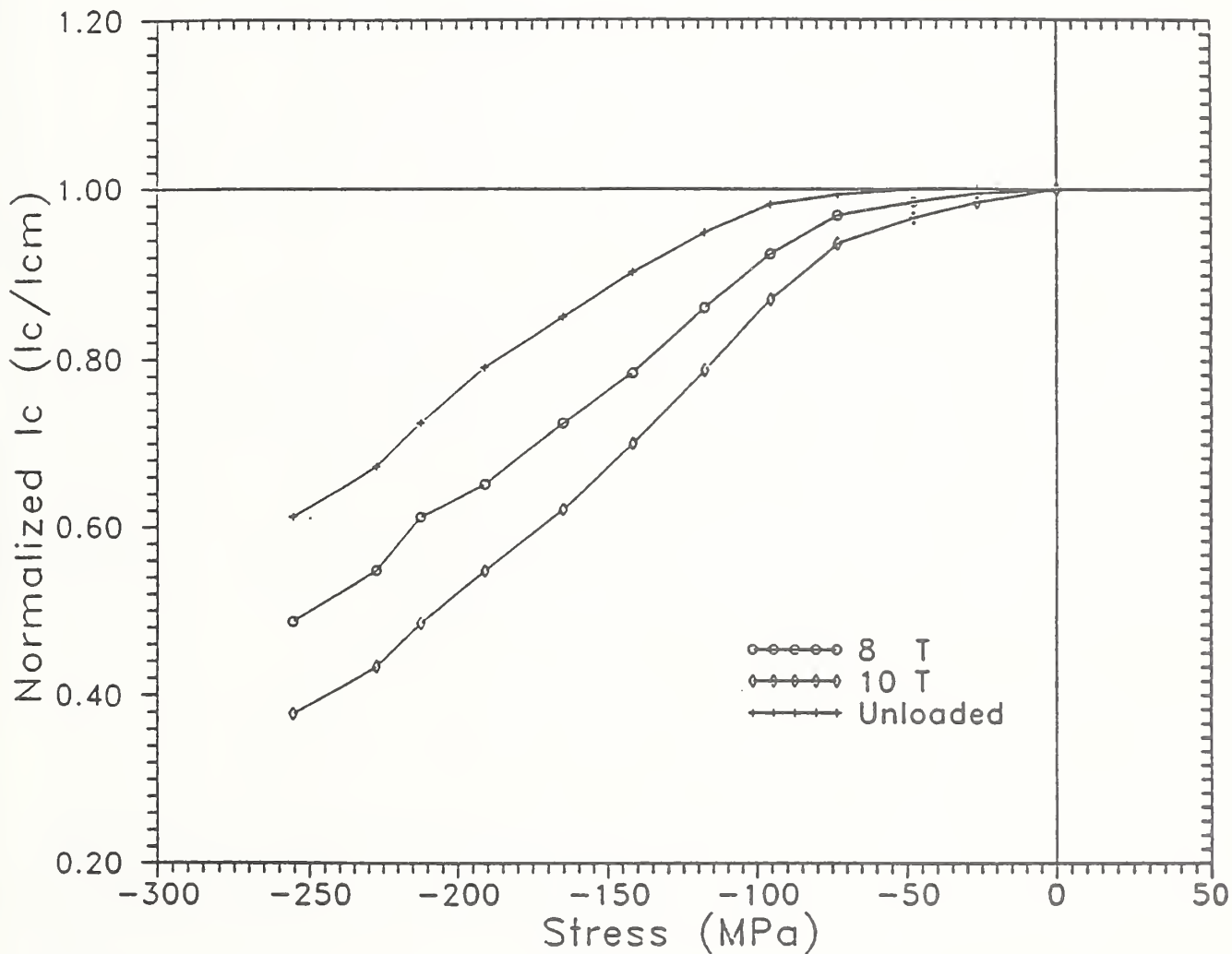
Fig. 1. Bronze process Nb_3Sn I_c-vs-stress curves at 8 and 10 T. The critical current has been normalized by its maximum value, Icm. The "Unloaded" data points indicate the measured I_c at 10 T after unloading the sample from the indicated stress level.
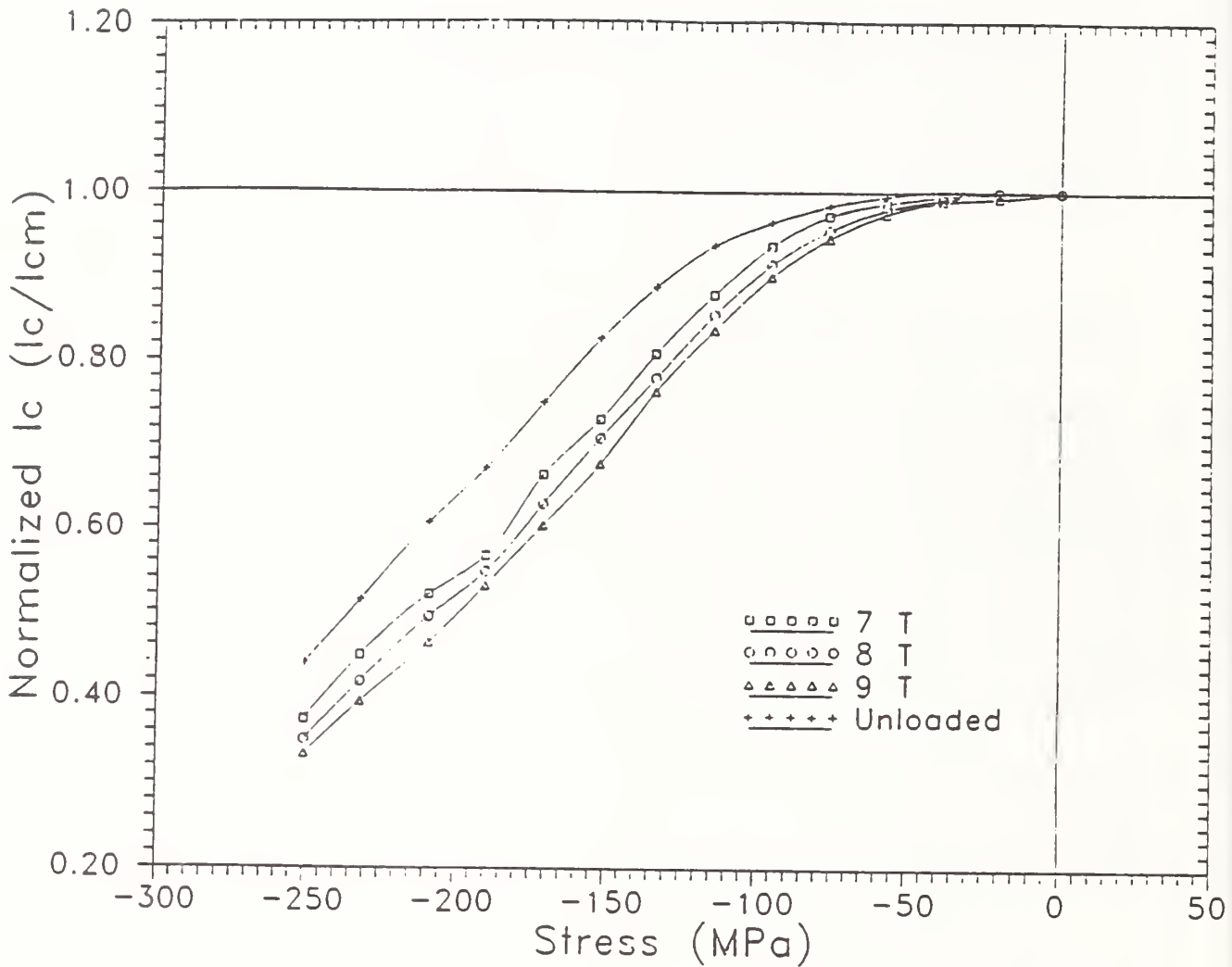
Fig. 2. Internal tin process Nb$_3$Sn I$_c$-vs-stress curves at 7, 8, and 9 T. The critical current has been normalized by its maximum value, Icm. The "Unloaded" data points indicate the measured I$_c$ at 9 T after unloading the sample from the indicated stress level.

References:

1. J. W. Ekin, Appl. Physics 62, 4829 (1987).

2. W. Specking, W. Goldacker, and R. Flukiger, Adv. Cryo. Eng. 34, 569 (1988).

3. M. Suenaga, "Metallurgy of Continuous Filamentary AIS Superconductors," in Superconductor Materials Science, edited by S. Foner and B. B. Schwartz, Plenum Press, New York 1980, pp. 201-274.

Effect of transverse stress on the critical current of bronze-process and internal-tin Nb₃Sn

J. W. Ekin, S. L. Bray, and W. L. Bahn

Electromagnetic Technology Division, National Institute of Standards and Technology, Boulder, Colorado 80303

The effect of transverse stress on the critical current of two substantially different Nb₃Sn superconductors, a bronze-process conductor and an internal-tin conductor, has been measured. Photomicrographs of the two conductors reveal a basic difference in their microstructure. The bronze-process conductor exhibits columnar grains that are radially oriented within the Nb₃Sn filaments, while the grains of the internal-tin conductor are more equiaxed and randomly oriented. The radial orientation of the bronze-process grains defines an anisotropy between the axial and transverse directions that might account for the greater sensitivity of the critical current to transverse stress reported previously. The effect of transverse stress measured on the internal-tin conductor, however, is comparable to that of the bronze-process conductor. Thus, these data indicate that the transverse stress effect is not highly dependent on either grain morphology or fabrication process. From an engineering standpoint the similarity of the transverse stress effect for these two types of Nb₃Sn superconductors represents an important simplification for setting first-order quantitative limits on the mechanical design of large superconducting magnets.

Internally generated stresses within the windings of a superconducting magnet can adversely affect its performance through a reduction in the superconductor's critical current (I_c). The superconducting wire is subjected to two dominant stress components, a tensile stress that is aligned with the wire's longitudinal axis (axial stress) and a compressive stress that is perpendicular to its axis (transverse stress). The effect of *axial* stress on the I_c of A15 superconductors has been the subject of extensive research.[1] More recently, the first measurement of the effect of *transverse* stress was made,[2] and it was significant in bronze-process Nb₃Sn, with the onset of degradation occurring at about 50 MPa. In an applied field of 10 T, the effect of transverse stress is about seven times the effect of axial tensile stress. Subsequently, the results of these measurements were substantiated at several other laboratories.[3–5] A bronze-process Nb₃Sn conductor was used for the initial transverse stress measurements and for several later measurements. The bronze process results in a characteristic grain morphology[6] that might explain the greater sensitivity of these conductors to transverse stress. Because of its dissimilarity to bronze-process conductors, an internal-tin Nb₃Sn conductor was selected for this study to directly address the effect of grain morphology on the transverse stress effect.

The apparatus allows measurement of the superconducting sample's I_c as a function of magnetic field and transverse stress at 4 K. Figure 1 shows the mutually perpendicular orientation of the current, magnetic field, and force. Force is applied to the sample through a pivoting self-aligning anvil that ensures uniform force application along the sample's compressed length. The voltage leads are soldered to the sample within this region so that the electric field is measured only over the uniformly stressed portion of the sample. The force is supplied by a servohydraulic test system, the current by a 900 A battery-powered supply, and the magnetic field by a 10 T split-pair magnet.

The characteristics of the two conductors that were tested are given in Table I. The cross section of each sample is shown in Fig. 2. The bronze-process conductor is stabilized with an external 64 vol% copper ring which surrounds the Nb₃Sn filament-bronze core and is separated from it by a tantalum diffusion barrier. The tin core modified jelly roll internal-tin conductor is stabilized with 65 vol% copper. The copper is separated from each of the conductor's 42 Nb₃Sn and bronze subelements by diffusion barriers consisting of a ring of niobium surrounded by a ring of vanadium.

Figures 3(a) and 3(b) show the shape and orientation of grains within the Nb₃Sn filaments for the bronze-process and internal-tin samples, respectively. The photographs show fractured transverse cross sections of the filaments. In the case of the bronze-process conductor, the grains have a columnar shape with their longitudinal axes oriented approximately radially within the filament. This microstructural anisotropy is a possible source of the conductor's greater sensitivity to transverse stress than to axial
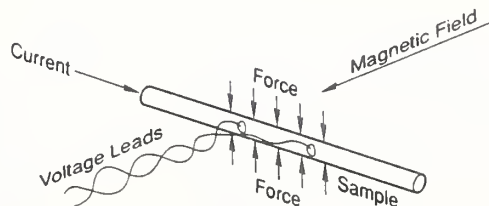
FIG. 1. Relative orientation of test sample, current, magnetic field, applied transverse force, and voltage sensing leads.

TABLE I. Sample characteristics.

	Bronze-process	Internal-tin
Diameter	0.70 mm	0.60 mm
No. filaments	2869	$\simeq 15\,800$
Filament size	3.8 μm	$\simeq 1.1\ \mu m \times (1.1–2.2)\mu m$
Filament twist pitch	25 mm	12.1 mm
Composition (vol%)	64% Cu	65% Cu
	25% bronze	12.0% Nb
	2.4% Ta	11.8% Cu
	8.6% Nb$_3$Sn and Nb	6.3% Sn Noncopper
		2.45% Nb
		2.45% V
Noncopper area	1.35×10^{-7} m^2	9.90×10^{-8} m^2
Reaction	96 h at 700 °C	220 h at 220 °C
	48 h at 730 °C	16 h at 340 °C ,
		110h at 650 °C

stress. In contrast, the internal-tin grains are more equiaxed, as described in Ref. 6. If the source of the transverse stress sensitivity of bronze-process Nb$_3$Sn is in fact the anisotropy, then the internal-tin conductor would be expected to show a smaller sensitivity to transverse stress.

The critical current of the test sample was measured at zero applied force and 4 K as a function of magnetic field. Force was then applied to the sample at 4 K and again the I_c was measured as a function of field. This process was continued while incrementally increasing the applied force to generate the data shown in Fig. 4.

The effective overall transverse stress is calculated by dividing the applied force by the compressed area of the sample. A projected area equal to the sample diameter multiplied by the length of the compressed region is used for this calculation. This simple technique is justified by the results of previous comparative measurements between otherwise identical round and rectangular Nb$_3$Sn samples.[2]
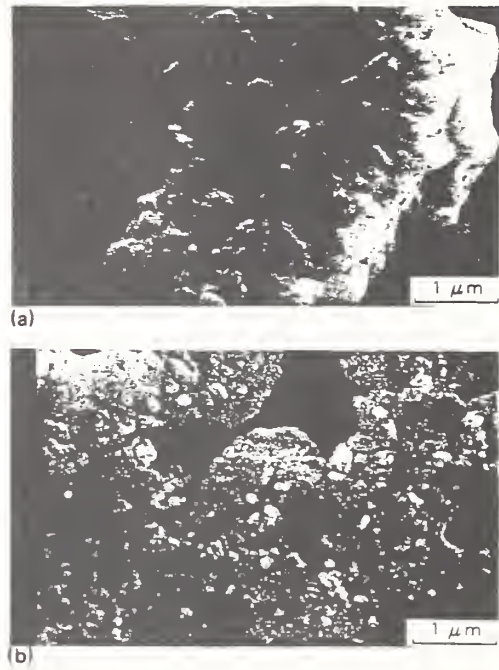
FIG. 3. Micrographs of bronze-process conductor (a) showing columnar radially oriented grains, and internal-tin conductor (b) showing more equiaxed and randomly oriented grains.

An electric-field criterion of 2 μV/cm was used to determine the I_c. The overall precision of the I_c data is about $\pm 3\%$.

Figure 4(a) shows the critical current of the internal-tin conductor as a function of transverse compressive stress for several applied magnetic fields. The ordinate is the measured critical current normalized to the starting (zero-stress) value, and the abscissa is the effective overall transverse stress. Figure 4(b) shows the 8 and 10 T internal-tin data compared with the bronze-process data.
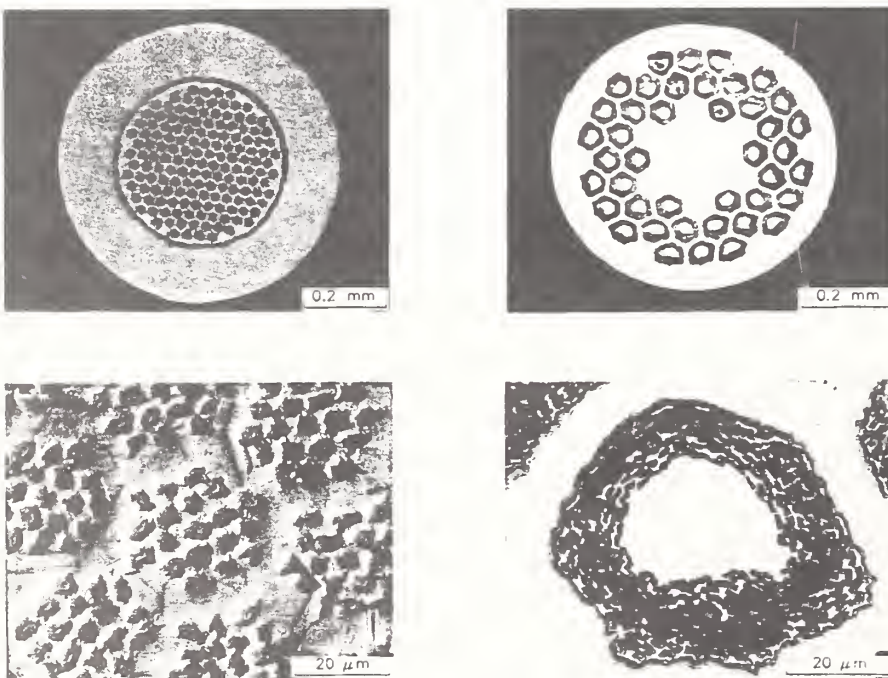
FIG. 2. Cross-sectional view of bronze-process sample (top) and internal-tin sample (bottom).

4437   J. Appl. Phys., Vol. 69, No. 8, 15 April 1991

20

Ekin, Bray, and Bahn   4437

(a)

(b)
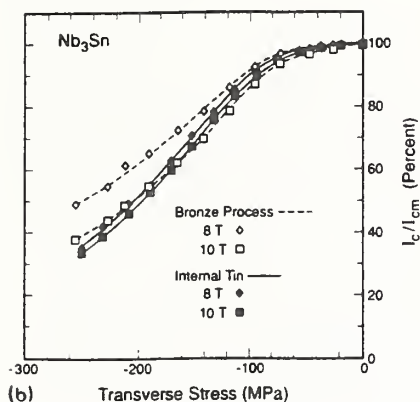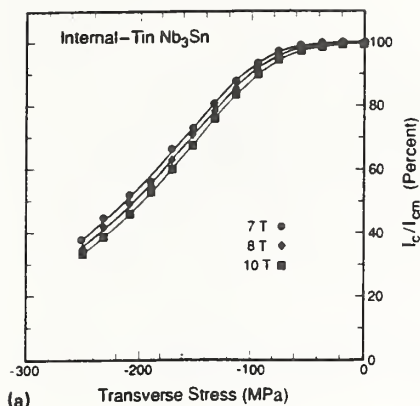
FIG. 4. Critical-current degradation as a function of transverse stress and magnetic field for the internal-tin conductor (a) and (b) a comparison of the effect in internal-tin and bronze-process conductors. By convention, the negative values of stress indicate compression.

Comparing the 8 T internal-tin and bronze-process data of Fig. 4(b), a 10% reduction in the I_c occurs at a transverse stress of approximately 100 MPa for both samples. Moreover, the two sets of results show nearly the same transverse stress effect, within the limits of error, over the entire measured range of transverse stress. If anything, the internal-tin sample has a slightly greater I_c degradation than the bronze-process sample, which is opposite to what would be expected if the columnar grain morphology was the source of the transverse stress sensitivity. At a stress of 200 MPa, the internal-tin sample shows a degradation of approximately 50%, whereas the bronze-process sample is degraded slightly less than 40%. Considering that the two test conductors were fabricated by different manufacturers using fundamentally different processes, the two data sets are in surprisingly close agreement.

The difference between the magnitude of the effect of axial and transverse stress on the I_c of Nb_3Sn is presently the source of speculation. Based on these data, however, the difference would not appear to be due to microstructural anisotropy. Moreover, recent measurements of the

transverse stress effect in Nb_3Al (Ref. 7) and $PbMo_6S_8$ (Ref. 8) demonstrate that the large difference between the two effects is not limited to Nb_3Sn or even to A15 superconductors. If, in general, this is a common characteristic of superconductors, the transverse stress effect may be important for developing a fundamental understanding of stress effects in superconductors. From a practical point of view, the relatively large magnitude of the transverse stress effect makes it a significant factor in the designing of large magnets where the large radial thickness of the conductor can lead to accumulation of high internal transverse stress loading of the strands within cabled conductors.[2] Although the effect of transverse stress on the I_c of Nb_3Sn is considerably greater than that of axial stress, their relative importance in magnet design may be comparable because the axial stress imposed on typical magnet conductors is usually greater than transverse stress. The main effect of transverse stress will be to place limits on the conductor thickness in the direction of the Lorentz force. This can be particularly significant in cabled conductors where stress concentrations can occur at strand crossover points.

The effect of transverse stress on the critical current of *internal-tin* Nb_3Sn superconductors was nearly identical to that measured for *bronze-process* Nb_3Sn. The magnitude of the effect was nearly the same even though photomicroscopic analysis revealed significant difference in grain morphology and orientation for the two conductor types; the bronze-process conductor grains had a columnar shape and were oriented in a radial pattern within each Nb_3Sn filament, while the internal-tin conductor grains were more equiaxed. These data also indicate that the transverse stress effect is not highly sensitive to the Nb_3Sn fabrication procedure. The data shown in Fig. 4, thus, should serve as a general starting point for determining the effect of transverse stress and setting engineering design limits for the conductor windings in Nb_3Sn magnets.

[1] See, for example, the references given in J. W. Ekin, Adv. Cryo. Eng. 30, 823 (1984).

[2] J. W. Ekin, J. Appl. Phys. 62, 4829 (1987).

[3] W. Specking, W. Goldacker, and R. Flükiger, Adv. Cryo. Eng. 34, 569 (1988).

[4] L. T. Summers and J. R. Miller, IEEE Trans. Magn. 25, 1835 (1989).

[5] H. Boschman and L. J. M. van de Klundert, Adv. Cryo. Eng. 36, 93 (1990).

[6] M. Suenaga, C. J. Klamut, N. Higuchi, and T. Kuroda. IEEE Trans. Magn. 21, 305 (1985).

[7] D. Zeritis, T. Ando, Y. Takahashi, M. Nishi, H. Nakajima, and S. Shimamoto, Appl. Phys. Lett 57, 506 (1990).

[8] W. Goldacker, W. Specking, F. Weiss, G. Rimikis, and R. Flükiger, Cryogenics 29, 955 (1989).

21

Transverse Stress and Crossover Effect in Nb_3Sn[*]

J. W. Ekin and S. L. Bray

Electromagnetic Technology Division, National Institute of Standards and Technology, Boulder, Colorado 80303

Abstract: The superconducting wires in an energized magnet coil are subjected to mechanical stresses caused by the Lorentz force. Previous measurements have shown that either axial tensile stress or transverse compressive stress, the two dominant stresses on the wire, can cause substantial degradation in the superconductor's critical current. The previous transverse stress measurements were made with uniformly applied stress; however, many superconductor applications employ cables where the strands experience stress concentrations at the points where they cross one another. For this study, a single stress concentration point was simulated by applying transverse stress to two Nb_3Sn wires, which were crossed over one another at an angle, while measuring the critical current of one of the wires at magnetic fields up to 9 T. A comparison between the crossover-transverse-stress measurements and the uniform-transverse-stress measurements shows a critical-current degradation at equivalent *load* that is significantly greater for the crossover situation due to the reduced area. However, these preliminary data indicate that the concentration effect can be simply predicted because the degradation in critical current is comparable at equivalent *stress*.

I. INTRODUCTION

The two dominant components of stress in a magnet winding are a tensile stress that is aligned with the wire's longitudinal axis (axial stress) and a compressive stress that is perpendicular to its axis (transverse stress). The effect of *axial* stress on the critical current (I_c) of A15 superconductors has been the subject of extensive research.[1] More recently, the effect of *transverse* stress on the I_c of Nb_3Sn has been studied,[2-6] and its effect is several times greater than that of axial stress. In previous measurements of the transverse stress effect, a uniform stress was applied over the length of the test wire.[2,6] In this study, stress was applied to the test wire through a second sample of the same wire (crossover wire) to simulate a concentrated-stress condition that can occur within the strands of a superconducting cable. The superconductor used for these measurements is a tin-core modified jelly roll Nb_3Sn wire. This is the wire that was used to construct the cable-in-conduit conductor for the US-Demonstration Poloidal Coil (US-DPC).

The test configuration of the crossover wire and the test wire are shown in Fig. 1. The voltage sensing leads were connected to the test wire outside its stressed region; consequently, an "effective voltage tap separation" was calculated from the crossover angle, Θ, and the wire diameter, d. The I_c values were determined using an electric field criterion of 2 μV/cm, where the electric field was calculated from the effective voltage tap separation. Moreover, the difference between I_c based on the actual tap separation and I_c based on the effective separation, at zero stress and all tested magnetic fields, was less than 6%. The overall precision of the I_c data is about ±3%.

Fig. 1.   Schematic diagram showing the test configuration
of the test wire and crossover (X-over) wire.

For the purposes of this study, the transverse compressive stress is defined as the applied load divided by the "projected stress area," which is also shown in Fig. 1. A crossover angle of 30° was selected for these measurements based on cable strand crossover angles observed in the US-DPC cable. All of the I_c measurements were made at a temperature of 4 K.

II. RESULTS

The results of the crossover measurements are shown in Fig. 2 where the I_c is plotted as a function of transverse load for several magnetic fields. The ordinate is the measured I_c normalized to the starting (zero-stress) value, and the abscissa is the transverse load applied to the test wire through the crossover wire. By convention, the load is negative to indicate compression. For comparison, the results of a uniform stress test on another sample of the same wire are also shown. In this case, the transverse load is evenly distributed along the length of the wire. At 9 T, a 60 % reduction in the I_c occurs at a load of approximately -1760 N for uniform stress and at only 1/6 this load (-290 N) for crossover stress. The stressed area of the conductor in the uniform stress test is 7.48 mm², and the stressed area of the crossover test wire is only 1.24 mm², also 1/6 the area.

Fig. 2. Critical-current degradation as a function of transverse load and magnetic field for uniform and crossover stress.

Figure 3 shows the same I_c data as Fig. 2, but in Fig. 3 it is plotted as a function of transverse stress instead of load. This plot shows that, for the same transverse *stress*, the I_c degradation is comparable up to -240 MPa for uniform or crossover stress. These data show that the I_c

Fig. 3. Critical-current degradation as a function of transverse
stress and magnetic field for uniform and crossover stress.

degradation caused by concentrated transverse stress at a strand crossover point is nearly the same as the degradation caused by uniform transverse stress. For both tests, there is no significant I_c recovery when the transverse load is removed from the test wire.

III. CONCLUSIONS

The transverse stress generated by the Lorentz force within the windings of a superconducting magnet can substantially degrade the I_c of the superconductor and the performance of the magnet. Distributed structural reinforcement of the windings can limit the peak transverse load, but its use is restricted by inductance and current-density requirements. These data show that the effect of transverse load on the superconductor greatly depends on the load distribution. At a load that caused no measurable I_c degradation for the uniform stress test, the I_c degradation was over 60% for the crossover test. Consequently, internal cable design may be important in controlling degradation from this effect. When the results of the crossover and uniform stress tests are compared based on the applied stress, rather than load, the I_c degradation is nearly the same for both tests. This is an important result from an engineering analysis standpoint because it may allow the estimation of I_c degradation and the design of cables from uniform transverse stress data and the cable strand geometry.

ACKNOWLEDGEMENT

REFERENCES

1. See, for example, the references given in J. W. Ekin, Adv. Cryog. Eng. 30:823 (1984).
2. J. W. Ekin, Effect of transverse compressive stress on the critical current and upper critical field of Nb_3Sn, J. Appl. Phys. 62:4829 (1987).
3. W. Specking, W. Goldacker, and R. Flükiger, Effect of transverse compression on I_c of Nb_3Sn multifilamentary wire, Adv. Cryog. Eng. 34:569 (1988).
4. L. T. Summers and J. R. Miller, The effect of transverse stress on the critical current of Nb_3Sn cable-in-conduit superconductors, IEEE Trans. Magn. 25:1835 (1989).
5. H. Boschman and L. J. M. van de Klundert, Effects of transverse stress on the current carrying capacity of multifilamentary wires, Adv. Cryog. Eng. 36:93 (1990).
6. J. W. Ekin and S. L. Bray, Effect of transverse stress on the critical current of bronze-process and internal-tin Nb_3Sn, J. Appl. Phys. 69:4436 (1991).

CRITICAL-CURRENT DEGRADATION IN Nb$_3$Sn COMPOSITE

WIRES DUE TO LOCALLY CONCENTRATED TRANSVERSE STRESS*

S. L. Bray and J. W. Ekin

Electromagnetic Technology Division
National Institute of Standards and Technology
Boulder, Colorado 80303

ABSTRACT

The superconducting wires in an energized magnet coil are subjected to mechanical stresses caused by the Lorentz force. Previous measurements have shown that either axial tensile stress or transverse compressive stress, the two dominant stresses on the wire, can cause substantial degradation in the superconductor's critical current. The previous transverse stress measurements were made with uniformly applied stress; however, many superconductor applications employ cables where the strands experience stress concentrations at the points where they cross one another. For this study, a single stress concentration point was simulated by applying transverse stress to two Nb$_3$Sn wires, which were crossed over one another at an angle, while measuring the critical current of one of the wires at magnetic fields up to 9 T. A comparison between the crossover-transverse-stress measurements and the uniform-transverse-stress measurements shows a critical-current degradation at equivalent *load* that is significantly greater for the crossover situation due to the reduced area. However, these preliminary data indicate that the concentration effect can be simply predicted because the degradation in critical current is comparable at equivalent *stress*.

INTRODUCTION

The Lorentz forces generated within the windings of a superconducting magnet can be large enough to significantly degrade the critical current (I$_c$) of the superconductor and, thus, the performance of the magnet. The two dominant components of stress are a tensile stress that is aligned with the wire's longitudinal axis (axial stress) and a compressive stress that is perpendicular to its axis (transverse stress). The effect of *axial* stress on the I$_c$ of A15 superconductors has been the subject of extensive research.[1] More recently, the effect of *transverse* stress on the I$_c$ of Nb$_3$Sn has been studied,[2-6] and its effect is several times greater than that of axial stress. In previous measurements of the transverse stress effect, a uniform stress was applied over the length of the test wire.[2-6] In this study, stress was applied to the test wire through a second sample of the same wire (crossover wire) to simulate a concentrated-stress condition that can occur within the strands of a superconducting cable. The superconductor used for these measurements is a tin-core modified jelly roll Nb$_3$Sn wire. This is the wire that was used to construct the cable-in-conduit conductor for the US-Demonstration Poloidal Coil (US-DPC).

---

*Contribution of NIST, not subject to copyright.
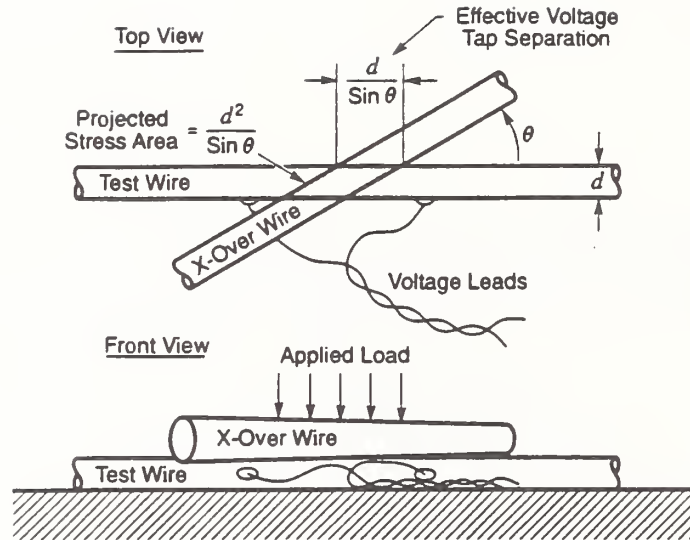
Advances in Cryogenic Engineering (Materials), Vol. 38
Edited by F. R. Fickett and R. P. Reed
Plenum Press, New York, 1992

27

Fig. 1. Schematic diagram showing the test configuration
of the test wire and crossover (X-over) wire.

EXPERIMENTAL DETAILS

The I_c of a Nb_3Sn superconducting wire was measured at 4 K as a function of magnetic field and transverse compressive stress. The relative orientations of the current, magnetic field, and stress were mutually perpendicular to simulate the conditions within the windings of a superconducting magnet. The current was supplied by a 900 A battery-powered supply, the magnetic field by a 9 T split-pair magnet, and the stress by a servohydraulic test system.

The test configuration of the crossover wire and the test wire are shown in Fig. 1. The voltage sensing leads were connected to the test wire outside its stressed region; consequently, an "effective voltage tap separation" was calculated from the crossover angle, Θ, and the wire diameter, d. The I_c values were determined using an electric field criterion of 2 µV/cm, where the electric field was calculated from the effective voltage tap separation. Moreover, the difference between I_c based on the actual tap separation and I_c based on the effective separation, at zero stress and all tested magnetic fields, was less than 6%. The overall precision of the I_c data is about ±3%.
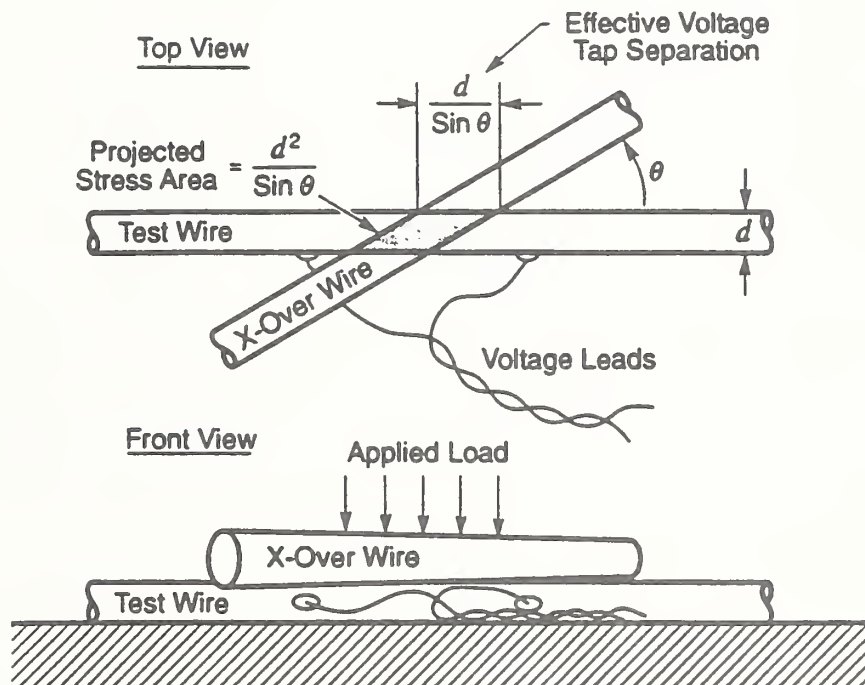
Table 1. Nb_3Sn Wire Specifications

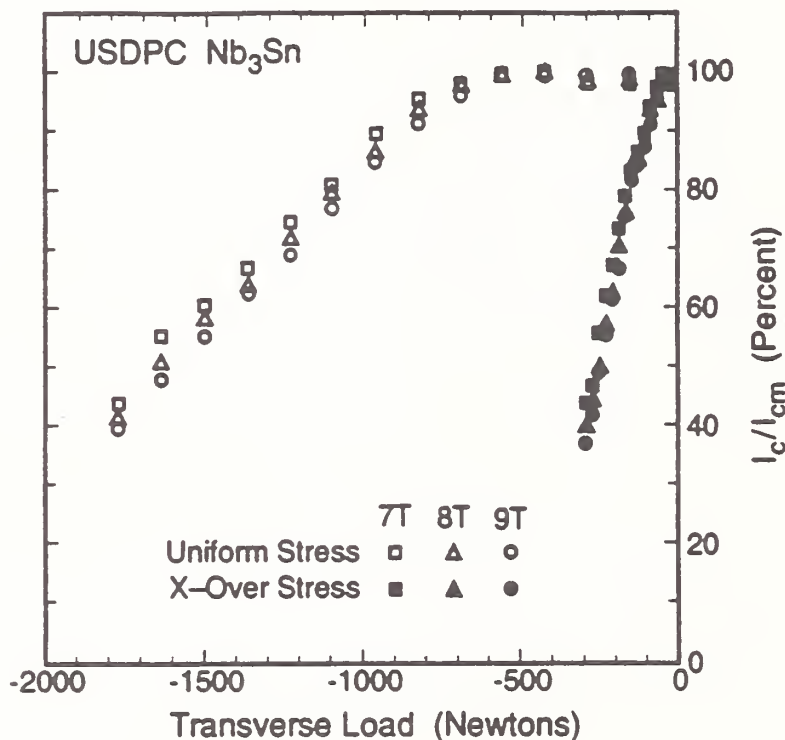|	
Wire Diameter	0.78 mm
Stabilizing Copper	54 vol.%
Non-Copper	46 vol.%
Nb Filament	22.9 vol.%
Copper	48.7 vol.%
Tin	15.8 vol.%
Vanadium	12.6 vol.%
Local Cu/Nb Ratio	1.7
Filament Size	3 µm
Filament Composition	Nb-1 wt.% Ti
Subelements	18
Twist Pitch	2 twists per inch
Critical Current	
7 Tesla	309 A
8 Tesla	256 A
9 Tesla	213 A
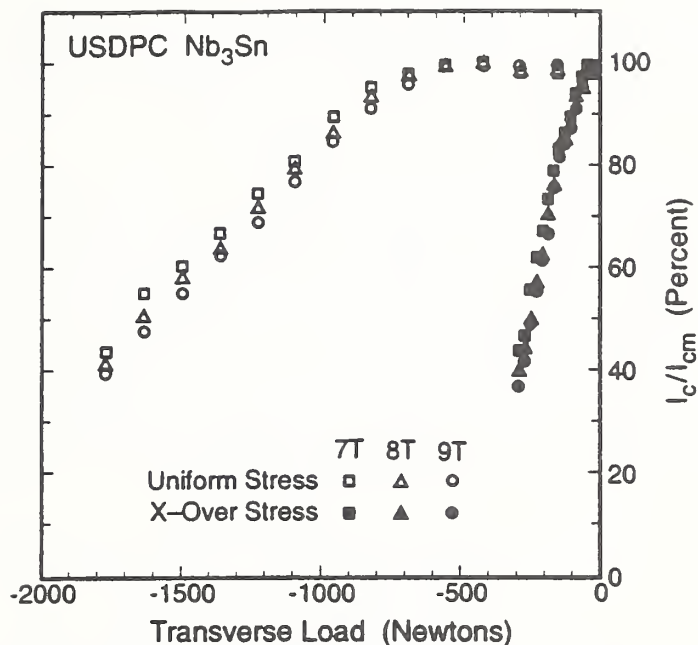
Fig. 2. Critical-current degradation as a function of transverse
load and magnetic field for uniform and crossover stress.

For the purposes of this study, the transverse compressive stress is defined as the applied load divided by the "projected stress area," which is also shown in Fig. 1. A crossover angle of 30° was selected for these measurements based on cable strand crossover angles observed in the US-DPC cable. The characteristics of the Nb_3Sn wire that was used for this study are given in Table 1.

RESULTS

The results of the crossover measurements are shown in Fig. 2 where the I_c is plotted as a function of transverse load for several magnetic fields. The ordinate is the measured I_c normalized to the starting (zero-stress) value, and the abscissa is the transverse load applied to the test wire through the crossover wire. By convention, the load is negative to indicate compression. For comparison, the results of a uniform stress test on another sample of the same wire are also shown. In this case, the transverse load is evenly distributed along the length of the wire. At 9 T, a 60 % reduction in the I_c occurs at a load of approximately -1760 N for uniform stress and at only 1/6 this load (-290 N) for crossover stress. The stressed area of the conductor in the uniform stress test is 7.48 mm², and the stressed area of the crossover test wire is only 1.24 mm², also 1/6 the area.

Figure 3 shows the same I_c data as Fig. 2, but in Fig. 3 it is plotted as a function of transverse stress instead of load. This plot shows that, for the same transverse *stress*, the I_c degradation is comparable up to -240 MPa for uniform or cr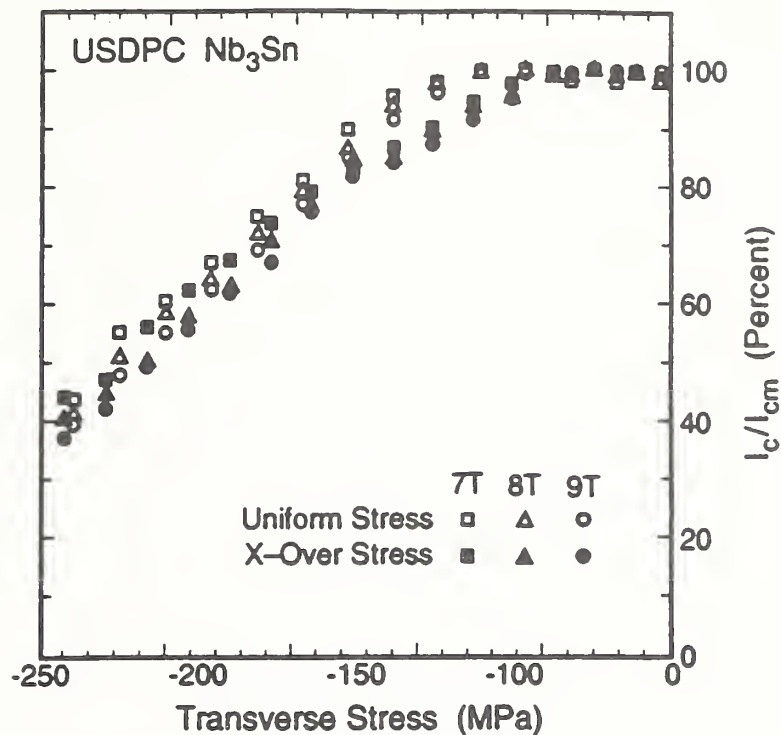ossover stress. These data show that the I_c degradation caused by concentrated transverse stress at a strand crossover point is nearly the same as the degradation caused by uniform transverse stress. For both tests, there is no significant I_c recovery when the transverse load is removed from the test wire.

DISCUSSION

The data analysis was greatly simplified by defining the stress as the applied load divided by the area projected from the compressed section of the test wire. For the uniform stress test this area is simply the diameter of the wire multiplied by its compressed length, and for the crossover test it
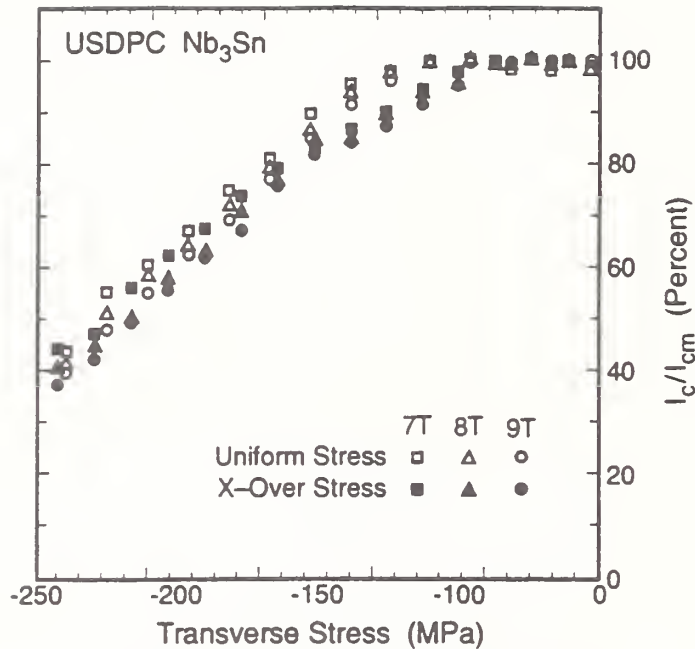
Fig. 3. Critical-current degradation as a function of transverse
stress and magnetic field for uniform and crossover stress.

is the area of the parallelogram shown in Fig. 1. The validity of this procedure was demonstrated for uniform transverse stress through comparative measurements of round and rectangular specimens of the same wire.[2]

There is a second simplifying assumption unique to the analysis of the crossover data. If the voltage taps are connected to the test wire with a separation equal to the compressed length of the wire, it is extremely difficult to precisely align the crossover wire with the voltage taps. Consequently, the voltage tap separation must be greater than the length of the test wire's compressed region to ensure that the voltage taps span this entire region. However, the "effective voltage tap separation," which is simply the length of this compressed region, (shown in Fig. 1) is used to calculate the electric field for I_c analysis. This procedure is appropriate because, at stresses where substantial degradation of the I_c occurs, the measured voltage will be generated over the stressed region of the conductor. Moreover, the difference between I_c based on the actual voltage tap separation and the effective separation is too small to affect the conclusions of the paper.

CONCLUSIONS

The transverse stress generated by the Lorentz force within the windings of a superconducting magnet can substantially degrade the I_c of the superconductor and the performance of the magnet. Distributed structural reinforcement of the windings can limit the peak transverse load, but its use is restricted by inductance and current-density requirements. These data show that the effect of transverse load on the superconductor greatly depends on the load distribution. At a load that caused no measurable I_c degradation for the uniform stress test, the I_c degradation was over 60% for the crossover test. Consequently, internal cable design may be important in controlling degradation from this effect. When the results of the crossover and uniform stress tests are compared based on the applied stress, rather than load, the I_c degradation is nearly the same for both tests. This is an important result from an engineering analysis standpoint because it may allow the estimation of I_c degradation and the design of cables from uniform transverse stress data and the cable strand geometry.

30

REFERENCES

1. See, for example, the references given in J. W. Ekin, Adv. Cryog. Eng. 30:823 (1984).
2. J. W. Ekin, Effect of transverse compressive stress on the critical current and upper critical field of Nb_3Sn, J. Appl. Phys. 62:4829 (1987).
3. W. Specking, W. Goldacker, and R. Flükiger, Effect of transverse compression on I_c of Nb_3Sn multifilamentary wire, Adv. Cryog. Eng. 34:569 (1988).
4. L. T. Summers and J. R. Miller, The effect of transverse stress on the critical current of Nb_3Sn cable-in-conduit superconductors, IEEE Trans. Magn. 25:1835 (1989).
5. H. Boschman and L. J. M. van de Klundert, Effects of transverse stress on the current carrying capacity of multifilamentary wires, Adv. Cryog. Eng. 36:93 (1990).
6. J. W. Ekin and S. L. Bray, Effect of transverse stress on the critical current of bronze-process and internal-tin Nb_3Sn, J. Appl. Phys. 69:4436 (1991).

US-DPC Nb₃Sn Cable Strand

A complete set of axial strain data was obtained for the critical current of the US-DPC cable strand at magnetic fields from 10 T to 24 T. The conductor specifications are shown in Table 1, and the measured data are shown in Table 2. The data are presented graphically in Figs. 1-4. The I_c and J_c values are based on an electric field criterion (E_c) of 2 μV/cm. The results show a zero-strain 12 T value of J_c (referred to the noncopper area) which was 0.54 GA/m^2 and a peak (strain-free) J_c value of 0.62 GA/m^2. The irreversible strain limit was reasonably high, 0.82%, and the compressive prestrain was 0.38%. The sample did not fracture until 1.31% strain.

Table 1. US-DPC Nb₃Sn conductor specifications.

Wire diameter	0.78 mm
Stabilizing Copper	54 vol.%
Noncopper	46 vol.%
Nb Filament	22.9 vol.%
Copper	48.7 vol.%
Tin	15.8 vol.%
Vanadium	12.6 vol.%
Local Cu:Nb Ratio	1.7:1
Filament Size	3 µm
Filament Composition	Nb-1 wt.% Ti
Subelements	18
Twist Pitch	2 twists per inch

Table 2. High-field critical current of US-DPC Nb_3Sn sample CRE 1087 B4H21 as a function of axial tensile strain applied at 4 K.

E (%)	Eo (%)	Ic (Amperes)	Field (Tesla)	Jc (GA/m^2)	JcB (GN/m^3)	Ic/Icm
0.00	-.38	183.460	10.00	0.819	8.190	
		121.140	12.00	0.541	6.490	0.8576
		74.870	14.00	0.334	4.679	
		42.423	16.00	0.189	3.030	
		19.799	18.00	0.088	1.591	
		7.209	20.00	0.032	0.644	
		3.793	21.00	0.017	0.356	
		1.724	22.00	0.008	0.169	
		0.665	23.00	0.003	0.068	
0.18	-.20	197.230	10.00	0.880	8.805	
		134.810	12.00	0.602	7.222	0.9543
0.23	-.16	138.430	12.00	0.618	7.416	0.9800
0.30	-.08	141.260	12.00	0.631	7.568	1.0000
0.41	0.03	140.020	12.00	0.625	7.501	0.9912
		90.757	14.00	0.405	5.672	
		53.369	16.00	0.238	3.812	
		27.644	18.00	0.123	2.221	
		11.528	20.00	0.051	1.029	
		6.746	21.00	0.030	0.632	
		3.503	22.00	0.016	0.344	
		1.581	23.00	0.007	0.162	
		0.538	24.00	0.002	0.058	
0.52	0.14	132.150	12.00	0.590	7.080	0.9355
0.63	0.25	117.940	12.00	0.527	6.318	0.8349
0.72	0.34	103.970	12.00	0.464	5.570	0.7360
0.33	-.05	140.880	12.00	0.629	7.547	0.9973
0.82	0.44	87.687	12.00	0.391	4.698	0.6208
0.40	0.02	135.650	12.00	0.606	7.267	0.9603
0.90	0.52	75.108	12.00	0.335	4.024	0.5317
0.45	0.07	127.270	12.00	0.568	6.818	0.9010
0.96	0.58	60.134	12.00	0.268	3.222	0.4257

33

Table 2 cont'd

E (%)	Eo (%)	Ic (Amperes)	Field (Tesla)	Jc (GA/m^2)	JcB (GN/m^3)	Ic/Icm
0.49	0.11	116.870	12.00	0.522	6.261	0.8273
1.07	0.69	40.730	12.00	0.182	2.182	0.2883
0.53	0.15	94.626	12.00	0.422	5.069	0.6699
1.17	0.79	24.363	12.00	0.109	1.305	0.1725
0.58	0.20	67.861	12.00	0.303	3.635	0.4804
1.27	0.89	11.251	12.00	0.050	0.603	0.0796
0.66	0.28	34.885	12.00	0.156	1.869	0.2470
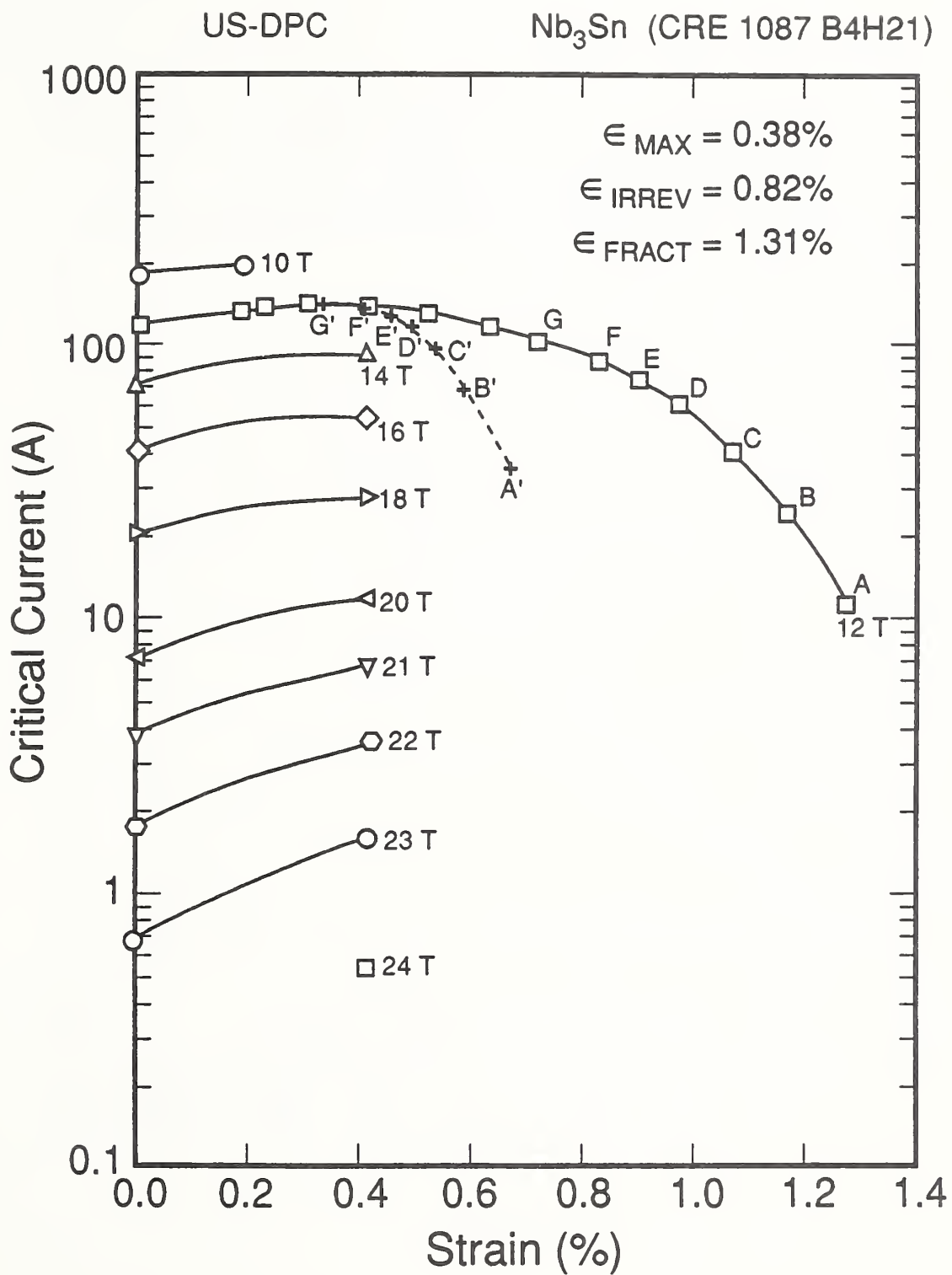
Figure 1. Effect of axial tensile strain on the critical current of US-DPC Nb_3Sn sample CRE 1087 B4H21 at 4 K and several magnetic fields.
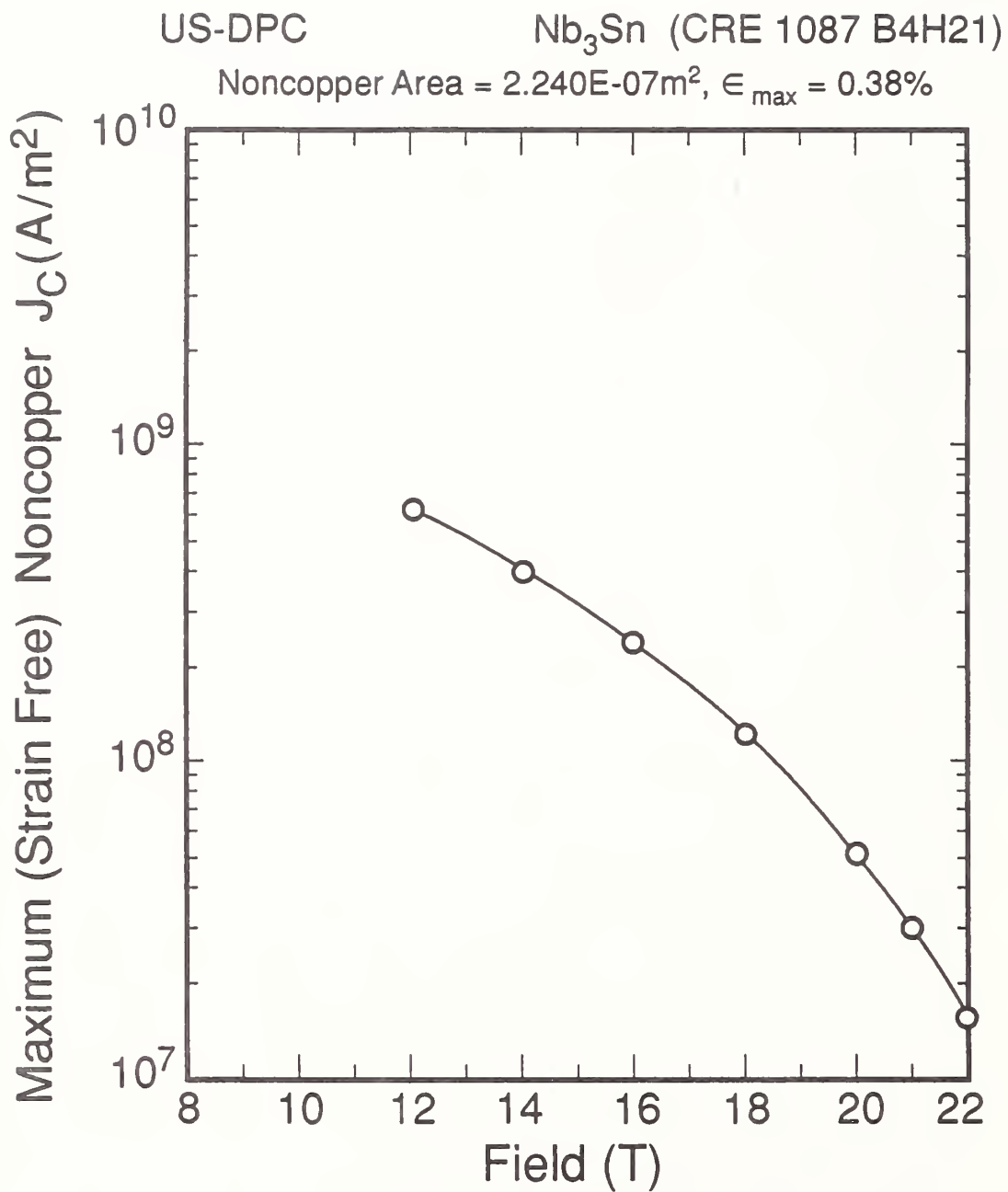
Figure 2. Effect of magnetic field on the critical current density of US-DPC Nb_3Sn sample CRE 1087 B4H21 at 4 K .
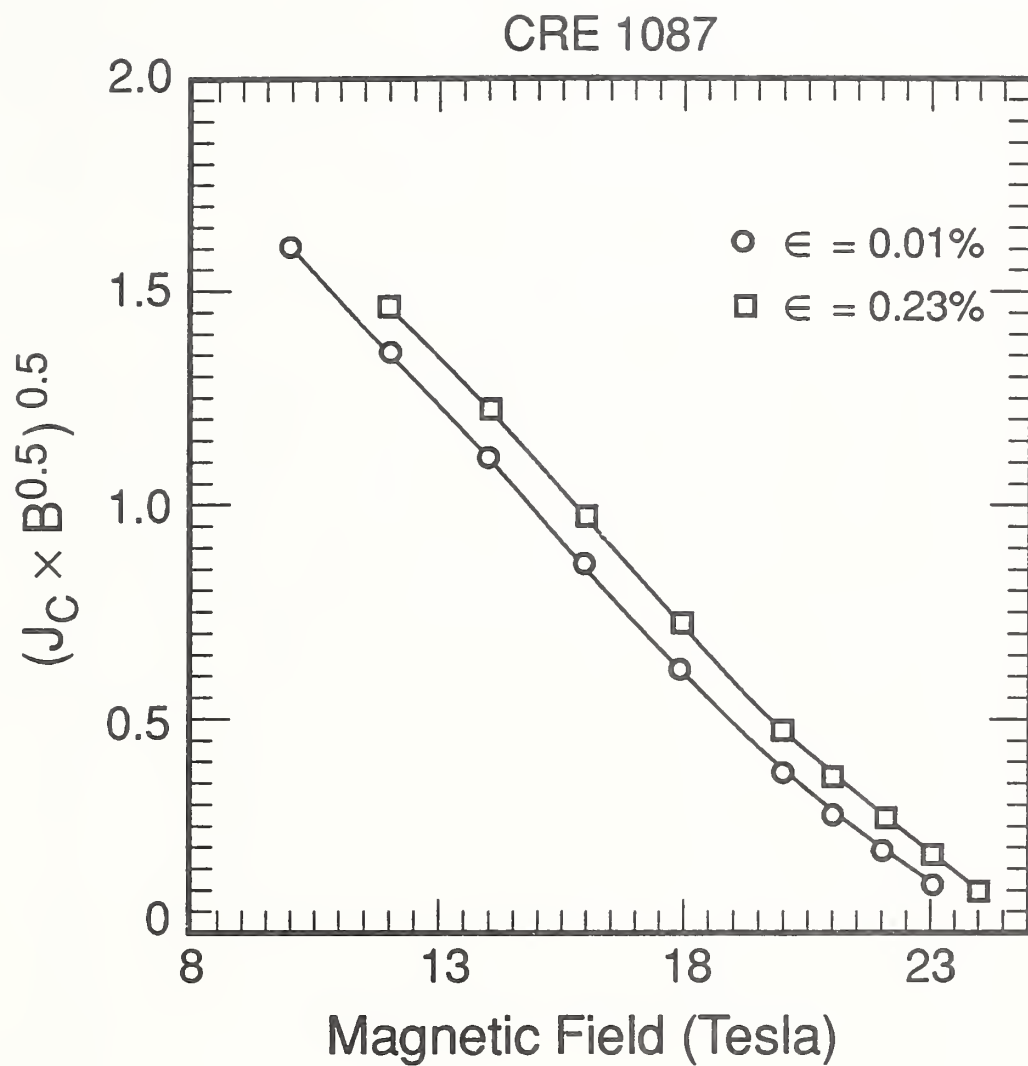
Figure 3. $(J_c \times B^{0.5})^{0.5}$ as a function of magnetic field for US-DPC Nb$_3$Sn sample CRE 1087 B4H21 at 0.01% and 0.23% strain.
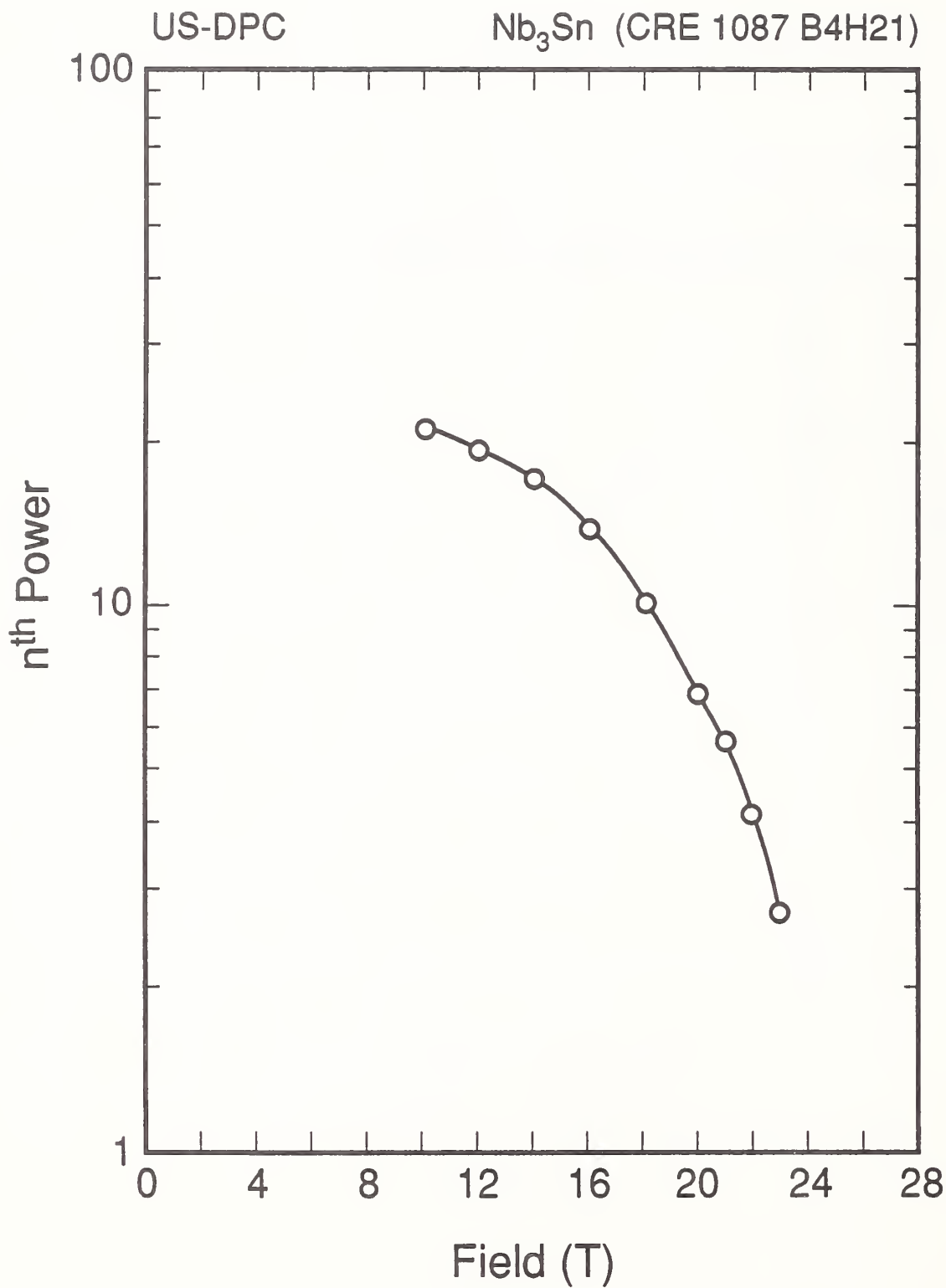
Figure 4. Effect of magnetic field on n^{th} power of US-DPC Nb_3Sn sample CRE 1087 B4H21 at 4 K.

Nb₃Sn LLNL Cable Test Strand

Axial strain characterization was completed for a Nb_3Sn conductor from Lawrence Livermore National Lab used in a transverse stress test of a cable-in-conduit conductor. The effect of axial strain on the critical current of the LLNL Nb_3Sn test strand was measured at magnetic fields from 8 T to 22 T. The conductor specifications are shown in Table 3, and the measured data are shown in Table 4. The data are presented graphically in Figs. 5 through 7. The I_c and J_c values are based on an electric field criterion (E_c) of 2 µV/cm. The zero-strain 12 T value of J_c (referred to the noncopper area) was measured to be 0.36 GA/m^2 and the peak (strain-free) J_c at 12 T was 0.39 GA/m^2. The irreversible strain limit was quite high, 1.0% strain, and the compressive prestrain was relatively low at 0.27%. Fracture strain was 1.10%.

Table 3.   LLNL Nb₃Sn cable test strand specifications.

Wire Diameter	0.533 mm
Local Cu:Nb Ratio	1.0:1.0
Copper Stabilizer	50%
7 Subelements	
Filament Composition	1.2 wt.% Ti
Filament Dia.	~4 µm
Nb Diffusion Barrier with Cu Interlayers	

Table 4.   High-field critical current of LLNL Nb$_3$Sn cable test strand.

E (%)	Eo (%)	Ic (Amperes)	Field (Tesla)	Jc (GA/m^2)	JcB (GN/m^3)	Ic/Icm
0.00	-.27	145.290	8.00	0.650	5.201	
		110.270	10.00	0.493	4.934	
		80.560	12.00	0.360	4.325	0.9400
		53.920	14.00	0.241	3.378	0.8841
		32.595	16.00	0.146	2.333	0.8267
		17.377	18.00	0.078	1.399	0.7837
		7.169	20.00	0.032	0.642	0.6709
		1.738	22.00	0.008	0.171	0.4791
0.11	-.16	117.860	10.00	0.527	5.273	
		83.413	12.00	0.373	4.479	0.9732
		58.083	14.00	0.260	3.638	0.9523
		37.288	16.00	0.167	2.669	0.9457
		20.045	18.00	0.090	1.614	0.9040
		8.838	20.00	0.040	0.791	0.8271
		2.782	22.00	0.012	0.274	0.7669
0.22	-.05	86.088	12.00	0.385	4.622	1.0044
		62.262	14.00	0.279	3.900	1.0208
		39.527	16.00	0.177	2.830	1.0025
		22.082	18.00	0.099	1.778	0.9959
		10.435	20.00	0.047	0.934	0.9765
		3.578	22.00	0.016	0.352	0.9862
0.30	0.03	85.707	12.00	0.383	4.602	1.0000
		60.991	14.00	0.273	3.820	1.0000
		39.428	16.00	0.176	2.823	1.0000
		22.173	18.00	0.099	1.786	1.0000
		10.686	20.00	0.048	0.956	1.0000
		3.628	22.00	0.016	0.357	1.0000
0.14	-.13	84.150	12.00	0.377	4.518	0.9818
0.42	0.15	81.861	12.00	0.366	4.395	0.9551
		56.325	14.00	0.252	3.528	0.9235
		35.765	16.00	0.160	2.560	0.9071
		19.807	18.00	0.089	1.595	0.8933
		8.360	20.00	0.037	0.748	0.7823
		2.605	22.00	0.012	0.256	0.7179
0.21	-.06	86.830	12.00	0.389	4.662	1.0131
0.58	0.31	68.364	12.00	0.306	3.671	0.7977

Table 4 cont'd

E (%)	Eo (%)	Ic (Amperes)	Field (Tesla)	Jc (GA/m^2)	JcB (GN/m^3)	Ic/Icm
0.58	0.31	43.135	14.00	0.193	2.702	0.7072
		25.307	16.00	0.113	1.812	0.6419
		11.253	18.00	0.050	0.906	0.5075
		3.882	20.00	0.017	0.347	0.3633
		0.821	22.00	0.004	0.081	0.2264
0.30	0.03	86.684	12.00	0.388	4.654	1.0114
0.72	0.45	54.983	12.00	0.246	2.952	0.6415
		32.503	14.00	0.145	2.036	0.5329
		15.588	16.00	0.070	1.116	0.3954
		5.680	18.00	0.025	0.457	0.2562
		1.214	20.00	0.005	0.109	0.1136
		0.153	22.00	0.001	0.015	0.0422
0.41	0.14	85.143	12.00	0.381	4.571	0.9934
0.82	0.55	48.772	12.00	0.218	2.619	0.5691
		25.524	14.00	0.114	1.599	0.4185
		9.981	16.00	0.045	0.715	0.2532
		2.889	18.00	0.013	0.233	0.1303
		0.395	20.00	0.002	0.035	0.0369
0.50	0.23	80.263	12.00	0.359	4.309	0.9365
0.96	0.69	37.542	12.00	0.168	2.016	0.4380
0.59	0.32	70.639	12.00	0.316	3.793	0.8242
1.03	0.76	25.740	12.00	0.115	1.382	0.3003
0.60	0.33	52.654	12.00	0.236	2.827	0.6144
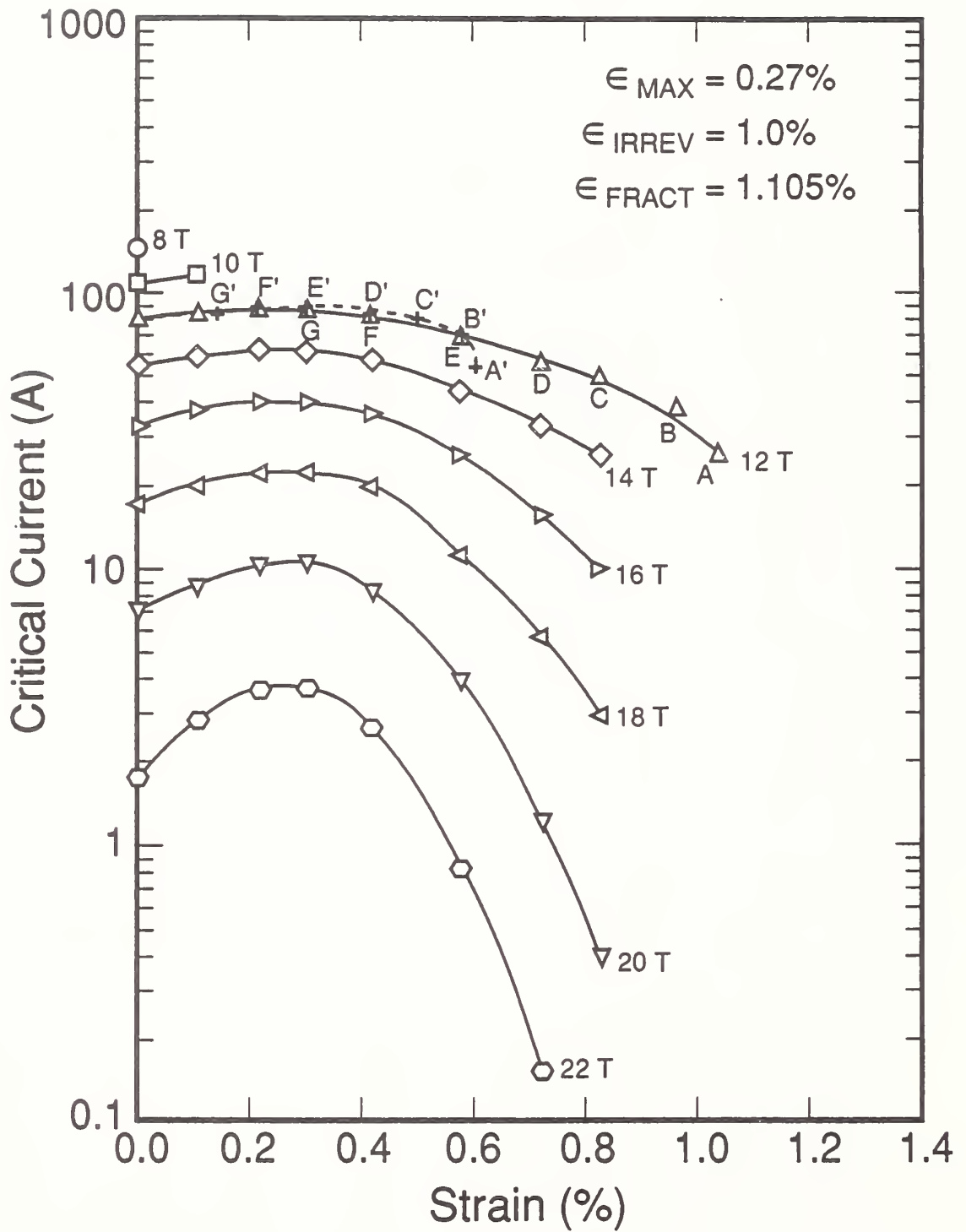
Figure 5. Effect of axial tensile strain on the critical current of LLNL Nb₃Sn cable test strand at 4 K and several magnetic fields.

Figure 6. Effect of magnetic field on the critical current density of LLNL Nb_3Sn cable test strand at 4 K.

Figure 7. Effect of magnetic field on the nth power of LLNL Nb_3Sn cable test strand at 4 K.

Nb$_3$Sn ITER Candidate Conductor

An internal-tin-process Nb$_3$Sn conductor, which is a prototype for the International Thermonuclear Experimental Reactor (ITER), was tested. The axial strain measurements were made over a range of magnetic fields from 15 to 25 T. The conductor specifications are given in Table 5, and the measured data are presented in Table 6 and Figs. 8 through 10. The I_c and J_c values are based on an electric field criterion (E_c) of 2 μV/cm. The results show a zero-strain 15 T value of J_c (referred to the noncopper area) which was 0.50 GA/m^2 and a peak (strain-free) J_c value of 0.55 GA/m^2. The irreversible strain limit was reasonably high, 0.92%, and the compressive prestrain was 0.28%. The sample did not fracture until 1.09% strain.

Table 5. ITER conductor specifications.

Wire Diameter	0.817 mm
Copper Stabilizer	46.5%
Nb Diffusion Barrier	
(of Non-Cu Area)	8.5%
Noncopper	53.5%
Filament No.	4902
Filament Dia.	3.5 μm
Subelement No.	19
Ti Addition	1.2%

Table 6. High-field critical current of Nb$_3$Sn ITER candidate conductor as a function of axial tensile strain applied at 4 K.

SP	E (%)	E0 (%)	FIELD (T)	Ic (A)	Jc (MA/m^2)	Ic/Icmax	N
0	0.048	-0.232	15	139.99	499.24	0.91	20.95
			16	109.56	390.73	0.90	17.73
			18	62.83	224.09	0.85	13.40
			20	27.43	97.82	0.74	8.33
			22	7.71	27.51	0.57	4.65
			24	0.47	1.68	0.23	1.78
			25				1.26
1	0.12	-0.16	15	149.89	534.55	0.97	18.47
			16	122.29	436.13	1.00	19.53
			18	72.23	257.60	0.97	15.16
			20	35.98	128.31	0.97	11.10
			22	11.86	42.31	0.88	6.02
			24	1.30	4.65	0.65	2.30
			25	0.11	0.41	0.50	1.48
2	0.232	-0.048	15	153.94	548.99	1.00	19.35
			16	117.86	420.34	0.96	13.27
			18	74.34	265.12	1.00	13.83
			20	37.00	131.94	1.00	9.19
			22	13.51	48.18	1.00	5.80
			24	2.01	7.17	1.00	2.59
			25	0.23	0.82	1.00	1.55
3	0.321	0.041	15	133.33	475.49	0.87	11.17
			16	118.64	423.11	0.97	17.35
			18	68.70	245.02	0.92	11.67
			20	34.23	122.06	0.93	8.53
			22	11.31	40.35	0.84	4.91
			24	1.75	6.24	0.87	2.50
			25	0.21	0.73	0.90	1.55
4	0.439	0.159	15	122.38	436.44	0.79	11.44
			16	97.63	348.18	0.80	11.35
			18	55.95	199.52	0.75	9.19
			20	25.39	90.55	0.69	6.53
			22	7.26	25.90	0.54	3.90
			24	0.71	2.52	0.35	1.92
			25	0.04	0.14	0.18	1.41
4U	0.221	-0.059	15	152.11	542.48	0.99	18.17
5	0.546	0.266	15	107.88	384.73	0.70	12.30

Table 6 cont'd

SP	E (%)	E0 (%)	FIELD (T)	Ic (A)	Jc (MA/m^2)	Ic/Icmax	N
			16	82.70	294.92	0.68	10.89
			18	41.28	147.22	0.56	7.35
			20	14.49	51.69	0.39	4.55
			22	3.23	11.51	0.24	2.83
			24	0.08	0.27	0.04	1.39
			25				1.15
5U	0.286	0.006	15	149.34	532.60	0.97	16.09
6	0.648	0.368	15	86.54	308.63	0.56	9.76
			16	64.56	230.24	0.53	9.20
			18	28.96	103.29	0.39	6.39
			20	8.13	28.98	0.22	3.67
			22	0.92	3.28	0.07	1.89
			24				1.19
6U	0.348	0.068	15	143.07	510.24	0.93	13.45
7	0.745	0.465	15	69.06	246.29	0.45	8.45
			16	50.40	179.73	0.41	8.09
			18	17.86	63.69	0.24	4.96
			20	3.37	12.01	0.09	2.64
			22	0.31	1.12	0.02	1.63
			24				1.07
7U	0.403	0.123	15	149.43	532.90	0.97	20.93
8	0.844	0.564	15	48.58	173.26	0.32	6.73
8U	0.464	0.184	15	116.39	415.08	0.76	9.17
9	0.919	0.639	15	34.64	123.54	0.23	5.40
9U	0.503	0.223	15	109.07	388.96	0.71	9.84
10	0.999	0.719	15	22.79	81.28	0.15	4.62
10U	0.55	0.27	15	74.68	266.35	0.49	6.05
11	1.088	0.808	15	13.20	47.09	0.09	3.52
11U	0.619	0.339	15	32.03	114.23	0.21	3.00
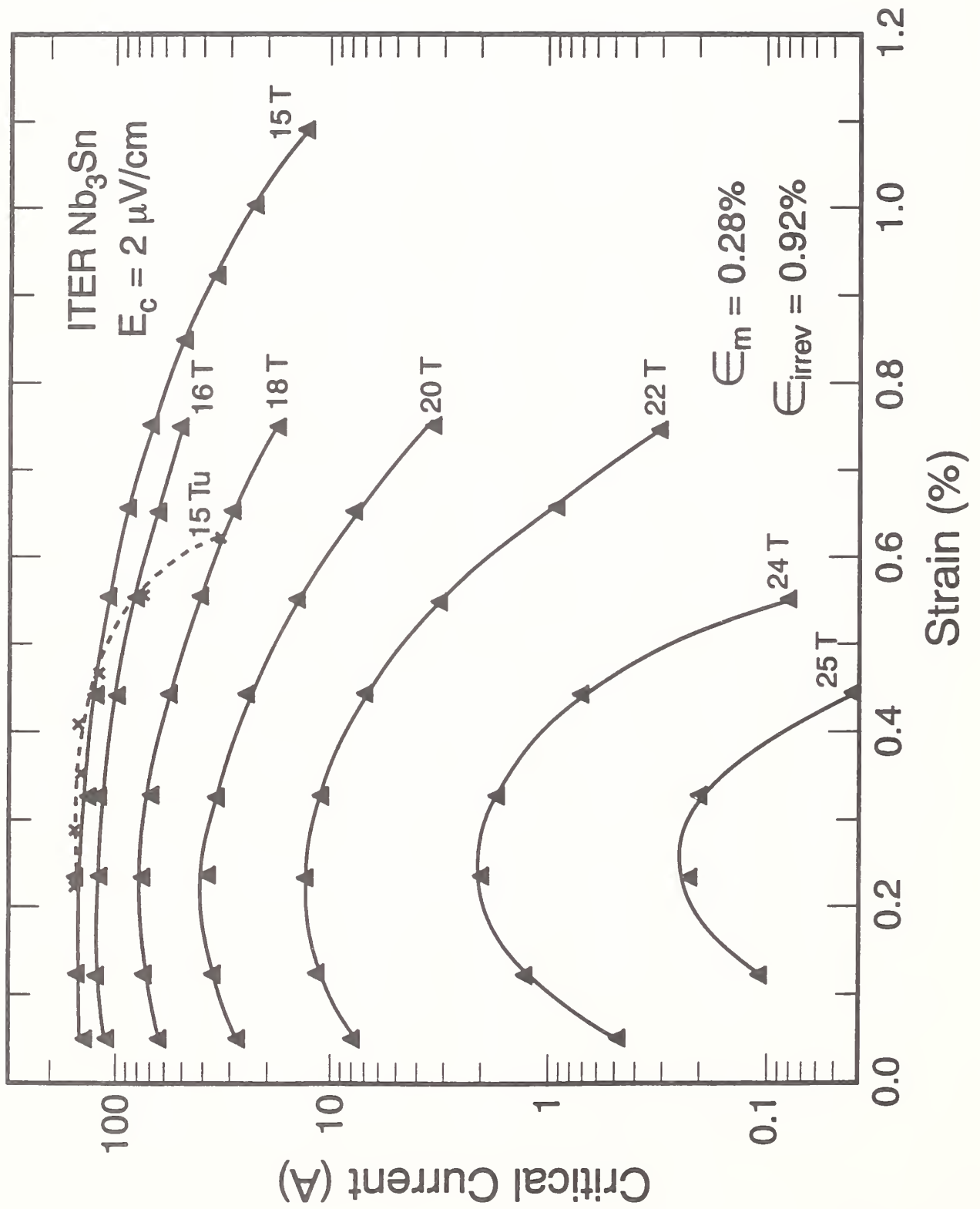
Figure 8. Effect of axial tensile strain on the critical current of the ITER Nb_3Sn candidate conductor at 4 K and several magnetic fields.
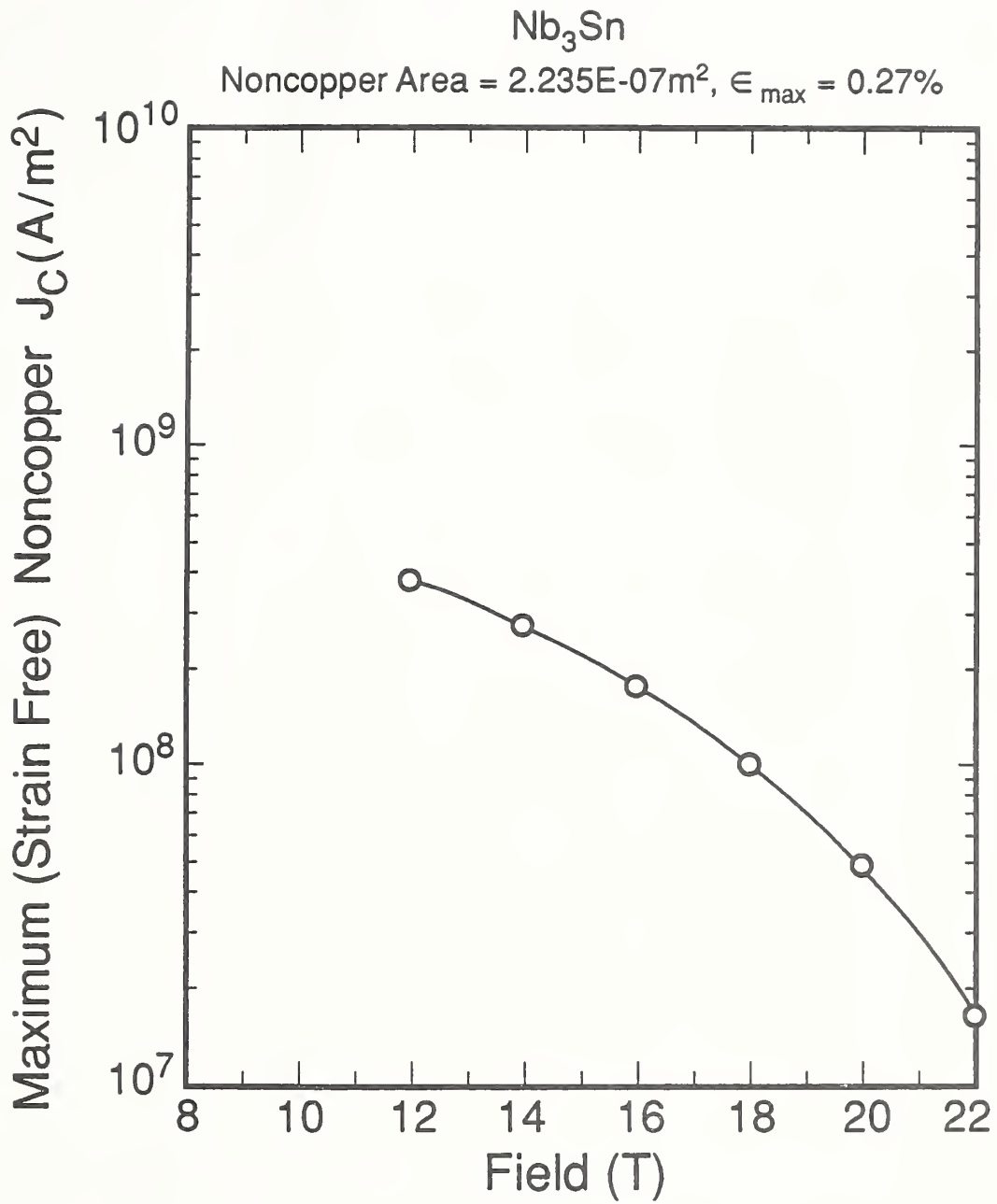
Figure 9. Effect of magnetic field on the critical current density of the ITER candidate conductor at 4 K.

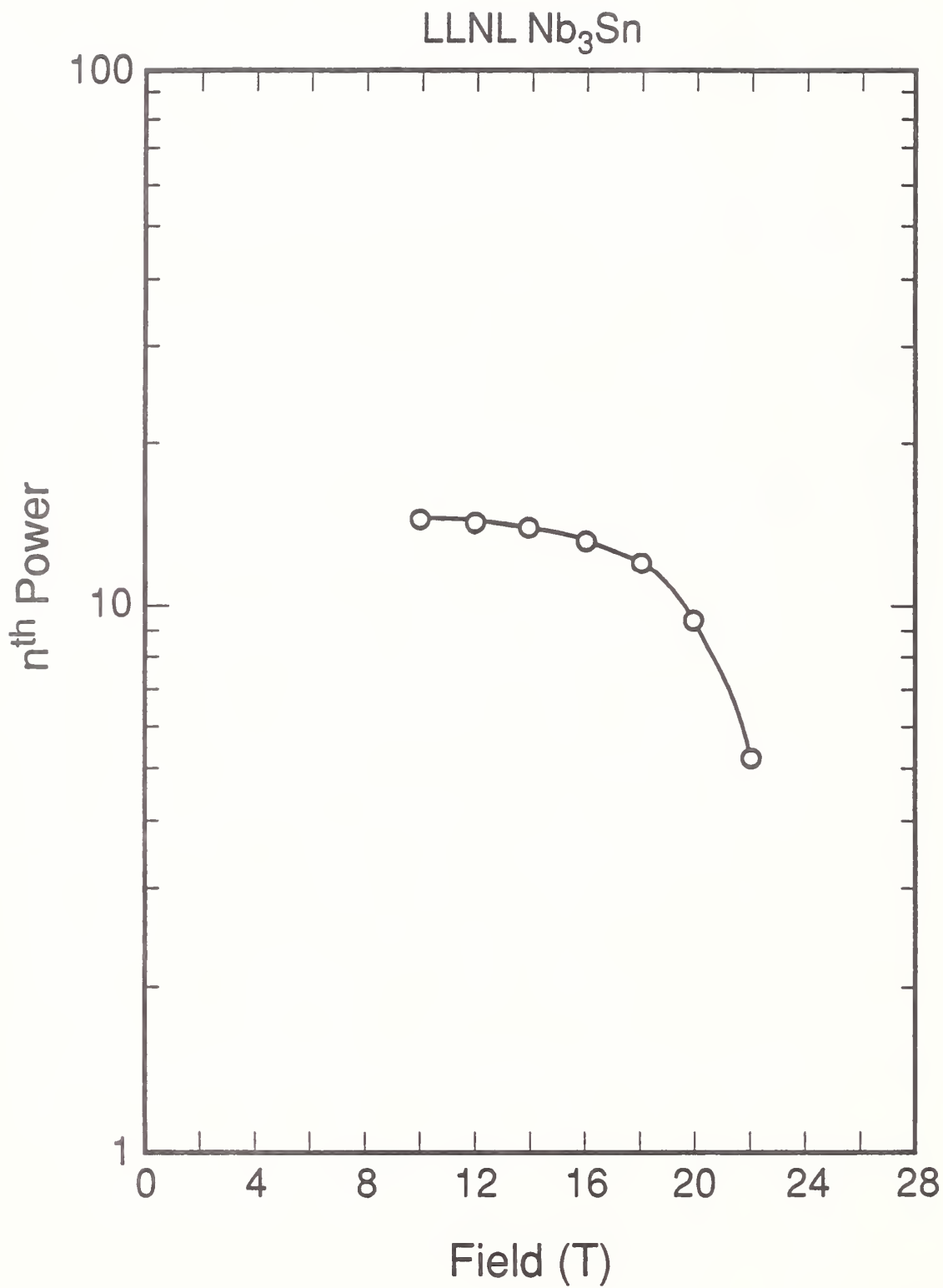Figure 10. Effect of magnetic field on the nth power of the ITER candidate conductor at 4 K.

Nb₃Sn Conductors Reinforced with Dispersion-Hardened Copper (DHC) Alloy

Nb$_3$Sn Conductors Reinforced with Dispersion-Hardened Copper (DHC) Alloy

The axial strain characteristics of a group of three similar experimental Nb$_3$Sn superconductors were measured over a broad range of magnetic fields. All three conductors were manufactured using the internal-tin process, and a dispersion-hardened-copper (DHC) reinforcement was used in each conductor for increased tensile strength. The first conductor has two concentric rings of stabilizing copper surrounding the noncopper core, which contains the internal tin. The inner ring is pure copper and the outer ring is DHC. The copper stabilizer makes up 72% of the conductor's total volume. Both of the other conductors have an internal-tin ring surrounding their cores and 56% external copper stabilizer. One of the conductors uses pure copper for the stabilizer and DHC for the core's matrix; the other conductor has the opposite configuration, a pure-copper matrix and DHC stabilizer. All three conductors have tantalum diffusion barriers between core and stabilizer. The conductor specifications are given in Tables 7 through 9. The I$_c$ and J$_c$ values are based on an electric field criterion (E$_c$) of 2 μV/cm.

The measured data for the tin-core conductor are presented in Table 10 and in Figs. 11 through 13. The large prestrain (ε_m=0.55%) for this conductor is caused by the high copper fraction, 72%. The I$_c$ doubles at 12 T between ε=0 and ε=ε_m because of the large value of ε_m. The noncopper peak J$_c$ (ε=ε_m) at 12 T is 850 A/mm^2.

The measured data for the tin-ring conductors are presented in Tables 11 and 12 and in Figs. 14 through 19. The lower copper-stabilizer fraction (56%) results in a smaller prestrain for both conductors (ε_m=0.3%). The noncopper peak J$_c$ (ε=ε_m) at 12 T is 1120 A/mm^2 for the pure-copper stabilized conductor and 1030 A/mm^2 for the DHC stabilized conductor. The low-field n-value for the pure-copper stabilized wire is ~30 and ~20 for the other wire. This difference is probably associated with the smaller filament diameter for the DHC stabilized conductor (1.7 μm compared to 3 μm).

Table 7. DHC reinforced tin-core Nb$_3$Sn conductor specifications.

Wire Diameter	0.389 mm
DHC (outside)	33%
Copper Stabilizer	39%
Noncopper Core	28%
Nb in Core	~31%
Ta Barrier	3.8%
Filament No.	37 x 894 = 33078
Filament Dia.	0.6 μm @ 0.389 mm dia.
Local Cu:Nb Ratio	0.8:1

Table 8. Conductor specifications for DHC reinforced tin-ring Nb$_3$Sn wire with pure-copper stabilizer.

Wire Diameter	0.267 mm
Noncopper Core	44%
DHC Core	
Pure Copper Stabilizer	56%
Ta Barrier	8%
Nb-1.3 wt.% Ti	~8%
Filament No.	624
Filament Dia.	~3 µm
Local Cu:Nb Ratio	1:1

Table 9. Conductor specifications for DHC reinforced tin-ring Nb$_3$Sn with DHC stabilizer.

Wire Diameter	0.267 mm
Local Cu:Nb Ratio	0.8:1
Noncopper Core	44%
DHC Stabilizer (outside)	56%
Ta Barrier	8%
Nb-1.3 wt.% Ti	13.5%
Filament No.	2796
Filament Dia.	~1.7 µm

Table 10. High-field critical current of copper-alloy reinforced tin-core Nb_3Sn as a function of axial tensile strain applied at 4 K.

| E (%)	Eo (%)	Ic (Amperes)	Field (Tesla)	Jc (GA/m^2)	JcB (GN/m^3)	Ic/Icm
0.00	-.55	74.630	8.00	2.241	17.929	0.7957
		36.650	10.00	1.101	11.006	
		14.918	12.00	0.448	5.376	
		4.284	14.00	0.129	1.801	
		0.747	16.00	0.022	0.359	
0.08	-.47	78.200	8.00	2.348	18.786	0.8338
0.23	-.32	87.400	8.00	2.625	20.997	0.9319
0.35	-.20	93.790	8.00	2.817	22.532	1.0000
0.51	-.04	54.605	10.00	1.640	16.398	
		28.265	12.00	0.849	10.186	
		12.293	14.00	0.369	5.168	
		3.971	16.00	0.119	1.908	
		0.765	18.00	0.023	0.414	
0.59	0.04	54.270	10.00	1.630	16.297	
0.71	0.16	43.855	10.00	1.317	13.170	
0.80	0.25	29.455	10.00	0.885	8.845	
0.41	-.14	31.195	10.00	0.937	9.368	
0.88	0.33	15.580	10.00	0.468	4.679	
0.47	-.08	18.260	10.00	0.548	5.484	
0.97	0.42	5.410	10.00	0.162	1.625	
0.53	-.02	3.450	10.00	0.104	1.036	
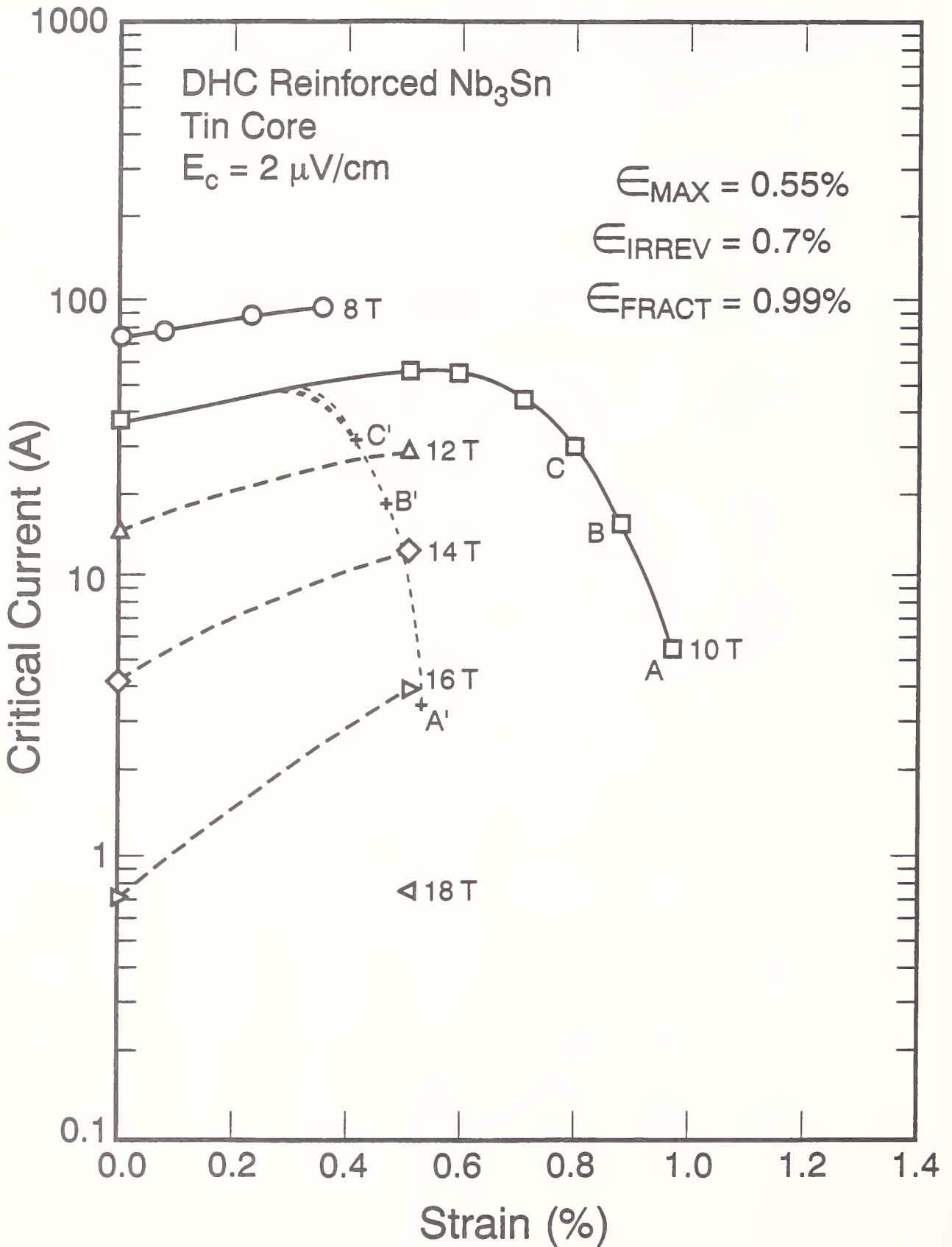
Figure 11. Effect of axial tensile strain on the critical current of DHC reinforced Nb_3Sn conductor at 4 K and several magnetic fields.
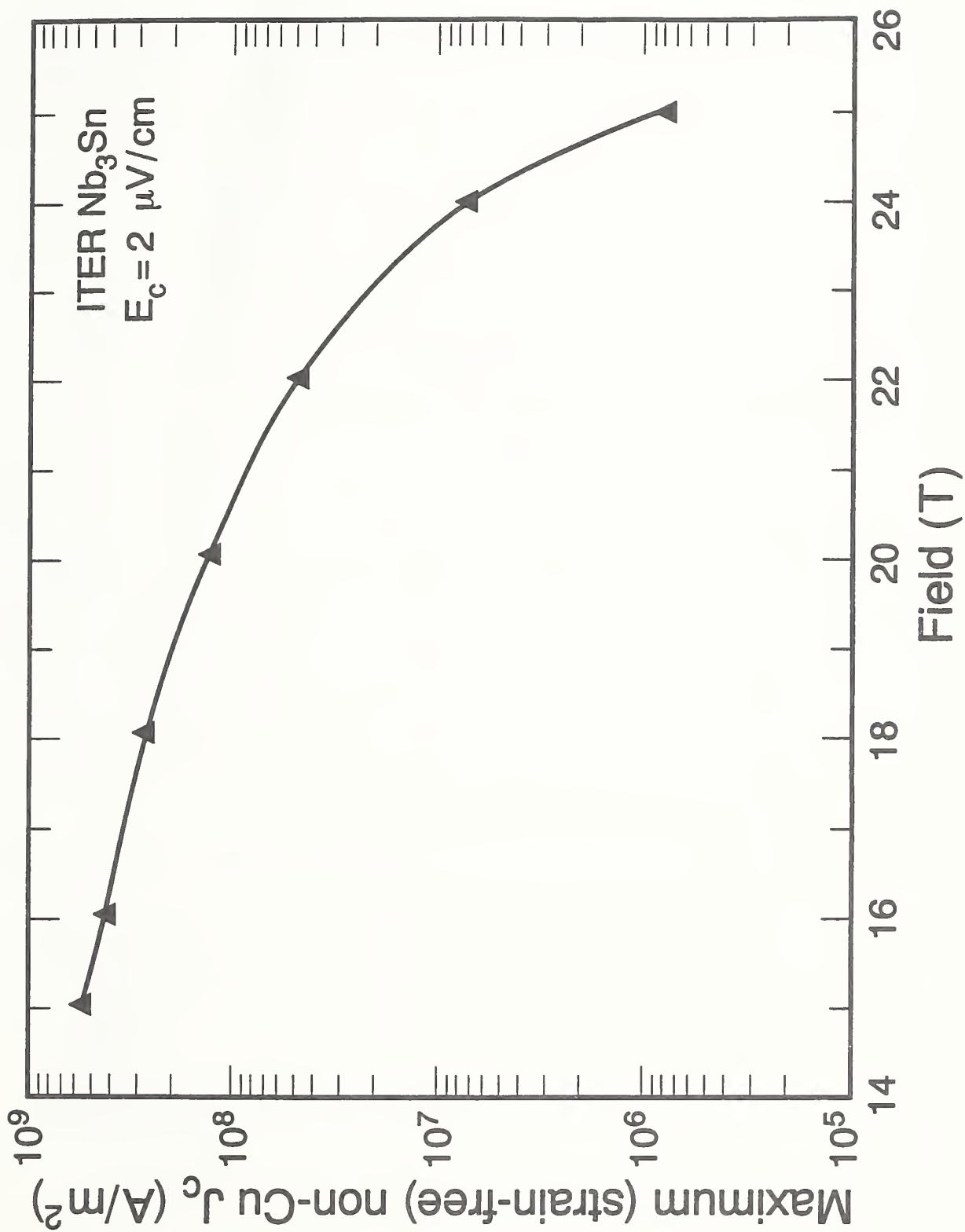
Figure 12. Effect of magnetic field on the critical current density of DHC reinforced
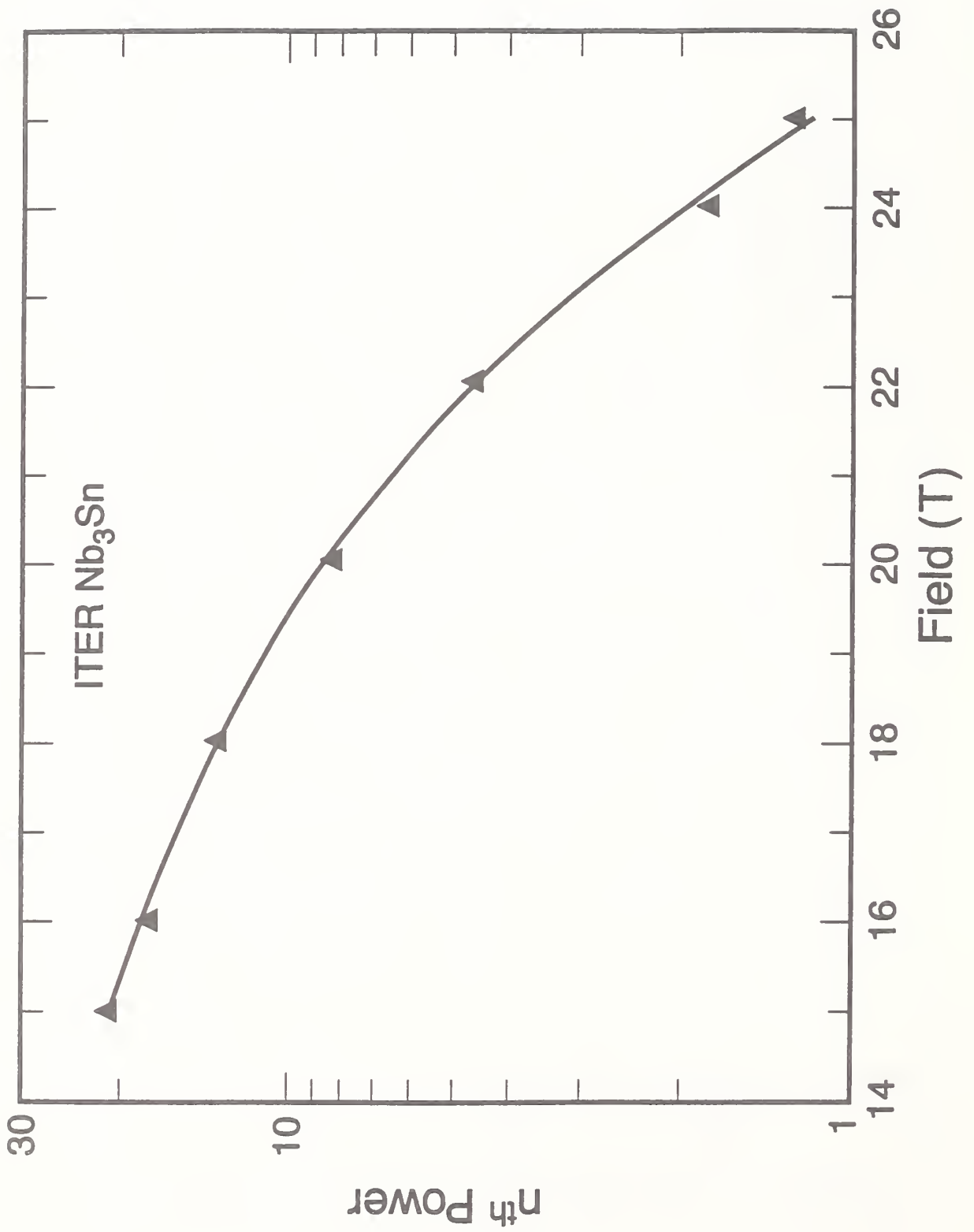Nb$_3$Sn conductor at 4 K.

Figure 13. Effect of magnetic field on the nth power of DHC reinforced Nb_3Sn conductor at 4 K.

Table 11. High-field critical current of DHC reinforced tin-ring Nb_3Sn with pure copper
stabilizer as a function of axial tensile strain applied at 4 K.

E (%)	Eo (%)	Field (T)	Ic (A)	Jc (MA/m^2)	Ic/Icm	n value
0.00	-.30	10.00	36.49	1484.72	0.958	30.0
		12.00	26.30	1070.00	0.957	30.3
		14.00	18.49	752.13	0.945	29.8
		16.00	12.28	499.54	0.926	28.5
		18.00	7.63	310.58	0.907	23.7
		20.00	4.08	165.99	0.866	17.8
		22.00	1.66	67.45	0.777	11.7
		.24.00	0.37	15.09	0.640	6.3
		25.00	0.10	4.27	0.529	3.6
0.09	-.21	10.00	36.68	1492.41	0.962	32.4
		12.00	26.30	1070.08	0.957	31.8
		14.00	18.45	750.44	0.943	30.7
		16.00	12.28	499.66	0.926	28.8
		18.00	7.52	305.80	0.893	23.1
		20.00	3.96	161.18	0.841	17.5
		22.00	1.58	64.10	0.738	11.1
		24.00	0.36	14.57	0.618	7.3
0.16	-.14	10.00	37.48	1524.77	0.983	32.1
		12.00	27.12	1103.40	0.987	34.6
		14.00	19.24	782.63	0.983	34.0
		16.00	13.06	531.45	0.985	33.3
		18.00	8.19	333.19	0.973	28.8
		20.00	4.45	180.85	0.943	19.8
		22.00	1.92	78.06	0.899	13.3
		24.00	0.46	18.89	0.801	6.5
		25.00	0.15	6.25	0.774	4.4
0.33	0.03	10.00	38.11	1550.59	1.000	35.8
		12.00	27.48	1117.80	1.000	33.3
		14.00	19.56	795.77	1.000	31.2
		16.00	13.26	539.65	1.000	29.5
		18.00	8.42	342.39	1.000	23.7
		20.00	4.71	191.69	1.000	18.1
		22.00	2.13	86.80	1.000	13.8
		24.00	0.58	23.58	1.000	7.4
		25.00	0.20	8.07	1.000	4.8
0.48	0.18	10.00	34.19	1391.03	0.897	27.4
		12.00	24.28	987.95	0.884	25.8
		14.00	16.68	678.64	0.853	25.1
		16.00	10.83	440.43	0.816	21.9
		18.00	6.26	254.68	0.744	14.5
		20.00	2.98	121.16	0.632	10.1

Table 11 cont'd

| E (%)	Eo (%)	Field (T)	Ic (A)	Jc (MA/m^2)	Ic/Icm	n value
		22.00	0.94	38.27	0.441	5.1
		24.00	0.15	5.91	0.251	3.2
		25.00	0.03	1.31	0.162	2.0
0.64	0.34	10.00	29.33	1193.16	0.769	24.7
		12.00	19.91	810.06	0.725	24.2
		14.00	12.74	518.15	0.651	21.1
		16.00	7.30	296.80	0.550	14.1
		18.00	3.40	138.16	0.404	10.4
		20.00	1.08	43.77	0.228	6.0
		22.00	0.18	7.30	0.084	3.9
0.33	0.03	10.00	36.53	1486.03	1.000	28.8
0.77	0.47	10.00	23.21	944.15	0.609	20.0
0.39	0.09	10.00	33.67	1369.79	0.922	23.4
0.87	0.57	10.00	18.68	760.07	0.490	21.5
0.44	0.14	10.00	28.84	1173.51	0.790	15.6
0.97	0.67	10.00	12.38	503.63	0.325	10.8
0.49	0.19	10.00	22.79	927.05	0.624	12.3
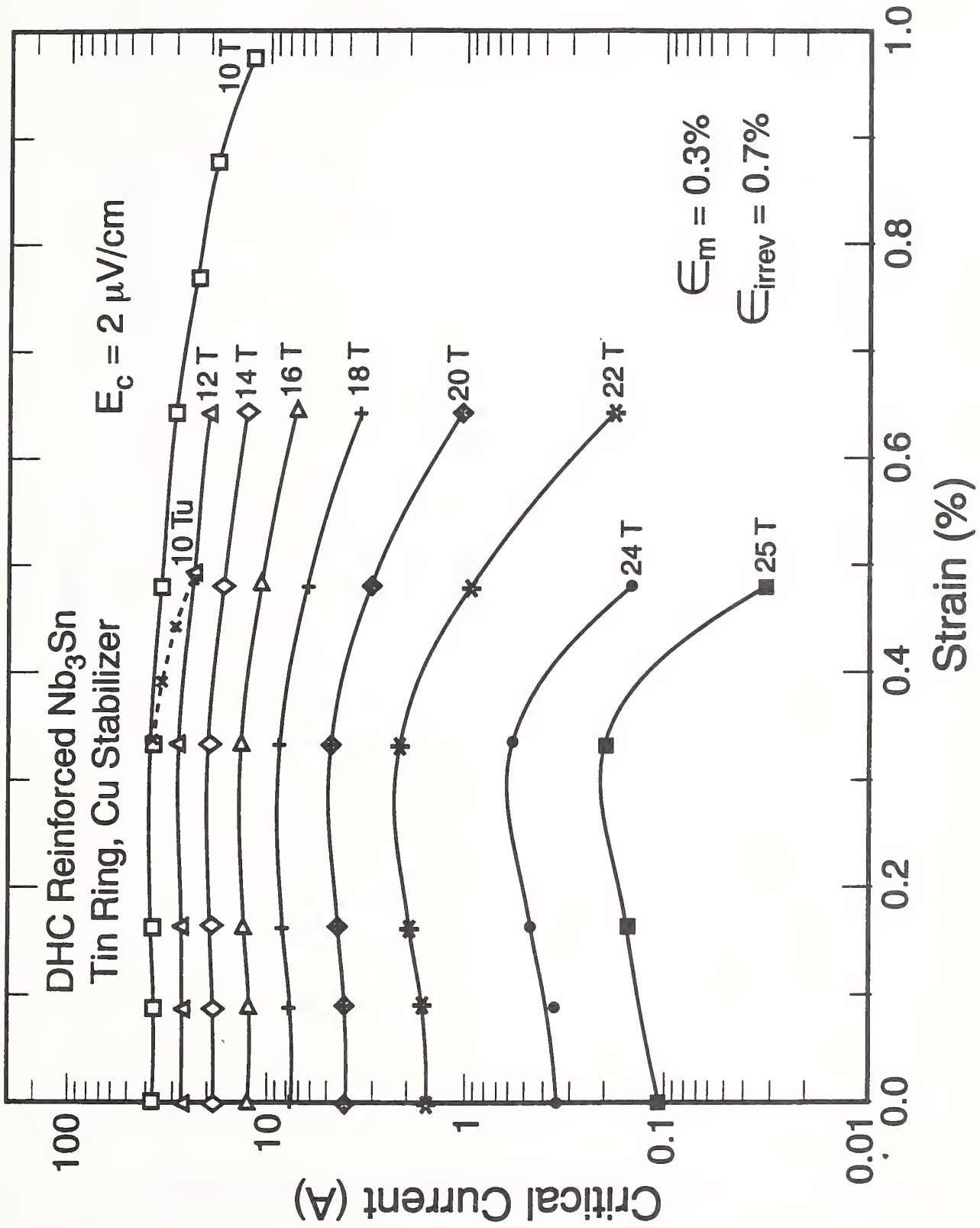
Figure 14. Effect of axial tensile strain on the critical current of DHC reinforced Nb$_3$Sn conductor at 4 K and several magnetic fields.
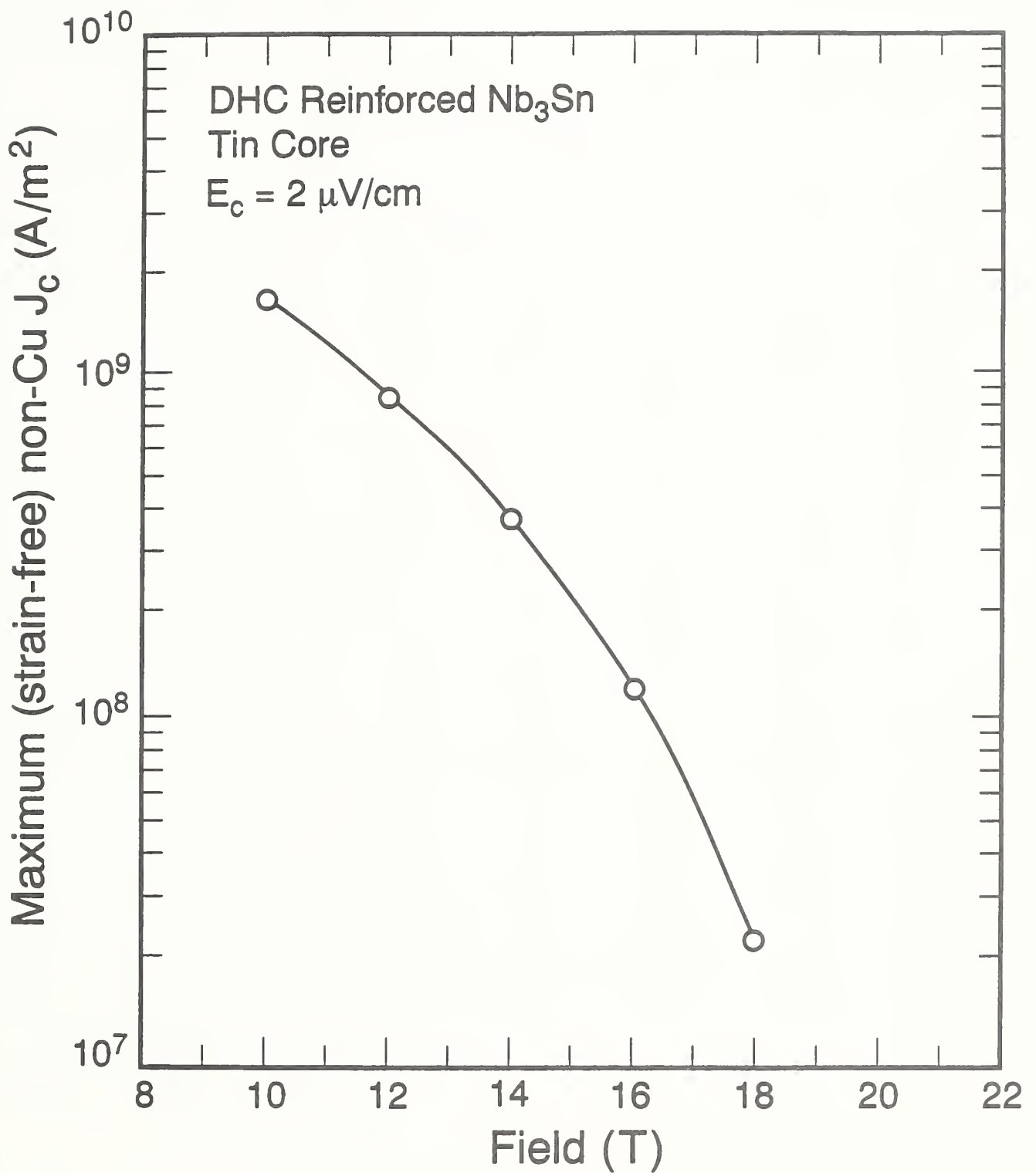
59

Figure 15. Effect of magnetic field on the critical current density of DHC reinforced Nb$_3$Sn conductor at 4 K.
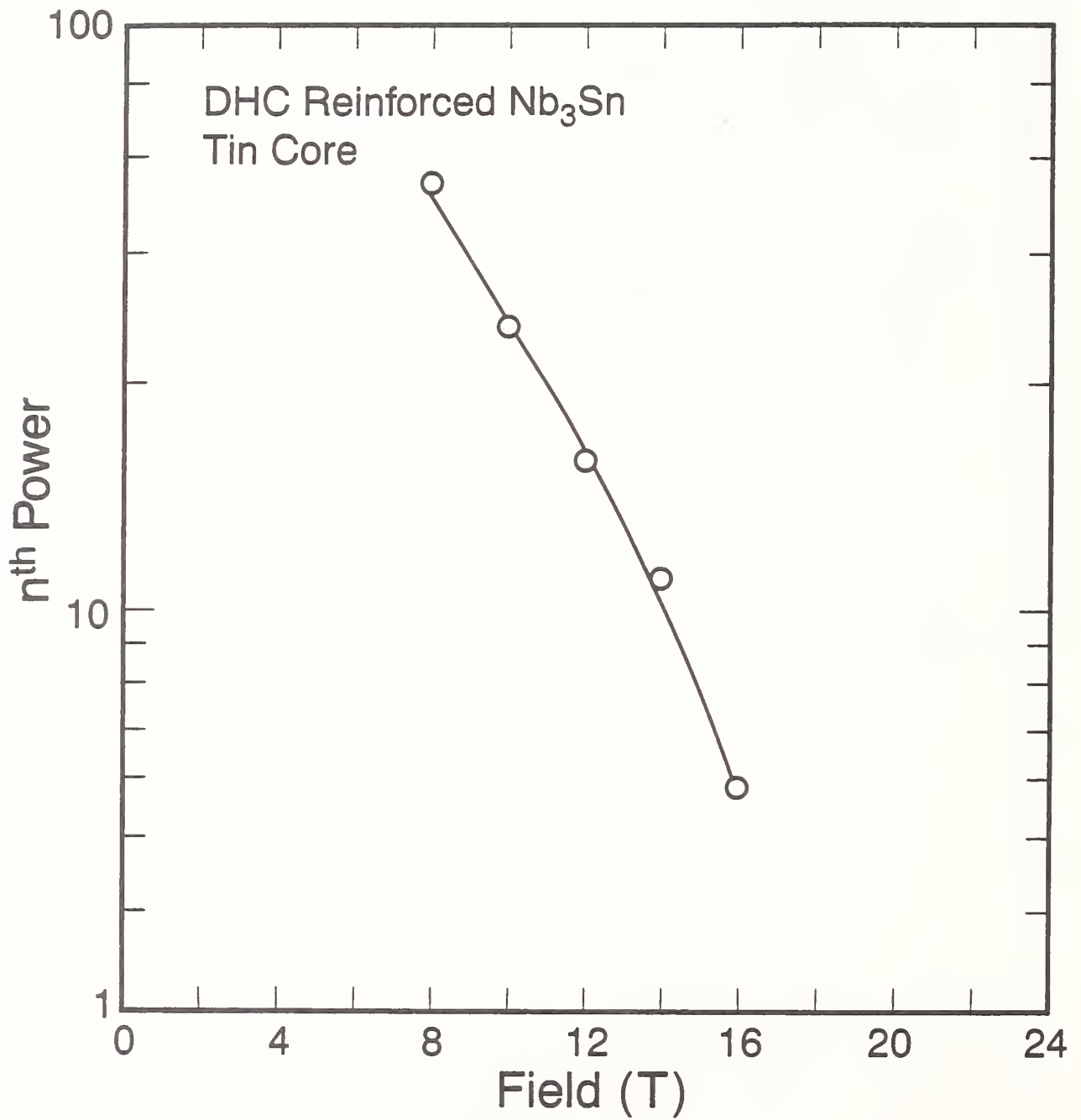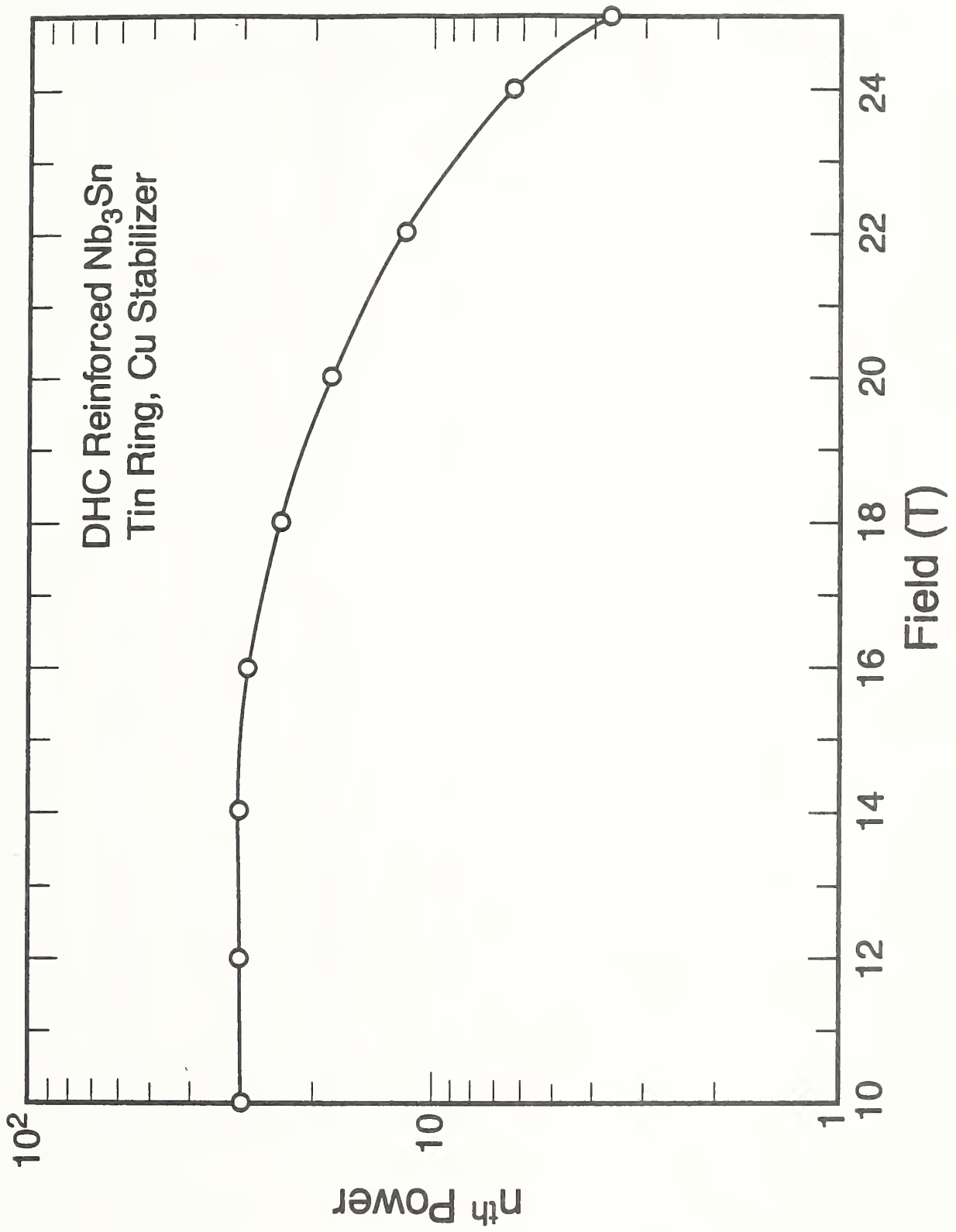
Figure 16. Effect of magnetic field on the nth power of DHC reinforced Nb_3Sn conductor at 4 K.

Table 12. High-field critical current of DHC reinforced tin-ring Nb$_3$Sn with DHC stabilizer as a function of axial tensile strain applied at 4 K.

SP	E (%)	E0 (%)	FIELD (T)	Ic (A)	Jc (MA/m^2)	Ic/Icmax	N
0	0.205	-0.095	10	33.85	1376.20	1.00	19.14
			12	24.62	1000.80	0.97	20.80
			14	17.09	694.69	0.96	19.93
			15	14.03	570.16	0.97	17.81
			16	11.25	457.51	0.97	17.76
			18	6.75	274.49	0.94	16.26
			20	3.39	137.68	0.90	14.26
			22	1.25	50.82	0.86	9.32
			24	0.22	8.94	0.78	4.77
			25	0.05	2.04	0.75	2.64
1	0.286	-0.014	12	25.45	1034.44	1.00	29.26
			14	17.73	720.73	1.00	25.60
			15	14.52	590.43	1.00	22.01
			16	11.65	473.74	1.00	18.06
			18	7.21	293.00	1.00	20.94
			20	3.75	152.55	1.00	15.15
			22	1.45	59.01	1.00	11.66
			24	0.28	11.41	1.00	5.40
			25	0.07	2.71	1.00	3.46
2	0.387	0.087	12	24.14	981.39	0.95	15.33
			14	17.06	693.31	0.96	18.67
			15	14.14	574.85	0.97	21.45
			16	11.34	461.04	0.97	17.70
			18	6.88	279.64	0.95	16.03
			20	3.49	141.97	0.93	14.06
			22	1.28	52.10	0.88	9.86
			24	0.20	8.20	0.72	4.69
			25	0.04	1.60	0.59	2.42
3	0.515	0.215	14	15.45	628.01	0.87	19.06
			15	12.15	493.83	0.84	16.12
			16	9.69	393.80	0.83	17.93
			18	5.40	219.53	0.75	13.89
			20	2.33	94.67	0.62	8.97
			22	0.62	25.09	0.43	5.25
			24	0.06	2.37	0.21	2.38
3U	0.298	-0.002	12	24.80	1008.03	0.97	15.24
4	0.643	0.343	14	12.25	497.83	0.69	16.40
			15	9.47	384.76	0.65	16.37

Table 12 cont'd

| SP	E (%)	E0 (%)	FIELD (T)	Ic (A)	Jc (MA/m^2)	Ic/Icmax	N
			16	6.96	282.84	0.60	12.69
			18	3.30	133.96	0.46	10.44
			20	0.96	39.05	0.26	5.42
			22	0.13	5.11	0.09	2.79
			24	0.01	0.51	0.04	1.38
4U	0.341	0.041	12	24.90	1012.01	0.98	21.63
5	0.755	0.455	12	15.70	638.11	0.62	14.49
5U	0.41	0.11	12	24.01	976.14	0.94	19.69
6	0.863	0.563	12	13.00	528.55	0.51	17.10
6U	0.48	0.18	12	22.83	928.24	0.90	20.82
7	0.972	0.672	12	10.15	412.76	0.40	13.83
7U	0.526	0.226	12	20.55	835.30	0.81	11.90
8	1.08	0.78	12	7.65	310.97	0.30	9.85
8U	0.581	0.281	12	17.88	726.83	0.70	10.38
9	1.188	0.888	12	6.37	259.12	0.28	7.07
9U	0.681	0.381	12	11.00	447.07	0.68	9.02
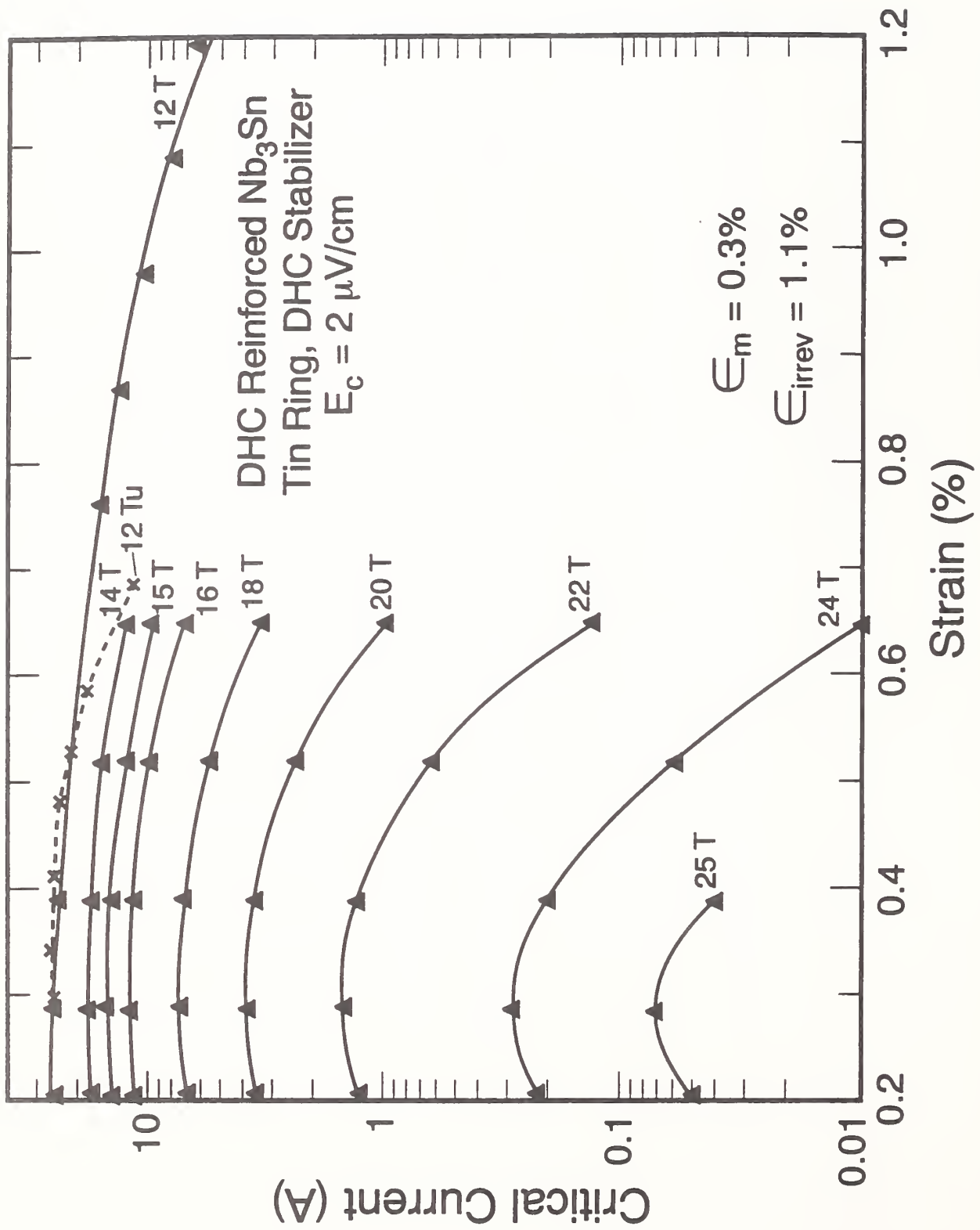
Figure 17. Effect of axial tensile strain on the critical current of DHC reinforced Nb_3Sn conductor at 4 K and several magnetic fields.
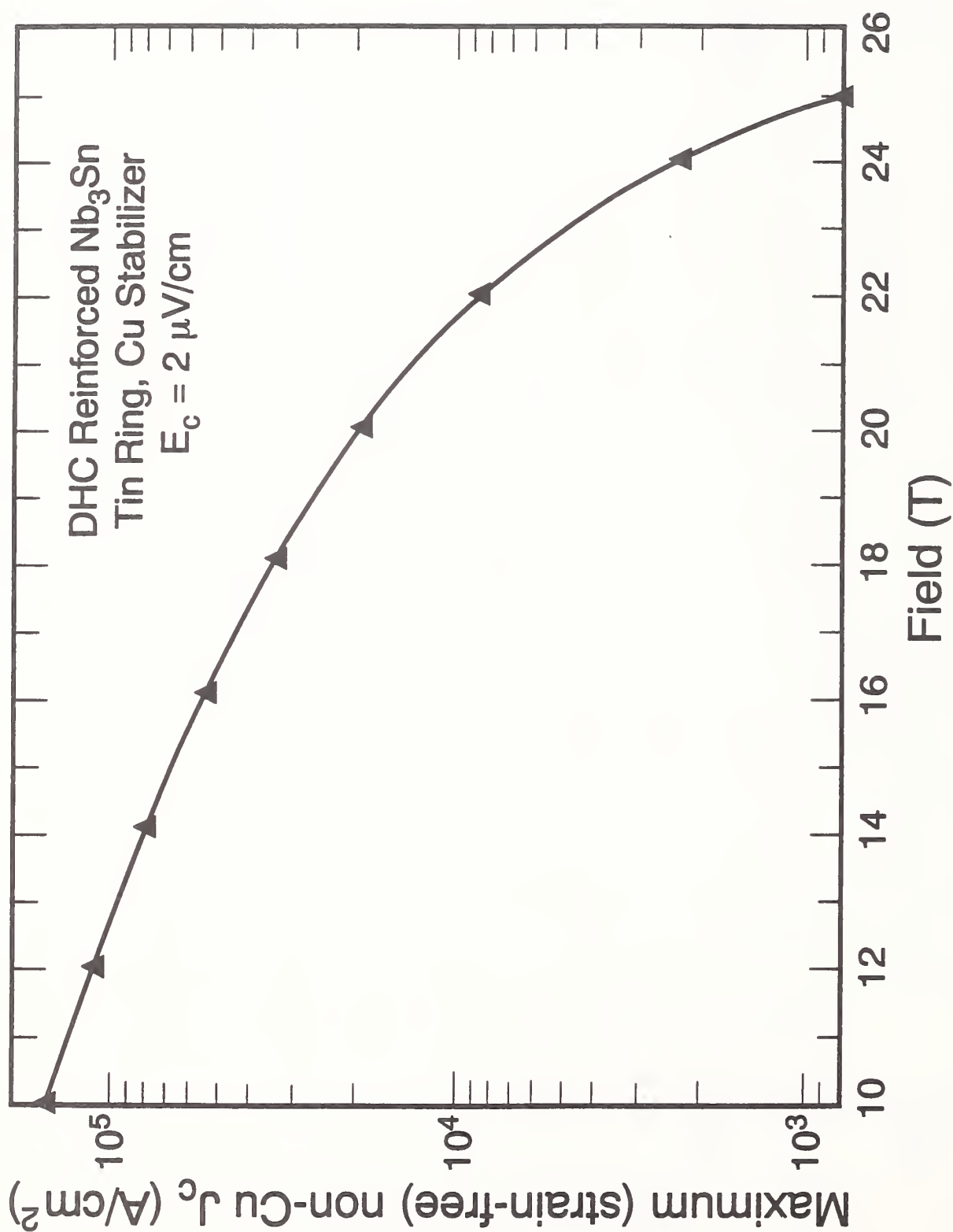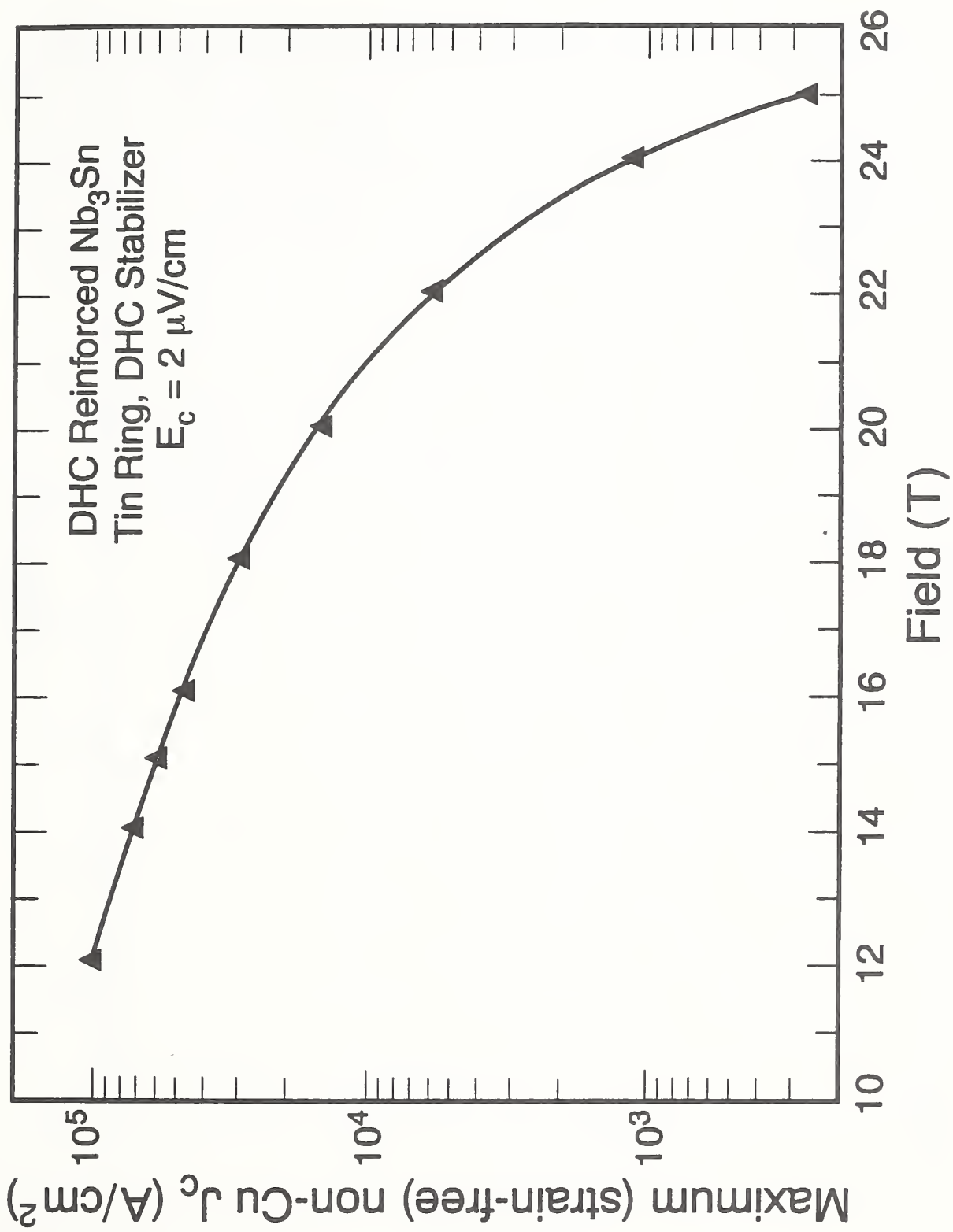
Figure 18. Effect of magnetic field on the critical current density of DHC reinforced Nb$_3$Sn conductor at 4 K.

65
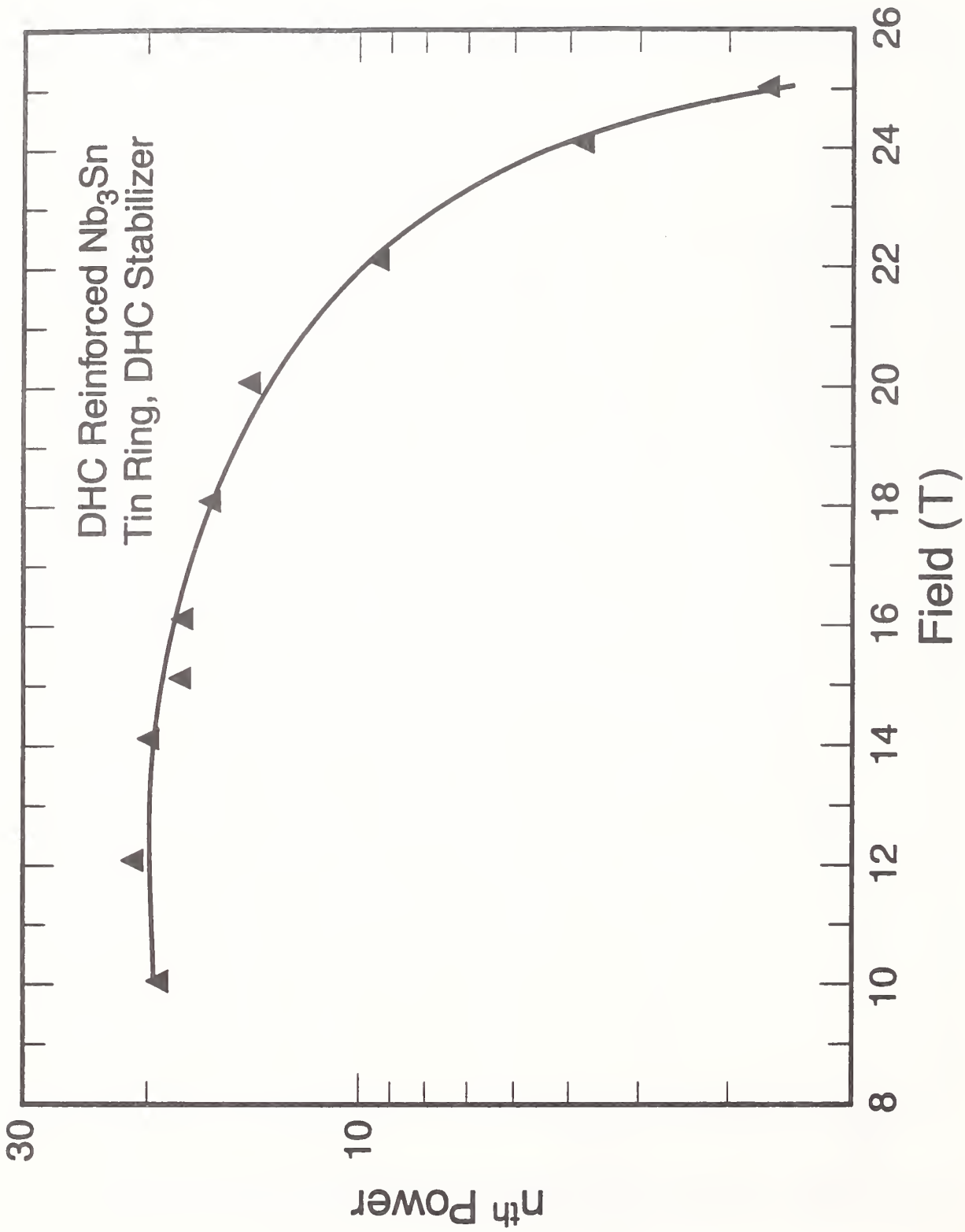
Figure 19. Effect of magnetic field on the nth power of DHC reinforced Nb_3Sn conductor at 4 K.

V$_3$Ga Tape

We also tested an experimental high-field V$_3$Ga tape conductor manufactured in Japan, which is not available from US manufacturers. The conductor specifications are shown in Table 13. The complete set of J$_c$ vs. strain data at magnetic fields from 10 T to 19.65 T is given in Table 14, and the data are presented graphically in Figs. 20 through 22. The I$_c$ and J$_c$ values are based on an electric field criterion (E$_c$) of 2 μV/cm. This material has good J$_c$ properties out to 20 T and is a viable candidate material for extending superconducting magnets to this field range. The results show a peak (strain-free) J$_c$ that is high and nearly constant out to 20 T. The initial prestrain, however, is very low, only about 0.05%, and the irreversible strain limit is only 0.2%.

Table 13. V$_3$Ga tape specifications.

In-Situ Process	
Cross-Sectional Dimensions	4 mm x 150 μm
Noncopper Area	0.440 mm^2
Superconductor Area	0.1016 mm^2
Core Composition	Cu-35at.%V

Table 14. High-field critical current of V_3Ga tape.

E (%)	Eo (%)	Ic (Amperes)	Field (Tesla)	Jc (GA/m^2)	JcB (GN/m^3)	Ic/Icm
0.00	-.05	154.700	10.00	0.103	1.031	0.9937
		143.530	12.00	0.096	1.148	1.0527
		126.130	14.00	0.084	1.177	0.9953
		117.850	16.00	0.079	1.257	0.9940
		103.680	18.00	0.069	1.244	1.0026
		87.320	19.00	0.058	1.106	1.0029
		69.980	19.65	0.047	0.917	0.9779
0.05	0.00	155.680	10.00	0.104	1.038	1.0000
		136.350	12.00	0.091	1.091	1.0000
		126.730	14.00	0.084	1.183	1.0000
		118.560	16.00	0.079	1.265	1.0000
		103.410	18.00	0.069	1.241	1.0000
		87.070	19.00	0.058	1.103	1.0000
		71.560	19.65	0.048	0.937	1.0000
0.16	0.11	152.730	10.00	0.102	1.018	0.9811
		132.000	12.00	0.088	1.056	0.9681
		118.300	14.00	0.079	1.104	0.9335
		102.970	16.00	0.069	1.098	0.8685
		83.980	18.00	0.056	1.008	0.8121
		69.720	19.00	0.046	0.883	0.8007
		58.090	19.65	0.039	0.761	0.8118
0.19	0.14	137.900	10.00	0.092	0.919	0.8859
		118.600	12.00	0.079	0.949	0.8698
		106.980	14.00	0.071	0.998	0.8442
		94.270	16.00	0.063	1.006	0.7951
		75.810	18.00	0.051	0.910	0.7331
		63.610	19.00	0.042	0.806	0.7306
		52.190	19.65	0.035	0.684	0.7293
0.07	0.02	136.500	10.00	0.091	0.910	0.8768
0.26	0.21	125.430	10.00	0.084	0.836	0.8057
		104.400	12.00	0.070	0.835	0.7657
		94.280	14.00	0.063	0.880	0.7439
		81.630	16.00	0.054	0.871	0.6885
		66.490	18.00	0.044	0.798	0.6430
		54.710	19.00	0.036	0.693	0.6284
		44.870	19.65	0.030	0.588	0.6270
0.09	0.04	117.050	10.00	0.078	0.780	0.7519

Table 14 cont'd

| E (%)	Eo (%)	Ic (Amperes)	Field (Tesla)	Jc (GA/m^2)	JcB (GN/m^3)	Ic/Icm
0.33	0.28	61.570	10.00	0.041	0.410	0.3955
		51.000	12.00	0.034	0.408	0.3740
		45.520	14.00	0.030	0.425	0.3592
		37.630	16.00	0.025	0.401	0.3174
		26.880	18.00	0.018	0.323	0.2599
		19.020	19.00	0.013	0.241	0.2184
		14.320	19.65	0.010	0.188	0.2001
0.11	0.06	60.430	10.00	0.040	0.403	0.3882
0.38	0.33	40.050	10.00	0.027	0.267	0.2573
		26.090	12.00	0.017	0.209	0.1914
		20.130	14.00	0.013	0.188	0.1588
		14.565	16.00	0.010	0.155	0.1229
		8.505	18.00	0.006	0.102	0.0822
		5.378	19.00	0.004	0.068	0.0618
		3.460	19.65	0.002	0.045	0.0484
0.13	0.08	47.850	10.00	0.032	0.319	0.3074

69
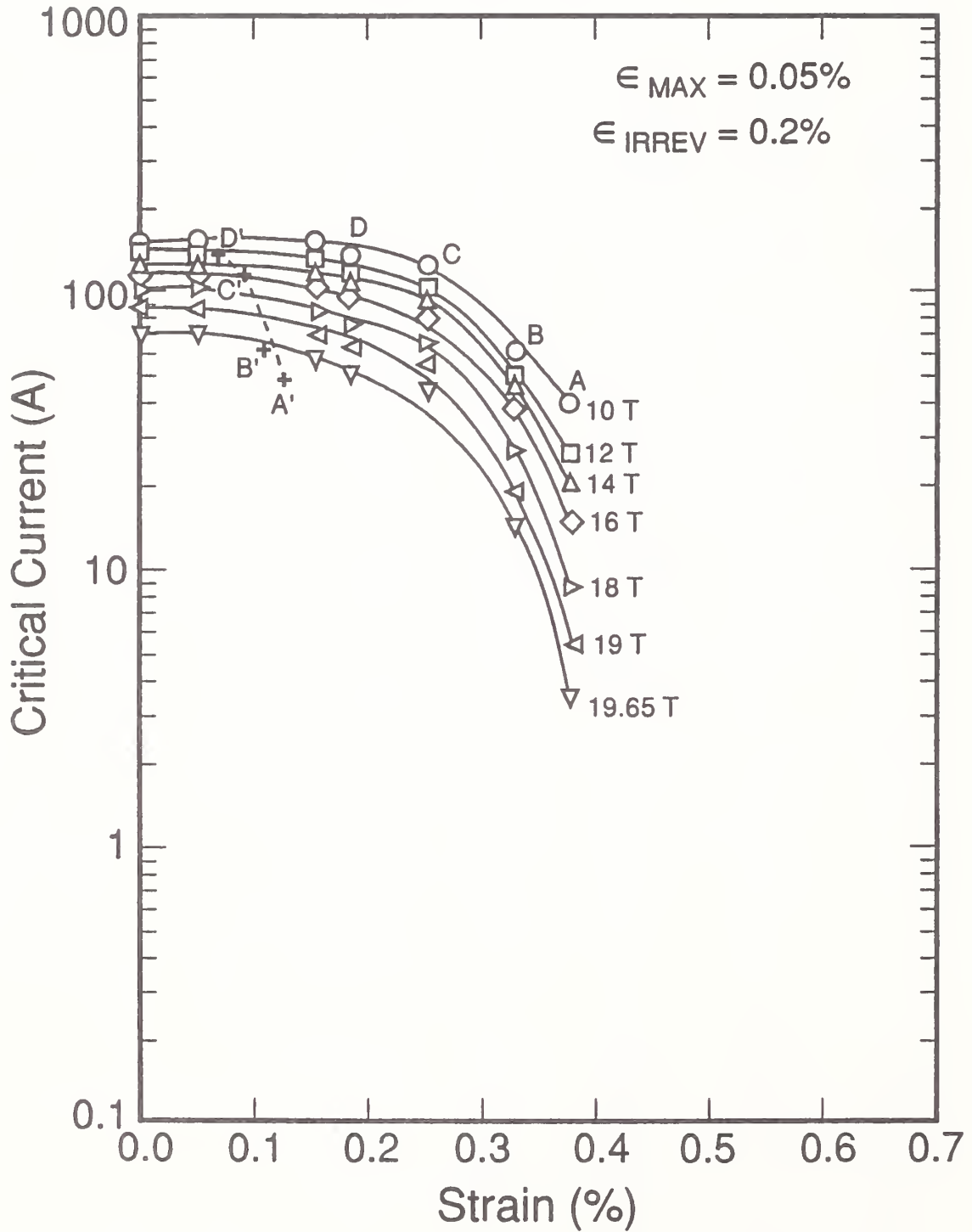
Figure 20. Effect of axial tensile strain on the critical current of V_3Ga tape at 4 K and several magnetic fields.
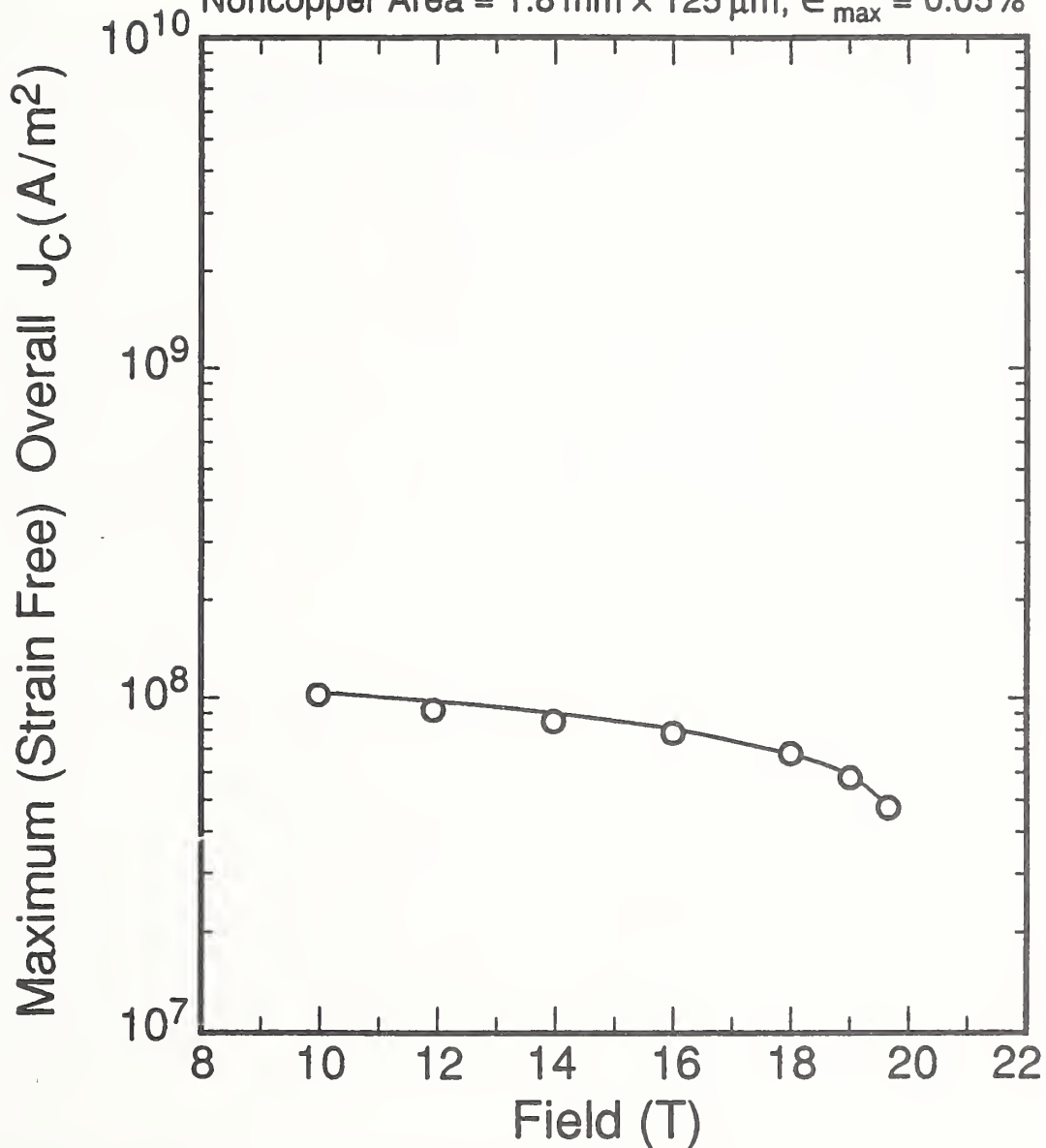
Figure 21. Effect of magnetic field on the critical current density of V_3Ga tape at 4 K.
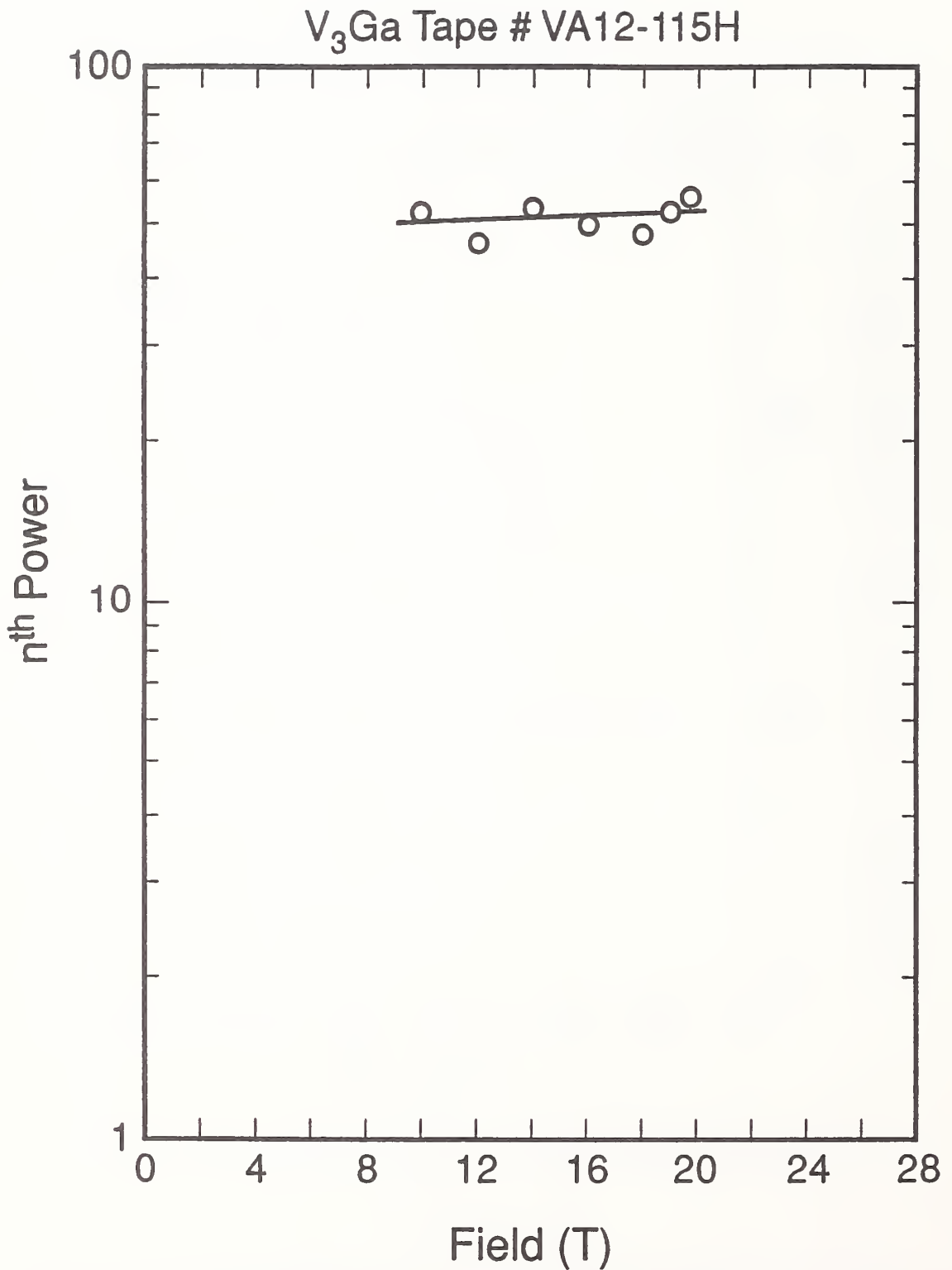
Figure 22. Effect of magnetic field on the nth power of V_3Ga tape at 4 K.

CRITICAL-CURRENT DEGRADATION IN MULTIFILAMENTARY Nb3Al WIRES FROM TRANSVERSE COMPRESSIVE AND AXIAL TENSILE STRESS

S. L. Bray and J. W. Ekin
National Institute of Standards and Technology
325 Broadway
Boulder, CO 80303

T. Kuroda
National Research Institute for Metals
Ibaraki 305, Japan

Abstract--The effect of transverse compressive stress and axial tensile stress on the critical current of multifilamentary Nb3Al superconducting wires has been measured. Compared with commercial Nb3Sn, Nb3Al exhibits a relatively small sensitivity to both axial and transverse stress. For a given degradation of critical current at 9 T, Nb3Al will tolerate about twice as much axial stress as Nb3Sn and about five times the transverse stress. The elastic modulus of Nb3Al, 169 ± 20 GPa, was measured for the first time at cryogenic temperatures and found comparable to that of Nb3Sn. A comparison between the effect of axial and transverse stress showed that Nb3Al, like Nb3Sn, is more sensitive to transverse stress than axial stress. For a given level of critical-current degradation, the transverse stress tolerance of Nb3Al is about half the axial stress tolerance. The favorable electromechanical characteristics of Nb3Al, compared with Nb3Sn, may allow increased operating limits for the next generation of large high-field superconducting magnets.

I. INTRODUCTION

Presently, the most common conductor material used in high-field (>10 T) superconducting magnet designs is Nb3Sn. Commercially available multifilamentary Nb3Sn conductors typically have noncopper critical-current densities (J_c) exceeding 10^5 A/cm^2 at a magnetic field of 10 T. High current densities and high fields interact within magnet windings to produce large Lorentz forces supported by the conductor and the magnet structure. The two dominant components of stress in the windings are a tensile stress aligned with the conductor's longitudinal axis (axial stress) and a compressive stress that is perpendicular to its axis (transverse stress). The J_c of Nb3Sn is highly sensitive to its stress state. Consequently, it is the internal stress state of the magnet windings, rather than the J_c of the unstressed superconductor, that determines the design limits for large high-field magnets.

As new magnet designs call for larger coils and higher fields, stresses must be limited by structural reinforcement of the windings. Control of the stress, which accumulates radially within the windings, requires distributed internal reinforcement. Aside from complicating the design and increasing the cost of the magnet, additional internal reinforcement limits the superconductor packing fraction and, thus, reduces the magnetic field. Also, internal stresses within cable-in-conduit conductors can be difficult to control; thus, a superconducting material that is less sensitive to stress but comparable to Nb3Sn in J_c has significant design advantages. A promising candidate material for this application is the A-15 superconductor Nb3Al.

Early measurements of Nb3Al wires demonstrated their relative insensitivity to axial stress [1], but these experimental conductors were only available in short test sample lengths, unsuitable for magnet applications. More recently, technologies have been developed that allow fabrication of multifilamentary Nb3Al wires of practical lengths [2]. In this paper, both the axial and transverse stress effects for these conductors are investigated, and their performance is compared with that of a commercial binary Nb3Sn conductor. Also, results from the first elastic-modulus measurements of Nb3Al at cryogenic temperatures, which were required to compare the axial and transverse stress effect in Nb3Al, are presented.

II. EXPERIMENTAL DETAILS

The critical-current (I_c) degradation of round multifilamentary Nb3Al composite wires, caused by both axial and transverse stress, was measured at a temperature of 4 K and as a function of magnetic field. An electric-field criterion of 2 μV/cm was used for determining the I_c. The overall precision of the I_c data is about $\pm 0.5\%$. In the case of the transverse tests, a servohydraulic actuator and load cell are used to apply a compressive transverse load to the sample. The apparatus design allows mutually perpendicular application of current, field, and load [3] to simulate the conditions within the windings of a magnet. The transverse stress is calculated by dividing the load by the projected area of the compressed region of the sample. This technique is justified by previous comparative transverse stress measurements between round and rectangular Nb3Sn samples [3].

In the case of the axial tests, an axial tensile load is applied to the sample and the resulting axial strain is measured with an extensometer [4]. The magnetic field is perpendicular to the strain and current, which are coaxial, again simulating the conditions within a magnet. The characteristics of the Nb3Al samples, which were prepared by the Nb-tube process [2], are given in Table 1.

Table 1. Nb₃Al Sample Characteristics	
Wire diameter	0.5-0.57 mm
Matrix material	Nb
Filament composition	Al-1 at% Cu-1 at% Ge (prior to heat treatment)
Matrix-to-filament volume ratio	31:1
No. filaments	1,728,000
Filament size	~80 nm
Heat treatment	3 hours at 800 °C
Overall J_c at 12 T	8,600 A/cm^2
Filament J_c at 12 T	274,000 A/cm^2

III. RESULTS

The results of the Nb₃Al *axial* strain measurements are shown in Fig. 1 where I_c is plotted as a function of axial strain for several magnetic fields. The ordinate is the measured I_c normalized to the starting (zero-strain) value (I_{cm}). For comparison, previously acquired data for a commercial bronze-process Nb₃Sn conductor [3] are also presented. The available data do not allow direct comparison of the Nb₃Al and Nb₃Sn conductors at a common field; however, interpolation of the Nb₃Sn data allows comparison at 9 T. For I_c degradations greater than 10%, the Nb₃Al will tolerate approximately twice the strain of the Nb₃Sn while undergoing the same degradation in I_c.
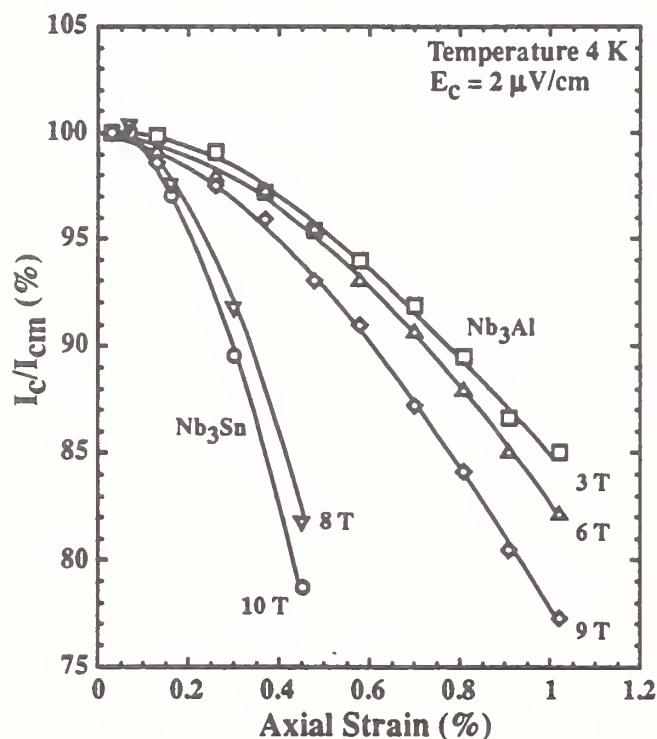

Fig. 1. Critical-current degradation caused by axial tensile strain.

Figure 2 shows a similar comparison between Nb₃Al and Nb₃Sn subjected to *transverse* stress. By convention, the stress is negative to indicate compression. The difference between Nb₃Al and Nb₃Sn is even greater in the case of transverse stress. For I_c degradations greater than 10% at 9 T,

the Nb₃Al will tolerate approximately five times the stress of the Nb₃Sn while undergoing equal I_c degradation.
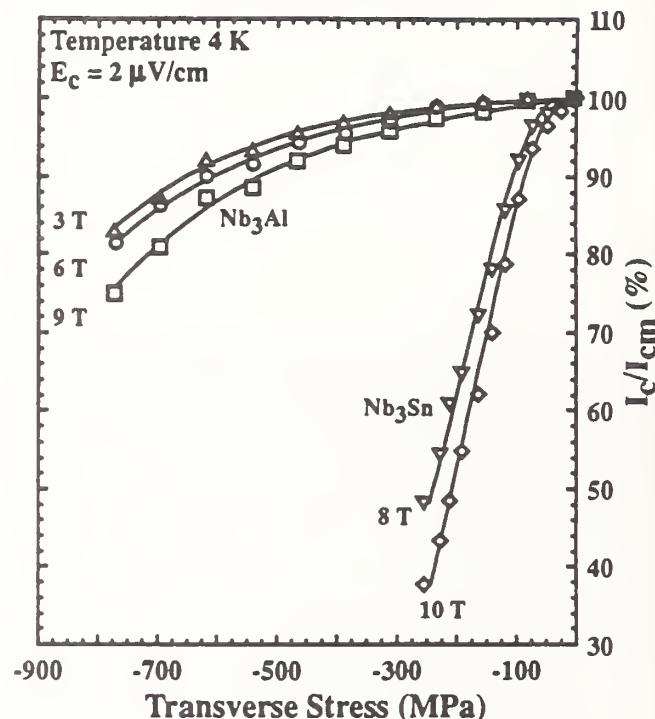

Fig. 2. Critical-current degradation caused by transverse compressive stress.

Previous studies comparing the axial and transverse stress effects in Nb₃Sn [3], [5], [6], [7] have all shown a much greater sensitivity to transverse stress than axial stress. This type of comparison requires a conversion of the axial strain data, the measured quantity, to axial stress. The relationship between stress and strain (elastic modulus) has previously been measured at cryogenic temperature for Nb₃Sn (165 GPa) [8] but not for Nb₃Al. Consequently, to allow comparison of axial and transverse stress effects, elastic-modulus measurements of Nb₃Al at cryogenic temperatures were made.

The Nb₃Al samples used in the I_c tests are not well suited for modulus measurements because of their ultra-fine filaments and small superconductor-to-matrix ratio. Consequently, a group of three different large monofilament Nb₃Al conductors were used for the modulus measurements. These are powder-process wires that vary in Nb₃Al content (45 ± 15%, 60 ± 10%, and 81 ± 2% Nb₃Al). A detailed description of the wires is contained in [9]. All of the samples were 5 cm long. The results of these measurements are shown in Fig. 3 where the elastic moduli of the three different conductors are plotted as a function of their Nb₃Al content. Since the sample with the highest Nb₃Al content is 81 ± 2% Nb₃Al, the elastic modulus of pure Nb₃Al was extrapolated from the measured data.

Two samples of the 60%-Nb₃Al conductor were measured at both 76 K and 4 K. For both samples, the difference between measurements at 4 K and 76 K was less than 5%.
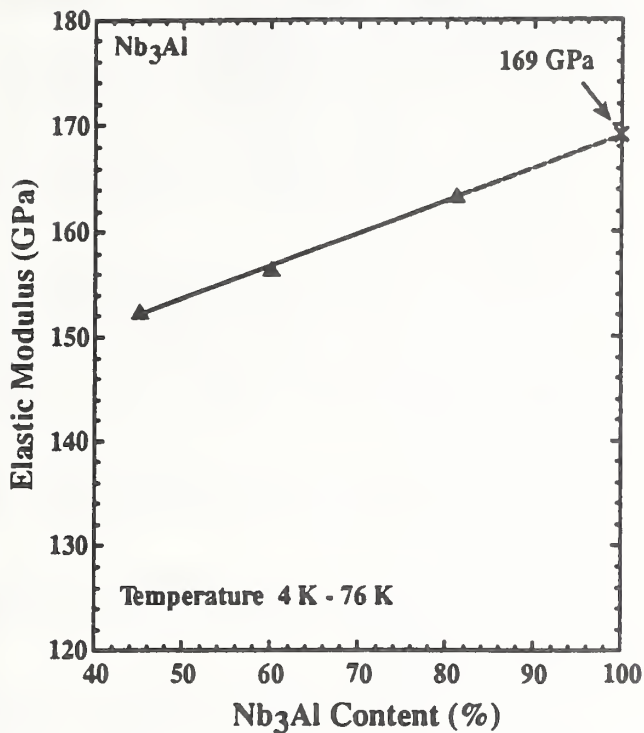
Fig. 3. Elastic modulus of three Nb₃Al wires, each with a different Nb₃Al content.

Given an overall experimental error of about 5% for the modulus measurements, the difference in the 4 K and 76 K measurements can reasonably be neglected.

Two 45%-Nb₃Al wires were measured, and the average of these measurements is plotted in the figure. The two measurements varied ± 1.6% from the mean. Seven total measurements of four different 60%-Nb₃Al wires were made with a maximum variation of ± 9.2% from the plotted mean value. For the 81%-Nb₃Al wire, two measurements were made, and the variation was ± 4.0%. The mean values are plotted for each type of conductor in Fig. 3; a linear extrapolation of the data yields an elastic modulus of approximately 169 ± 20 GPa.

Using this modulus value, axial stress values were calculated from the axial strain data and plotted in Fig. 4 for comparison with the transverse data. Like Nb₃Sn, Nb₃Al is more sensitive to transverse stress than to axial stress; however, the difference in sensitivity is much greater for Nb₃Sn than for Nb₃Al. From Fig. 4, the stress that causes a given amount of I_C degradation at 9 T is almost two times smaller for transverse stress than for axial stress. In contrast, this ratio for Nb₃Sn at 10 T is approximately five [3].

As indicated in Fig. 4, transverse *compressive* stress is being compared with axial *tensile* stress. There are two practical reasons for this. First, these are the conditions that actually exist in the windings of an energized magnet, thus these data are useful from an engineering design standpoint for estimating magnet performance. Also, it is difficult to apply axial compressive stress to a superconducting wire. The

effect of axial compressive stress has been measured in Nb₃Sn by taking advantage of the compressive prestrain of the superconductor [4]. The Nb₃Al samples did not exhibit this prestrain, so the effect of axial compressive stress could not conveniently be measured. However, assuming that Nb₃Al behaves similarly to Nb₃Sn, in which the effects of tensile and compressive axial stress are approximately equal, the sense of the axial stress does not affect these results.

IV. CONCLUSIONS

For a given degradation of I_C at 9 T, Nb₃Al will tolerate about twice as much axial stress as Nb₃Sn and about five times the transverse stress. The elastic modulus of Nb₃Al, 169 ± 20 GPa, was measured for the first time at cryogenic temperatures and found comparable to that of Nb₃Sn, 165 GPa. The elastic modulus of Nb₃Al was needed in this study for comparing the axial and transverse stress effects, but, in a more general sense, it will ultimately be important for Nb₃Al magnet design.
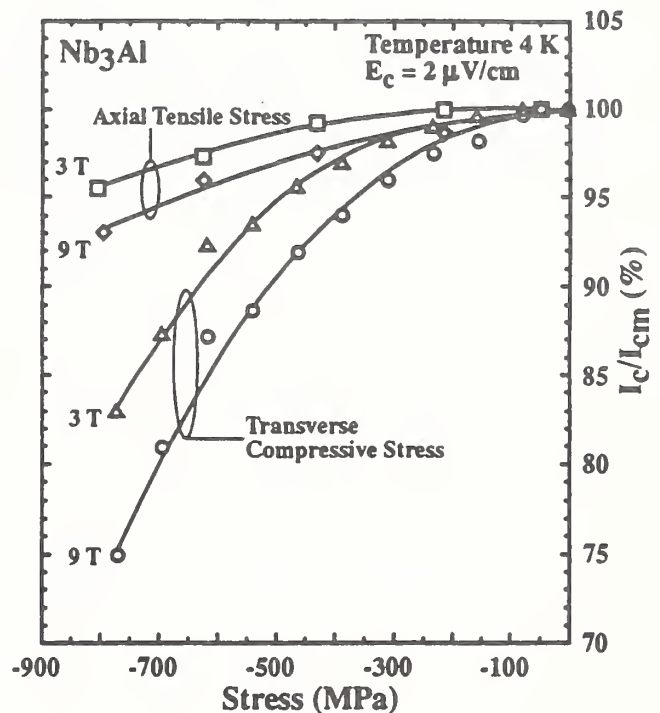
Fig. 4. Comparison between axial and transverse stress effects.

Nb₃Al conductors are more sensitive to transverse stress than axial stress. This suggests that the anisotropy in stress degradation, which was first observed in Nb₃Sn conductors, is not associated with a particular processing method or even a particular material. However, the difference between axial and transverse sensitivity is less for Nb₃Al than Nb₃Sn. A given level of I_C degradation at 10 T in Nb₃Sn requires about five times less transverse stress than axial stress; for Nb₃Al at 9 T, the ratio is only about two.

There are many factors that determine the suitability of a superconducting material for a particular application. Critical-

current density, critical magnetic field, cost, available conductor length, and handling properties are important considerations for most applications. For the large high-field magnets needed in fusion applications, stress effects often dictate the design operating limits of the magnet. The present interest in Nb_3Al superconductors is partially due to its relative insensitivity to stress. Ultimately, if Nb_3Al conductors can be developed that are otherwise comparable to the existing high-field commercial superconductors, their favorable electromechanical properties may extend the operating limits for future magnet designs.

REFERENCES

[1] J. W. Ekin, "Strain effects in superconducting compounds," Adv. Cryog. Eng., vol. 30, pp. 823-836, 1984.

[2] T. Takeuchi, Y. Iijima, T. Kuroda, M. Yuyama, and K. Inoue, "Effects of additive elements on continuous ultra-fine Nb_3Al mf superconductor," IEEE Trans. Magn., vol. 25, pp. 2068-2075, Mar. 1989.

[3] J. W. Ekin, "Effect of transverse compressive stress on the critical current and upper critical field of Nb_3Sn," J. Appl. Phys., vol. 62, pp. 4829-4834, Dec. 1987.

[4] J. W. Ekin, "Strain scaling law for flux pinning in practical superconductors. Part 1: Basic relationship and application to Nb_3Sn conductors," Cryogenics, vol. 20, pp. 611-624, Nov. 1980.

[5] W. Specking, W. Goldacker, and R. Flükiger, "Effect of transverse compression on I_c of Nb_3Sn multifilamentary wire," Adv. Cryog. Eng., vol. 34, pp. 569-575, 1988.

[6] L. T. Summers and J. R. Miller, "The effect of transverse stress on the critical current of Nb_3Sn cable-in-conduit superconductors," IEEE Trans. Magn., vol. 25, pp. 1835-1838, Mar. 1989.

[7] H. Boschman and L. J. M. van de Klundert, "Effects of transverse stress on the current carrying capacity of multifilamentary wires," Adv. Cryog. Eng., vol. 36, pp. 93-100, 1990.

[8] D. S. Easton, D. M. Kroeger, W. Specking, and C. C. Koch, "A prediction of the stress state in Nb_3Sn superconducting composites," J. Appl. Phys., vol. 51, pp. 2748-2757, May 1980.

[9] C. L. H. Thieme, "The production of Nb_3Al superconducting wire by the powder metallurgy process," University of Twente, The Netherlands, Ph.D. dissertation, 1988.

J. W. Ekin, "Superconductor Specification," Concise Encyclopedia of Magnetic & Superconducting Materials, ed by J. E. Evetts, p. 575 (1992).

Table 1
Example of superconductor wire specification

Specification	Typical value	Test specimen or sample
Physical		
superconductor material	(Nb–1.5 at.%Ti)$_3$Sn	
stabilizer material	oxygen-free copper	
wire diameter	0.808 ± 0.005 mm	each 150 m, middle and end of each billet
copper-to-noncopper ratio	(1.5 ± 0.1):1	both ends of each billet
filament size and spacing	6 μm > 1.0 μm	both ends of each billet
twist pitch	1.0 ± 0.1 clockwise twists cm^{-1}	beginning and end of each continuous wire
piece length	1.5 km	
Electrical		
critical current (min at 12 T)	164 A at 10^{-14} Ω m and 4.22 K for magnetic field ⊥ wire axis	beginning and end of each continuous wire length
resistance max R_{295K} max R_{19K}	565 μΩ cm^{-1} 6.8 μΩ cm^{-1}	beginning and end of each continuous wire length
Mechanical		
prestrain	0.15–0.25%	both ends of each billet
irreversible strain	> 0.7%	both ends of each billet

Superconducting Materials: Specification

The specification of superconductors is needed both in the purchase of practical superconductors and in the characterization of superconductor materials for research. Parameters such as the critical temperature T_c and the upper critical field H_{c2} are intrinsic to the material and are usually adequately specified just by specifying the material (i.e., by the ratio of elements in the superconducting alloy or compound). Extrinsic parameters that vary with processing technique and conductor design, on the other hand, are much more variable and need to be specified and measured on a conductor-to-conductor basis, especially for the procurement of superconductors for practical applications (see *Multifilamentary Superconducting Composites*). Such parameters include the physical shape of the conductor, critical current, matrix resistivity and mechanical properties. In this article, the emphasis will be on practical superconductor materials and, primarily, specification of their extrinsic parameters.

Furthermore, the article concentrates on the specification of single-strand multifilamentary conductors and does not include additional parameters needed for cable specification. The single-strand multifilamentary parameters, however, form the basis for most conductor specification and are a key element for the more complex cable conductors.

The extrinsic parameters of single-strand conductors are described here under three general headings: physical, electrical and mechanical specifications. An example of a set of typical superconductor specifications for a Nb$_3$Sn superconductor is given in Table 1.

1. Physical Specifications

1.1 Superconductor Material

Superconductor material should be specified in order to determine T_c and H_{c2}. Also, the mechanical properties inherent to the material will need to be considered in application of the material. For example, NbTi superconductors are easy to handle mechanically, because they are ductile. However, they are commonly used in magnet applications up to a magnetic field of only about 8 T. Nb$_3$Sn superconductors, on the other hand, are commonly used at higher fields up to about 14 T, but, being brittle, they require special handling and special mechanical design for applications.

Furthermore, the specific superconductor composi-

578

tion should be prescribed because some compositions are better for obtaining high current density J_c at high magnetic field, while other compositions are better for low fields. For example, in NbTi superconductors, the nominal composition of niobium and titanium should be prescribed along with alloy homogeneity. For Nb_3Sn, the superconductors either can be binary (just niobium and tin) or third (and sometimes fourth) elements, such as titanium or tantalum, can be added in order to increase J_c at very high magnetic fields.

1.2 Stabilizer Material

The type of material used as a stabilization matrix (see Fig. 1) should be specified in order to ensure adequate electrical and thermal conductivity to protect the conductor against thermal runaway. For example, oxygen-free copper is a common stabilizer material. Specification of the type of stabilizer material ensures that the conductor will be adequate to meet the residual resistivity ratio requirements discussed in Sect. 2.2.

1.3 Conductor Size

The cross-sectional dimensions of the conductor should be specified so that they are consistent with the current capability of the power supply and the desired magnet inductance. The tolerance for variation in these dimensions can be critical for some magnet applications. The cross-sectional dimensions are also needed to calculate the critical current density from the critical current, described in Sect. 2.1.

1.4 Copper-to-Noncopper Ratio

The copper-to-noncopper ratio specifies the volume of stabilizer material relative to the superconductor

material. It must not be too low, or the conductor will be unstable and susceptible to thermal runaway. If the ratio is too high, on the other hand, the overall critical current density suffers. Values from 1:1 to 5:1 are typical, with the higher ratios needed to ensure stability in large magnets where the stored energy can be very great.

The copper-to-noncopper ratio is usually measured by weighing a sample of the conductor, chemically etching away the copper with a 50% nitric acid solution, drying the remaining superconducting filaments, and reweighing. The copper mass is obtained from the difference. The copper-to-noncopper ratio is then determined by taking the ratio of the weight of copper to the remains and dividing by the ratio of specific gravities for copper and the noncopper material.

1.5 Filament Size and Spacing

The diameter of the superconducting filaments should be specified in order to ensure that hysteretic ac losses in the conductor filaments are reduced to an acceptable level. The smaller the filament size, the lower the losses. Too small a diameter, however, results in filament cross-sectional inhomogeneities and a lowering of the critical current density. A filament diameter of about 5 µm is a typical compromise.

The spacing between filaments must also be kept above a minimum value, typically 1 µm or more, edge to edge, in order to electrically decouple neighboring filaments. If the filaments couple, low-field ac losses can reach unacceptable levels.

Filament size and spacing are usually determined from a photomicrograph of a polished cross section of the conductor. Several filament diameters and spacings are measured and the results averaged.

Instead of specifying filament diameter and spacing, the maximum acceptable level of ac loss can be stipulated, along with the method by which it should be measured. This is usually preferable because it ensures a minimum performance level. Two methods are in common use: magnetization and calorimetry. The calorimetric method (using a boil-off technique, for example) measures a total ac loss and is therefore usually favored, but it is more difficult than magnetization measurements.

1.6 Twist Pitch

The filaments in a practical superconductor are twisted to reduce ac loss heating that would otherwise occur when the conductor is subjected to magnetic fields that change with time (see *AC Applications of Superconducting Materials*; *AC Losses in Superconducting Materials*). The rates of change can be particularly large in pulsed magnet applications, but can be significant in dc magnets as well, because of the need to charge and discharge the magnet. The number of twists per unit length, or the twist pitch (the length of one twist), is specified in order to ensure that ac
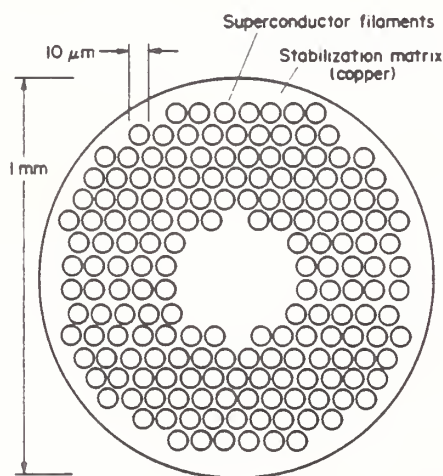

Figure 1
Cross-sectional view of a typical NbTi, copper-stabilized superconducting composite (after Ekin 1983b)

losses are reduced to an acceptable level. A twist pitch of about one centimeter is typical for a small (1 mm diameter) conductor.

1.7 Piece Length

The minimum acceptable length of continuous superconductor is usually specified in order to avoid an excessive number of joints between lengths. Sometimes the minimum length is determined by requirements on the joint location as well. For example, in superconducting electromagnets, the piece length needs to be long enough that the joints between conductors can be made in a low-magnetic-field region.

2. Electrical Specification

2.1 Critical Current

The critical current I_c is perhaps the most important parameter from a practical standpoint. Because the rise in the voltage–current (V–I) characteristic of a superconductor is not infinitely sharp (see Fig. 2), the critical current is arbitrary, unless a criterion is specified to determine the critical current (see *Critical Current Density*). This is usually done by using an electric field criterion or resistivity criterion. For example, the critical current I_c can be defined as the current at which the electric field E along the conductor reaches a specific value, such as $1 \, \mu V \, cm^{-1}$. This is shown by the intersection of the V–I curve and the horizontal dashed line in Fig. 2. Alternatively, I_c can be defined as the current at which the resistivity of the conductor rises to a specific value, such as 10 pΩ cm, shown by the dashed line passing through the origin in Fig. 2. When using the resistivity criterion, the cross-sectional area to be used in the determination should be specified. Finally, when the rise in the V–I characteristic is very gradual, much of the arbitrariness and variability is eliminated by using the offset criterion. As shown in Fig. 2, it is determined by taking the tangent to the V–I curve at a specified electric field.

The critical current density J_c is defined as the critical current divided by the cross-sectional area A of the superconductor,

$$J_c \equiv I_c / A$$

Usually the area A is taken as just the cross-sectional area of the conductor minus the cross-sectional area of the copper stabilizer; this is commonly referred to as the noncopper area.

Sometimes the shape of the voltage–current curve is also specified to indicate the quality of the superconductor. A sharp transition is desirable, indicating the rapid disappearance of resistivity below the nominal value of I_c. A common method for representing the sharpness of the resistive transition is through the use of the n value defined by a simple power law
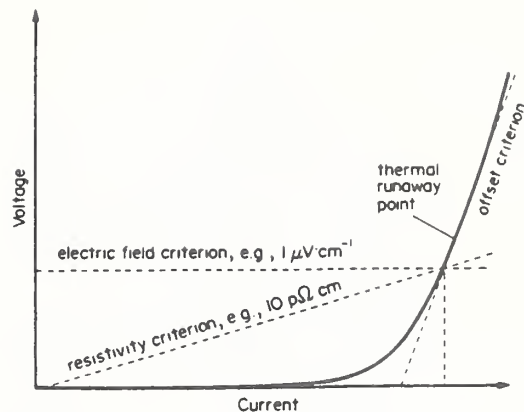

Figure 2
The voltage–current characteristic of a practical superconductor, showing electric-field and resistivity criteria for determining critical current

$$V \propto I^n$$

or equivalently

$$E \propto J^n$$

Here E is the electric field along the conductor and J is the current density. Values of the power n are easily determined by plotting the V–I or E–J curves on a log–log plot and determining the slope of the curve at a designated electric field (the curve is typically linear over a considerable range of electric field). Values of n generally lie between 20 and 100 for high-quality superconductors (see *Resistive Transition and Flux Flow in Superconducting Materials*). Lower n values usually indicate inhomogeneities in the local critical current density. Other methods of fitting the shape of the V–I curve are also used, usually involving more fitting parameters. However, this empirical formula is simple, involves only a single fitting parameter (other than a proportionality constant) and, consequently, is easy to use.

The critical current is also strongly dependent on the magnetic field magnitude (see Fig. 3) and direction. Typically, I_c values are prescribed at one or more magnetic fields, usually for the magnetic field applied perpendicular to the wire axis. This perpendicular orientation for the magnetic field usually corresponds to the worst case (lowest I_c), but is the most common orientation in superconductor magnet applications.

The critical current is also strongly dependent on temperature (see Fig. 3). Usually the temperature at which liquid helium boils at atmospheric pressure is used, that is, 4.2 K. If the critical current measurement cannot be carried out at precisely 4.2 K, small temperature corrections can be made to the measured I_c values using the "linear temperature" formula
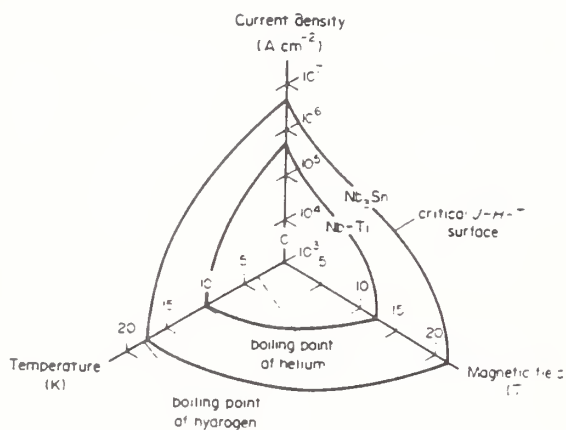
580

Figure 3
Interrelation of critical current density, magnetic field and temperature for Nb$_3$Sn and NbTi (courtesy of W. A. Fietz). In the region between the origin and the critical J–B–T surface the material is superconducting; beyond this critical surface the material is in the normal state

$$I_c/I_m = (T_c - T)/(T_c - T_m)$$

where T_c is the transition temperature at the specified magnetic field, I_m is the current measured at temperature T_m and I_c is the critical current at the specified temperature T.

Usually, the critical current is measured on samples taken from each continuous length of conductor. For testing, these samples are wound typically onto a cylindrical sample holder, such as shown in Fig. 4, and a four-terminal transport I_c measurement is carried out in accordance with a specific measurement procedure such as American Society for Testing and Materials (ASTM) Standard Test Method B714–82. A minimum length of sample for the critical current measurement should be prescribed, since inhomogeneities along the conductor have a greater effect on I_c over longer conductor lengths. A 25 cm length of sample between the voltage taps in Fig. 4 would be a typical test length. Long test lengths also allow a more sensitive measurement of low electric fields along the conductor, which permits a sensitive critical current criterion to be used.

2.2 Resistance at Room Temperature and T_c

The conductor resistance at room temperature (R_{295K}) is determined mainly by the amount of copper matrix. Thus, it can be used to provide an independent measure of the volume of copper to superconductor. The conductor resistance just above the superconducting transition temperature R_{T_c} is mainly determined by the purity of the matrix material. Thus, the resistance just above T_c is important because it gives a measure of the ability of the matrix to stabilize and protect the conductor from thermal runaway, should

a disturbance raise a portion of the superconductor above T_c. Typically the ratio, R_{295K}/R_{T_c}, called the residual resistance ratio (RRR), is specified. The higher the RRR value, the greater the purity of the copper matrix material and the better the stabilization of the conductor. Values of RRR of about 70 or more are typically achieved using oxygen-free copper.

Room-temperature resistance is usually measured using a four-terminal resistance measurement technique, similar to the critical current measurement, except that the V–I curve is linear and the measuring current is kept small to avoid sample heating. Temperature control for measuring R_{T_c} just above T_c can be achieved fairly easily by lowering the sample into a liquid helium bath and then raising it above the liquid helium a couple of centimeters and recording the resistance as the temperature rises through T_c. The superconductor is thus used as a fixed-point thermometer: as the temperature of the conductor increases, the resistance rises rapidly at T_c, then becomes constant just above T_c. This region of relatively constant resistance on warming is taken to be R_{T_c}. The RRR is then just the quotient R_{295K}/R_{T_c} of these two measured resistances.

3. Mechanical Parameters

For compound superconductors, such as Nb$_3$Sn, V$_3$Ga or Nb$_3$Al, several mechanical parameters need to be specified because of the sensitivity of the critical current of these materials to strain.
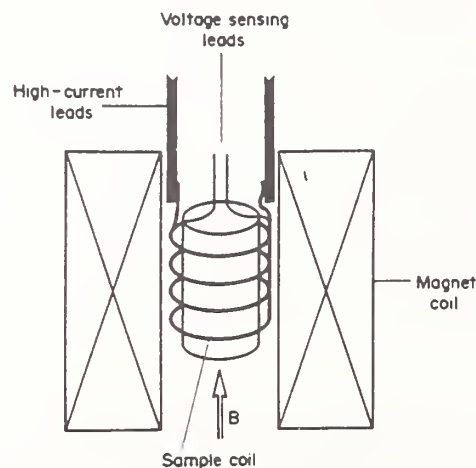
Figure 4
A typical cylindrical sample holder for measuring the critical current of a spirally wrapped superconducting wire sample (adapted from Goodrich and Fickett 1982). The sample holder assembly is placed inside the bore of a solenoid magnet that provides a background field along the axis of the holder (perpendicular to the sample). In this way, a long superconducting sample can be tested in the confined space of a high-field background magnet

581

3.1 Prestrain

The different materials that make up a composite superconductor (stabilizer matrix, tin–bronze matrix for Nb₃Sn conductors, superconducting material and diffusion barriers) all thermally contract by different amounts as the conductor is cooled from its fabrication temperature (typically 700 °C). This places the superconducting material under an initial prestrain ε_m, usually compressive, which arises from differential thermal contraction of the various materials making up the conductor.

The value of the prestrain ε_m is also needed to compare critical currents in different samples equally. Either compressive or tensile strain ε degrades the superconductor; thus, because of the inital compressive prestrain, the critical current will start at a degraded value (see Fig. 5), then pass through a maximum at zero "intrinsic" strain where the applied tensile strain removes all the precompression and the superconducting material itself is in a relatively strain-free state, and then again decrease when the intrinsic strain within the superconducting material becomes tensile. This results in the peaked curves shown in Fig. 5. The value of the prestrain can be determined by applying tension to a conductor and measuring the strain where the critical current passes through a maximum. Critical currents should be compared at the peak, or at comparable intrinsic strain relative to the peak, for the purpose of selecting conductors.

Because of the effect of strain on the critical current, the compressive prestrain ε_m from differential thermal contraction should be specified in order to set strain limits in designing magnets and specifying reinforcing structures for magnets. Ideally, the superconductor should operate just on the compressive side of maximum (about 0.1–0.2% intrinsic compressive strain) when the conductor is under full operating load. In such a case J_c is near maximum, but there is still a sufficient margin for additional strain.

3.2 Irreversible Strain

Irreversible strain specifies the strain beyond which the conductor is permanently damaged and J_c is irreversibly degraded. The importance of this parameter is that it sets a strain-handling limit in bending and spooling a conductor during magnet fabrication. It also defines the ultimate practical strain the conductor can tolerate in the mechanical design of the conductor support structure.

The irreversible strain is determined by measuring the critical current of a conductor as a function of tensile strain and periodically unloading the conductor to determine if the J_c vs ε curve retraces itself, that is, to see whether it is reversible. For example, in Fig. 6, the critical current on unloading from strain point A was measured to be at the + marked A′, right on the original curve. The same was true after unloading from strain point B; that is, the critical current was reversible. However, after unloading from strain
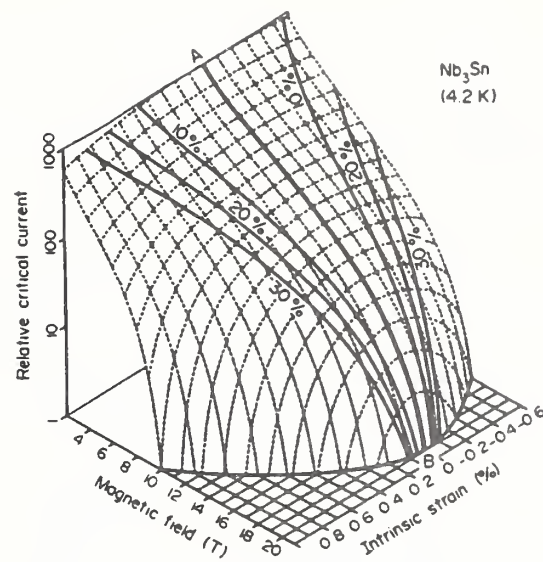
Figure 5
J–B–ε critical surface for Nb₃Sn showing the reversible degradation of critical current at either tensile or compressive strain as a function of magnetic field (after Ekin 1983a). Line A–B represents the maximum (strain-free) value of the critical current as a function of magnetic field. Corresponding pairs of curves on either side of line A–B show the strain window for mechanical design which will result in a critical current within the indicated percentage of maximum

point C, the critical current was irreversible as shown by point C′, which falls below the original I_c vs strain curve. Thus, the reversibility of the I_c vs ε curve is lost and permanent damage occurs to the superconducting material when the conductor is strained beyond point B, which is defined as the irreversible strain limit.

4. Future Specification Needs

Future needs for specification parameters will change with both applications and materials. For example, in new applications, superconductor magnets that use very rapidly changing ac currents will impose severe ac-loss requirements on the conductor. This problem is overcome by using very-small-diameter filaments and a short twist pitch (see *AC Applications of Superconducting Materials*). However, the very small filament diameter may well require a filament uniformity specification to avoid a lowering of the critical current from localized necking of the filament. Alternatively, the critical current may have to be specified at a very low criterion level to discriminate against the low voltages associated with such filament nonuniformity.

In the materials area, the advent of high-T_c super-

Figure 6
Illustration of the irreversible strain limit (after Ekin 1981). Corresponding loaded and unloaded data points are labelled by letters (A, B, C, etc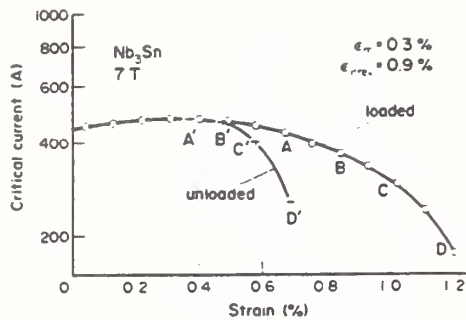.). The irreversible strain limit ε_{irr} occurs just beyond point B, after the conductor has been loaded to about 0.9%

conductors brings with it a new set of specifications. Mechanical parameters will become particularly important in these brittle ceramic materials. Also, the very low critical current densities of some bulk high-T_c conductors and the gradual rise of the V–I characteristic (see Fig. 2) make the specification of a critical current somewhat arbitrary with conventional criteria. More universal critical current criteria such as the offset criterion are being used to meet this need.

See also: Measurements in Superconducting Materials; Multifilamentary Superconducting Composites; Resistive Transition and Flux Flow in Superconducting Materials; Superconducting Magnets

Bibliography

Annual Book of ASTM Standards 1982a Standard definitions of terms relating to superconductors, ASTM B713–82. American Society for Testing and Materials, Philadelphia, PA

Annual Book of ASTM Standards 1982b Standard test method for dc critical current of composite superconductors, ASTM B714–82. American Society for Testing and Materials, Philadelphia, PA

Clark A F, Ekin J W 1977 Defining critical current. *IEEE Trans. Magn.* 13: 38–40

Ekin J W 1981 Mechanical properties and strain effects in superconductors. In: Foner S, Schwartz B (eds.) 1981 *Superconducting Materials Science: Metallurgy, Fabrication and Applications*. Plenum, New York, pp. 455–510

Ekin J W 1983a Four dimensional J–B–T–ε critical surface for superconductors. *J. Appl. Phys.* 54: 303–6

Ekin J W 1983b Superconductors. In: Reed R P, Clark A F (ed.) 1983 *Materials at Low Temperatures*. American Society for Metals, Metals Park, OH, pp. 465–513

Ekin J W 1987 Irregularity in Nb–Ti filament area and electric field vs current characteristics. *Cryogenics* 27: 603–7

Ekin J W 1989 Offset criterion for determining superconductor critical current. *Appl. Phys. Lett.* 55: 905–7

Goodrich L F, Bray S L 1990 High-T_c superconductors and critical current measurement. *Cryogenics* 30: 667–7

Goodrich L F, Fickett F R 1982 Critical current measurements: a compendium of experimental results. *Cryogenics* 22: 225–41

Larbalestier D C, West A W, Starch W, Warnes W, Lee P, McDonald W K, Olarey P, Hemachalam K, Zeitlin B, Scanlan R 1985 High critical current densities in industrial scale composites made from high homogeneity Nb 46.5 Ti. *IEEE Trans. Magn.* 21: 269–72

Plummer C J G, Evetts J E 1987 Dependence of the resistive transition on composite inhomogeneity in multifilamentary wires. *IEEE Trans. Magn.* 23: 1179–82.

J. W. Ekin
[National Institute of Standards and Technology, Boulder, Colorado, USA]

THE DEVELOPMENT OF AN INTERNAL-TIN NB3SN STRAND FOR FUSION APPLICATIONS

E. GREGORY[1], J.W EKIN[2] G. GRUNBLATT[3], H.G. KY[3], G.M. OZERYANSKY[1] AND B.A. ZEITLIN[1]

[1]IGC / Advanced Superconductors, 1875 Thomaston Avenue, Waterbury, CT 06704, U.S.A.
[2]Electromagnetic Technology Division, National Institute of Standards and Technology, Boulder, CO 80303, U.S.A.
[3]Alsthom Intermagnetics (AISA), 3 avenue des trois Chênes, 90018 Belfort, France

A high J_c internal-tin Nb3Sn strand with relatively low losses has been developed for fusion applications. This paper will present the results obtained on this strand as fabricated and supplied for the European fusion program. More than 10 km of chrome plated strand has been supplied in a variety of configurations and with different barriers. The test results on some of these strands, after they have been given different heat treatment cycles, are reported. The manner in which fabrication problems have been overcome are explained and methods to improve reliability and reproducibility of properties along the length of these strands, are also described. It has been shown that applying hot isostatic pressure (HIP) to the wire at the intermediate homogenization temperature of 580°C doubles the intrinsic irreverible strain.

1. INTRODUCTION

There is a need, in the fusion field for a reliable, economical material which will exhibit high current densities and low losses in the 12 to 15 T field region.

Nb_3Sn is one of the very few material options available for these applications and, while the material has been obtainable for thirty years (ref. 1), its wide application for large magnets has been relatively limited. The reasons for this are many and varied. They involve the strand, the total conductor, the insulation, the magnet design and its fabrication.

Nb_3Sn is a less forgiving material than NbTi and therefore the interrelationships of all these factors is of greater importance if we are to ensure the reliable performance of magnets in the size and field range required for fusion. In this paper, however, we will concern ourselves only with the optimization of the strand in such a way as to achieve high J_c, low losses and good mechanical and electrical reliability of the composites. It has been known, for some time, that internal-tin material can provide high J_c's (ref. 2) and in recent years, we have been exploring various methods of increasing piece length, reducing losses and improving ease of fabrication and reliability of performance (ref. 3-5).

Some strands supplied earlier for the NET program, and the properties which they exhibited, are reported upon. Areas in which work is being carried out to improve these products are also described.

2. SAMPLE MATERIAL SUPPLIED TO NET

Over a year ago some trial samples of 7 and 19 subelement internal-tin materials were supplied to NET for evaluation. Cross sections of the materials which contain filaments of Nb 7.5 wt.% Ta, are shown in Figures 1 & 2. The properties were close to those required to meet the NET specification.

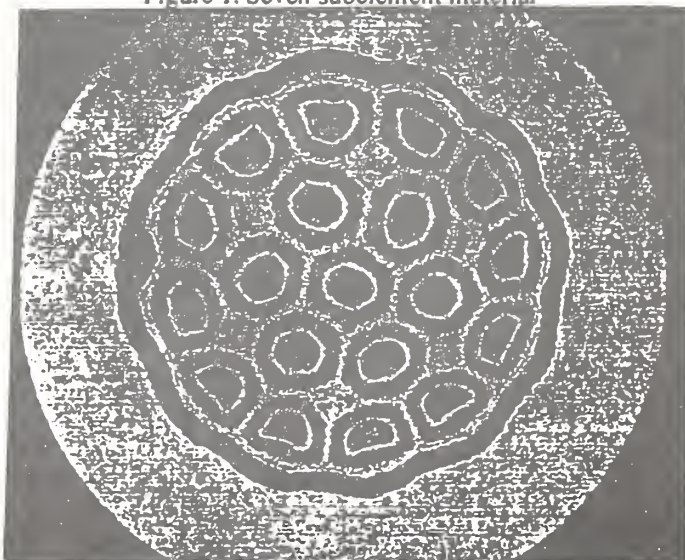Figure 1. Seven subelement material

Figure 2. Nineteen subelement material

The strand diameter was 0.73 mm, the Cu to non Cu ratio was 1.5:1 and the strand twist pitch length was less than 10 mm. The heat treatment used on both materials to provide homogenization was 200°C 96 h + 375°C 24 h + 580°C 48 h. This was followed by a 700°C reaction heat treatment which was for 180 h in the case of the 7 subelement material and 96 h for the 19 subelement array.

3. TESTS PERFORMED

The material was tested for I_c at the University of Twente and four samples were measured for each design. The hysteresis loss specimens were prepared at ECN and tested at the Rutherford Laboratory. The RRR measurements were made between room temperature and 20 K and measured at the Rutherford Laboratory and the University of Twente. The reported results were obtained from 5 specimens of each type. The results of these tests are shown in Table 1

4. RESULTS

Since the acceptance requirement for NET was $J_c > 635 \pm 5$ A/mm^2 at 12.5T, 4.2 K and 0.1 μV/cm, neither group of samples fully meets the J_c specification. The 7 subelement material, while it has an average J_c that is higher than the specification shows a wide variation from sample to sample and a low "n" value. The 19 subelement material is more consistent in J_c and shows higher "n" values but it needs to be optimized further to meet the J_c specification. The hysteresis losses are lower than the specification but the results on the 19 subelement material indicate that the smaller filaments lead to more bridging.

Measurements on the heat treated non Cr-plated specimens show good results while those on materials which have been heat treated after plating, are poor, particularly in the case of the 7 subelement material that was heated for a longer time at 700°C. It appears that the problem is not a result of barrier breakdown but one related to diffusion of the Cr (or more likely impurities in the Cr) into the Cu.

5. RECENT WORK

5.1 Current density and variability of J_c

Since the 7 subelement material shows low "n" values and a considerable variability in properties, it was decided to concentrate, in our present and future work, on the 19 subelement material that has performed well in the past when it

contained an extruded Nb barrier (ref. 6,7). At the time when the specimens described above were prepared, extruded barrier material was not available and a wrapped barrier technique was employed. When this assembly method is used for 19 subelement arrays, it is necessary to incorporate an internal copper tube below the barrier to ensure that a uniform array can be established. This results in a ring of bronze between the filament array and the barrier and this reduces the J_c by over 20 % (ref. 6).

Since this time we have developed a new facility for barrier extrusion and Figure 3 shows a 19 subelement material with material with an extruded tantalum barrier and no "under barrier" copper. This material we expect to yield a J_c well within the NET specification.

Although in Table 1, the 19 subelement material shows less variability in J_c than the 7 subelement material, it still shows a dispersion of ± 4.5 %.

5.2 HIP Experiments

In order to improve the uniformity of properties, hot isostatic pressure (HIP) experiments have been carried out on these wires, both at the final heat treatment temperature of 700°C and also at 580°C (ref. 5). The idea of HIP'ing the
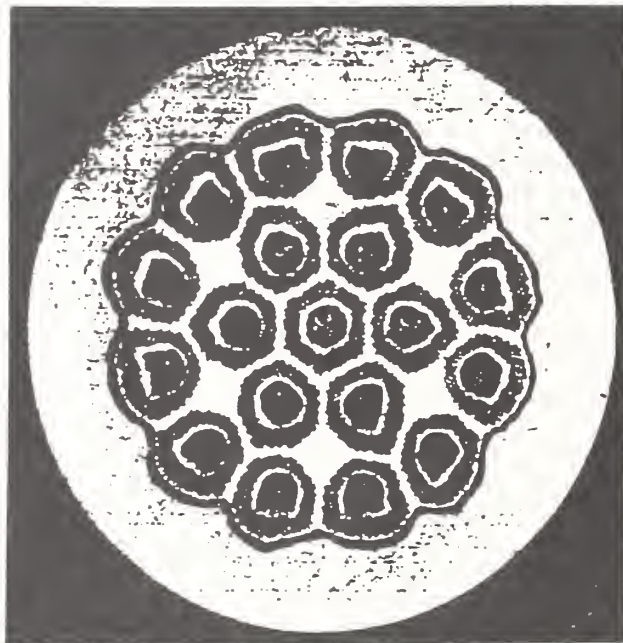
Figure 3. 19 subelement with an extruded Ta barrier

TABLE I
MEASURED PROPERTIES OF NET SAMPLES

PROPERTIES	SPECIFICATIONS	7 SUBELEMENTS	19 SUBELEMENTS
Heat treatment		180 h at 700°C	96 h 700°C
J_c (0.1 μV/cm, 12.5 T 4.2 K)	635	627, 716, 663, 615. Mean 655.5, Dispersion ± 7.7%	561, 609, 609, 615. Mean 598.8, Dispersion ± 4.5%
	n > 20	n = 17	n = 25
Hysteresis Losses ± 3T mJ/cc	<850	533	682
RRR (bare)		207 Rutherford, 219 Twente	309 Rutherford, 290 Twente
(Cr plated)	>100	33.8 Rutherford, 34.4 Twente	78.3 Rutherford, 81.5 Twente

84

TABLE 2.
COMPARISON OF J_c IN HIP'D AND UNHIP'D MATERIAL

Field	J_c (A/mm^2) (Non HIP'd) Sample 1	J_c (A/mm^2) (Non HIP'd) Sample 2	J_c (A/mm^2) (HIP'd) Sample 1	J_c (A/inm^2) (HIP'd) Sample 2
9	1101.8	1101.8		
10	916.2	916.2		
11	749.0	766.5		
12	622.8	622.8		808.4
13	507.8	515.0		658.7
14	401.2	407.2	419.2	438.3
15	316.2	318.6	299.4	330.5
16	239.5	241.9	215.6	227.5
17	174.3	178.4	149.7	155.7
18	121	122.8	101.8	103.6
19	76.2	79.5	64.7	64.7
20	46.0	48.4	35.9	37.1

material at 580°C was to fully homogenize the bronze and then densify it completely before significant Nb_3Sn formation takes place. The subsequent final heat treatment at 700°C does not lead to the redevelopment of large areas of porosity. Thus the properties can be expected to be more uniform after HIP'ing. In Table II and Figure 4 a comparison is made of the 19 subelement material HIP'd and unHIP'd. This work which was reported some time ago (ref. 5), was performed at the Francis Bitter National Magnet Laboratory of the Massachusetts Institute of Technology (MIT) by Dr. M. Suenaga of the Brookhaven National Laboratory (BNL). While the data were limited, there appeared to be an additional residual effect of HIP'ing that, at high fields, overrides the improved J_c noted at fields below 15 T.

5.3 Jc vs axial strain

In order to seek an explanation for this, we compared J_c vs strain for HIP'd and unHIP'd NET subelement material, shown in Figures 5 & 6. Unfortunately comparisons of the 12 T data are the only ones that can be made from these figures. While the zero strain Jc's are only slightly different, the most interesting result of the NIST tests is the apparent enhancement of the irreversible strain ε_{irrev} as a result of HIP'ing at the intermediate temperature of 580°C. The irreversible strain limit for permanent damage was increased from 0.9% in the unHIP'd material to 1.4% in the material that was HIP'd at 580°C. This corresponds to an enhancement of the *intrinsic* irreversible strain ($\equiv \varepsilon_{irrev} - \varepsilon_m$) increase from 0.6% to over 1.1% - essentially a doubling. A similar effect was found by Ekin some years ago on Japanese material, HIP'd after the final heat treatment (ref. 8)

The "n" values showed that at 12 T, HIP'd material had a value of 22 as compared with 17 in the unHIP'd material.

The aim would be to HIP the cabled material after the bronze has been homogenized and before the cable is introduced into the conduit. The chrome plating would prevent sintering and, if the amount of Nb_3Sn reaction is small, the brittleness of the high tin bronze may not cause damage that cannot be healed during final reaction heat treatment. Experiments are underway to determine if such a treatment can be performed
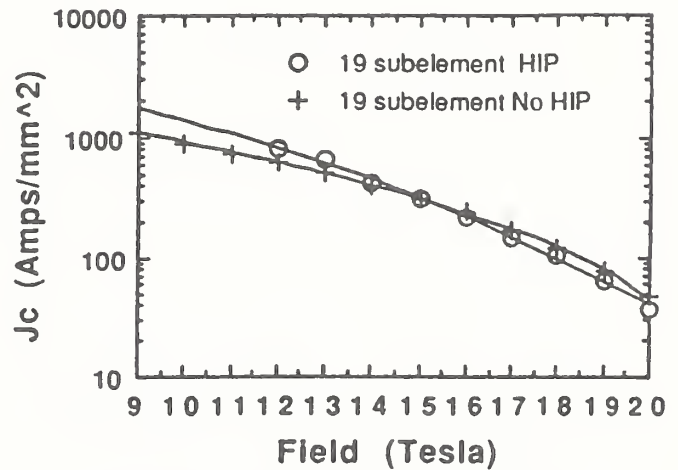
Figure 4. Comparison of J_c in HIP'd and unHIP'd 19 subelement material.
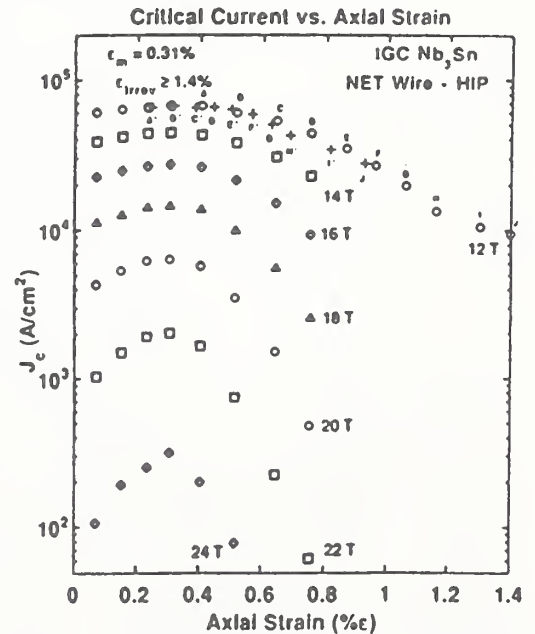
Figure 5. J_c vs. axial strain for HIP'd 19 subelement wire. ε_{irrev} is the irreversible strain and ε_m is the strain where J_c is a maximum.

85
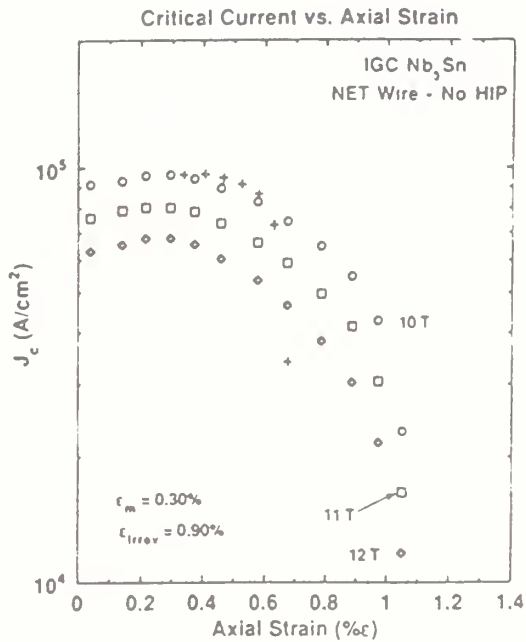
Figure 6. J_c vs. Axial Strain for unHIP'd 19 subelement wire.

practically. When the cable is in the homogenized condition rather than the reacted one, it should be much easier to handle without causing permanent damage.

The extent to which HIP'ing increases the ac losses is also being investigated. Significantly more bridging occurs in the HIP'd material than in the unHIP'd material as can be seen in Figures 7 & 8. Tentative results of squid magnetometer work on HIP'd and un-HIP'd material is shown in Figure 9. The work was carried out at BNL by Dr. M. Suenaga
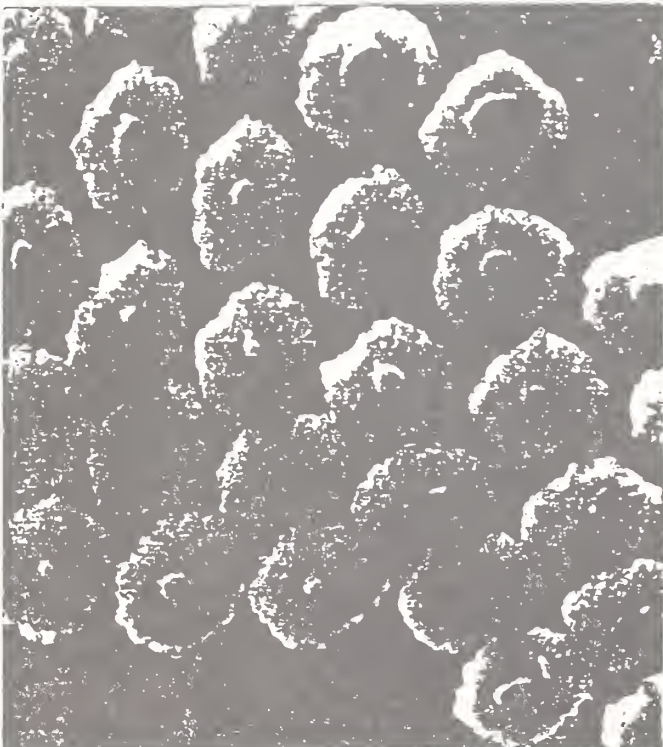
Figure 7 Cross section of filaments in HIP'd material after reaction

Figure 8 Cross section of filaments in unHIP'd material after reaction
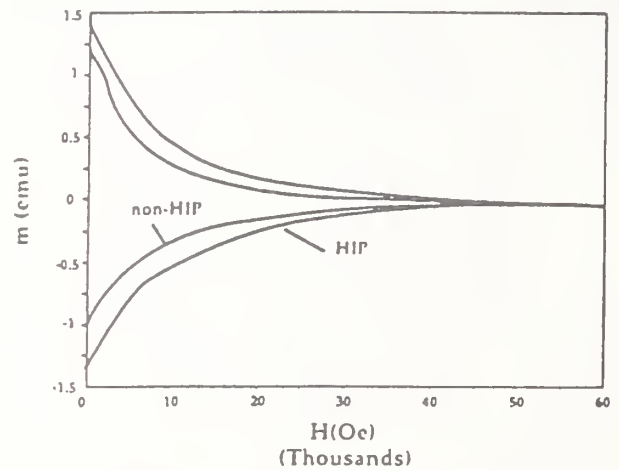
Figure 9 Comparison of hysteresis measurements on HIP'd and unHIP'd materials

6 . CONCLUSIONS

The poor RRR values obtained after prolonged heat treatments appear to be related to contaminants in the Cr plating bath and methods of improving the cleanliness of the process and the use of alternative insulation techniques are being explored.

It has been shown that the 19 subelement material with an extruded Ta barrier and no copper ring immediately under it, can be successfully fabricated to the NET size and beyond without problems. It is expected that this material will meet the NET J_c specification with a comfortable margin. The material is already within the NET specification for losses, (Table 1).

There are indications that HIP'ing the 19 subelement material at 580°C doubles the intrinsic irreversible strain as measured in tensile tests. Investigations are being carried out to determine the extent to which HIP'ing improves J_c, "n", and reliability of properties along the length of the wires. Also work is being carried out to determine the extent to which wires and cables can be handled after HIP'ing at intermediate temperatures without creating permanent damage.

ACKNOWLEDGMENTS

REFERENCES

1. J.E. Kunzler, E. Buehler, F.S.L. Hsu and J.H. Wernick, Phys. Rev. Lett, 1961, Vol 6 p 86.
2. R.E. Schwall, G. M. Ozeryansky, D.W. Hazelton, S.F. Cogan and R.M. Rose, "Properties and Performance of High Current Density Sn-Core Process MF Nb3Sn", IEEE Trans. ,MAG-19, 3, pp. 1135-1138, (1983).
3. E. Gregory, G.M. Ozeryansky, R.M. Schaedler, H.C. Kanithi and B.A. Zeitlin, "An Internal Tin Conductor with Nb 1 wt. % Ti Filaments", Adv. in Cryo. Eng. Vol. 36 pp. 147-155, eds. R.P. Reed and F.R. Fickett, Plenum Press, New York, NY, 1990.
4. E. Gregory, G.M. Ozeryansky, and B.A. Zeitlin, "Improvement of the structure and properties of internal tin Nb3Sn, Adv. in Cryo. Eng. Vol. 38b pp. 579-586 eds. F.R. Fickett and R.P. Reed , Plenum Press, New York, NY, 1992.
5. E. Gregory, G.M. Ozeryansky, and M. Suenaga, "Some effects of porosity and HIP'ing on critical currents in internal tin-processed multifilamentary Nb3Sn wires", 7th US-Japan Workshop on High Field Superconductors, Fukuoka, 21-23 Oct. 1991.
6. L.T. Summers, A.R. Duenas and C.E. Karlsen, G.M. Ozeryansky and E. Gregory, "A Characterization of Internal -Sn Nb3Sn Superconductors for use in the Proof of Principles (POP) Coil", IEEE Trans. 27, 2, pp. 1763-1766, (1991).
7. W.D. Markiewicz, G.M. Ciancetta, A.W. Grandin, D.W. Hazelton, and H.P. Hwang, "20 T Model Coil for a Very High Field NMR Spectrometer Magnet", Adv. in Cryo. Eng. Vol. 37a pp. 361-368 ed.. R.W. Fast, Plenum Press, New York, NY, 1992.
8. J.W. Ekin 5th US-Japan Workshop on High Field Superconductors, Tsukuba, Japan, 1987

VAMAS INTERCOMPARISON OF CRITICAL CURRENT MEASUREMENT IN Nb$_3$Sn WIRES

K. Tachikawa*, K. Itoh**, H. Wada**, D. Gould***, H. Jones[+],
C.R. Walters[++], L.F. Goodrich[+++], J.W. Ekin[+++] and S.L. Bray[+++]

*Tokai University, Hiratsuka, Kanagawa 259-12, Japan
**National research Institute for Metals, Tsukuba, Ibaraki 305, Japan
***Commission of the European Communities, Brussels, B-1049, Belgium
+Clarendon Laboratory, Oxford, OX1 3PU, United Kingdom
++Rutherford Appleton Laboratory, Didcot, OX11 0QX, United Kingdom
+++National Bureau of Standards, Boulder, Co 80303, USA

Abstract

The VAMAS technical working party in the area of superconducting and cryogenic structural materials has recently carried out the first world-wide intercomparison of critical current, I_c, measurement on multifilamentary Nb$_3$Sn wires. Three sample wires were supplied from each of EC (European Communities), Japan and USA. The total number of participant labs were 24 (EC 11, Japan 8 and USA 5). There were few restrictions for the I_c measurement at participant labs. The standard deviations of the I_c values reported from these labs varied among test samples, and were 6-21% of averaged I_c's at 12 Tesla.

Introduction

The superconductivity technology may have tremendous impact on important areas of science and technology and should be developed under the concept of the long term project whereby international cooperation would play an essential role. This is the underlying idea in the VAMAS which stands for the Versailles Projects among summit participant countries on Advanced Materials and Standards.[1] The VAMAS Technical Working Party (TWP) on superconducting and cryogenic structural materials consists of representatives of participant countries. The TWP has carried out an intercomparison on the critical current, I_c, measurement in Nb$_3$Sn multifilamentary wires: I_c is the most important superconducting parameter from the practical point of view.

The purpose of the present intercomparison (round robin) test on I_c is to identify parameters affecting the I_c by accumulating and evaluating the measurement results. The eventual goal of the research is to provide recommendations for the performance of short sample critical-current measurements of Nb$_3$Sn superconductors.

Participants, Samples and Test Procedure

11 EC, 8 Japanese and 5 US laboratories listed in Table I have participated in the round robin test on the I_c. The distribution of test samples and accumulation of resulting I_c data in EC, Japan and USA were performed by the respective central labs; BCMN(Belgium), NRIM, and NBS.

Multifilamentary Nb$_3$Sn wires with relatively small current carrying capacity (<500 A at 8 Tesla) were chosen as the test samples which could easily be tested at any participant laboratory. Three sample wires were supplied, one from each of EC, Japan and USA; these samples are labeled disorderly just as sample A, B and C in this paper.

Sample A fabricated by a bronze method has a wire diameter of 0.8 mm and 114 sub-bundles each containing 90 Nb-Ta filaments in a bronze matrix. The Cu stabilizer is located at the center of the wire and separated from the filament region by a Ta barrier. The volume fraction of Cu stabilizer in the wire is much smaller compared to those in other 2 samples.

Sample B has a wire diameter of 1.0 mm and 7 sub-bundles each separated by a Nb barrier from the Cu stabilizer outside. Each sub-bundle contains 721 Nb filaments in a Cu-Sn-Ti alloy matrix. This sample was also fabricated by a bronze process.

Sample C prepared by an internal-Sn diffusion method has a wire diameter of 0.68 mm and 37 sub-bundles each containing 150 Nb filaments. The filament region is separated from the outer layer of Cu by a single Ta barrier.

Specifications and the cross sectional views of these samples are given in Fig 1. Upper critical fields, H_{c2}, for sample A and sample B are enhanced by

Table I. Participant laboratories in I_c round robin test.

Europe (11)
Atominstitut der Oesterreichischen Univ. (Austria)
Inst. Experimental Physik, Oester. Univ. (Austria)
S.C.K./C.E.N (Belgium)
S.N.C.I., C.N.R.S. (France)
Kernforschungszentrum Karlsruhe (FRG)
Siemens AG (FRG)
Vacuumschmelze GmbH (FRG)
E.N.E.A, Centro di Frascati (Italy)
High Field Magnet Lab., U. Nijmegen (Netherlands)
Clarendon Laboratory (UK)
Rutherford Appleton Laboratory (UK)

Japan (8)
Electrotechnical Laboratory
Furukawa Electric Co., Ltd.
Hitachi Ltd.
I.M.R., Tohoku University
I.S.I.R., Osaka University
Japan Atomic Energy Research Institute
Kobe Steel, Ltd.
National Research Institute for Metals

USA (5)
Brookhaven National Laboratory
F.B.N.M.L., Massachusetts Institute of Technology
Lawrence Livermore National Laboratory
National Bureau of Standards
University of Wisconsin

additions of Ta and Ti, respectively.

Specimen wires from these samples, each several meters long, were distributed to participant labs through relevant central labs. Such wires were cut into parts as specimens at each participant lab and one specimen, wound on a heat treatment holder of drum shape, was collected from participant labs and heat treated at the relevant central labs (central reaction). The reacted specimens were then returned to the participant labs for measurements. In some cases, the participant labs also performed their own heat treatments on additional specimens of the samples (self reaction). The self reaction of samples was not possible at all labs.

Specifications of heat treatment holders were different from lab to lab. At most of the labs stainless steel tubes with a spiral groove on the outer surface were used to have a definite coil pitch. The surfaces of such tubes were usually coated with ceramics or oxidized prior to specimen mounting, in order to avoid reaction of the specimen with the holder. At some labs the same holders were used for both heat treatment and measurement, thereby reducing the possibility to damage the specimen by handling.

Central reaction was carried out in the following manner. For samples A and B, all specimens were heat treated in one vacuum furnace at once. The temperature of the furnaces was well controlled within ± 5 °C with time and in space. For sample C, specimens were individually heat treated in a dynamic vacuum. Both ends of a specimen of internal-Sn processed sample C were extended to a position where the temperature was kept below the melting point of Sn in order to avoid the outflow of molten Sn from the wire. The heat treatment conditions for samples A, B and C were 700 °C for 96hr, 670 °C for 200hr and 700 °C for 48hr, respectively.

More than half of self reactions were done in vacuum. At other labs specimens were encapsulated and heat treated in an argon or a hydrogen atmosphere. The

heat treatment temperature was also well regulated in the self reaction.

### Apparatuses and Measurement Conditions

Informations about measurement apparatuses and experimental conditions at each laboratory were described in formatted sheets prepared and distributed prior to the measurements.

At most of participant labs superconducting solenoid magnets were used to generate fields of 8-16.5 Tesla. At some labs copper solenoid magnets or hybrid type magnets were used which can generate fields over 20 Tesla. In any of these magnets rms ripple fields which may cause heat generation in the specimen, were less than 0.1% of the field generated. Field determination was carried out by means of NMR, Hall probe or rotating coil magnetometer, with estimated accuracies of 0.1% to 1%.

At most of the labs transistor type power sources were used to supply electric currents to the specimen. rms ripple noises were less than 0.1% of the full power. The accuracy of current determination was within 0.5% at most of the labs. In order to amplify the voltage signals generated in the specimen, nanovoltmeters were used at most of the labs. At some labs the signals were directly led to high sensitive XY recorders. The typical level of noises observed varied from 0.01 µV to 2 µV, depending on the apparatuses used.

The total length of a specimen, the distance between voltage taps and the distance between a current tap and its nearest voltage tap were much varied among labs. The shortest specimen used in a lab had a total length of about 215 mm and 1.5 turns of winding on the measurement holder. The longest specimen used was 2000 mm long and had 30 turns on the holder.

The variety of materials, e.g., fiberglass reinforced plastic (FRP), stainless steel, alumina, hastelloy and brass were used as the measurement holder. The
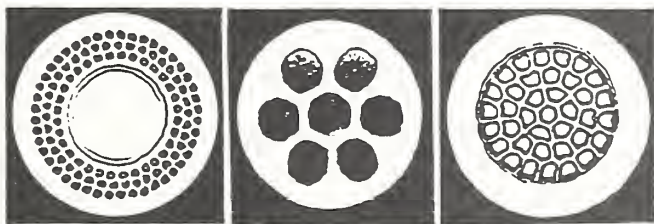
	sample A	sample B	sample C
Fabrication Method	Bronze	Bronze	Internal Sn
Wire Diameter (mm)	0.8	1.0	0.68
Structure	NbTa/CuSn	Nb/CuSnTi	Nb/Cu/Sn
Cu/non-Cu	0.22	1.68	0.88
Bronze/Cores	2.8	2.5	3.1
Filament Diam.(µm)	3.6	4.5	2.7
No. Filaments	10,000	5,047	5,550
Heat Treatment	700 C	670 C	700 C
	96h	200h	48h

Fig.1 Specifications and cross sectional views of round robin test samples.

Table II. Homogeneity study on sample A at SCK/CEN. Averages and standard deviations of I_c's for fields of 7-10 Tesla.

Field (Tesla)	7	8	9	10
Average (A)	424.5	354.8	296.6	246.4
Std. Dev. (A)	6.0	5.8	5.0	5.8
Std.Dev/Ave(%)	1.5	1.7	1.7	2.4

Table III. Homogeneity study on sample B at Clarendon Lab. Averages and standard deviations of I_c's for fields of 8-14 Tesla.

Field (Tesla)	8	10	12	14
Average (A)	303.8	214.1	150.9	102.3
Std. Dev. (A)	2.5	2.8	1.6	1.0
Std.Dev/Ave(%)	0.8	1.3	1.0	1.0

holders had ring or bar shaped current terminals of copper. Most of holders had a spiral groove on them. The specimen was mounted in a groove on the holder with both ends soldered to current terminals, and fixed using a bond such as grease, varnish, epoxy, and solder. In some cases no bond was used.

The Lorentz force caused by the interaction of the transport current with the applied field has an essential effect on the I_c. This force acts as a tensile or compressive stress to specimen when the spiral specimen generates a central field parallel or antiparallel to the direction of the applied field. At most labs, the direction of both fields were antiparallel. The effect of the field direction on the I_c was examined at several labs.

The I_c was defined at a current where a certain voltage gradient or a certain resistivity appeared along the superconducting specimen. Values of I_c at 5, 10, and 100 μV/m and at integer numbers of magnetic fields were requested to be reported in the present round robin test; I_c values at 10^{-14} and 10^{-13} Ωm were optional.

The relationship between the voltage V, and the transport current, I is empirically expressed as
$$V \propto I^n$$
where the exponent n is nearly constant in the small voltage region. A larger n corresponds to a sharper transition in the specimen. n values were also requested to be reported. In the case where n values were not reported by the participant, they were estimated by using the following relation,
$$n = 1/\log I_c(100\mu V/m)/I_c(10\mu V/m).$$

Homogeneity Study

As the purpose of this test was the intercomparison of results obtained at different labs, it was absolutely important that all the test specimens supplied should have identical superconducting properties. It is difficult, however, to fabricate a sample with homogeneous properties along the whole length of a wire because of the complicated structure of Nb_3Sn multifilamentary composite. The homogeneity in superconducting properties was examined on sample A at SCK/CEN and on sample B at Clarendon Lab.

The homogeneity study at SCK/CEN was performed on 21 specimens of sample A. Specimens were taken from the various parts of a test wire, each wound on a holder and heat treated at Rutherford Lab together with those of central reaction. The I_c measurement was carried out at 4.3 K and at 7-10 Tesla.

115 I_c data defined at a voltage of 10 μV/m for 21 specimens were analyzed at SCK/CEN. For voltages larger than 10μV/m specimens showed a tendency to quenching. 15 specimens quenched under a voltage of 10μV/m. The quench currents were usually lower compared to the true I_c's expected, and were not taken into account in the statistical treatment of the I_c data. For each magnetic field averages and standard deviations of I_c's were calculated according to the 10μV/m voltage and listed in Table II. Standard deviations are 2.4% of average of I_c's at 10 Tesla and decrease to 1.5% at 7 Tesla.

The homogeneity in sample B was examined at Clarendon Lab. 7 specimens were taken from the test wire, each mounted onto a stainless steel holder, and heat treated at Rutherford Lab altogether in a furnace. The I_c measurements were carried out at 4.2 K and at 7-15 Tesla. Averaged I_c's at a voltage of 10 μV/m and standard deviations are summarized in Table III.

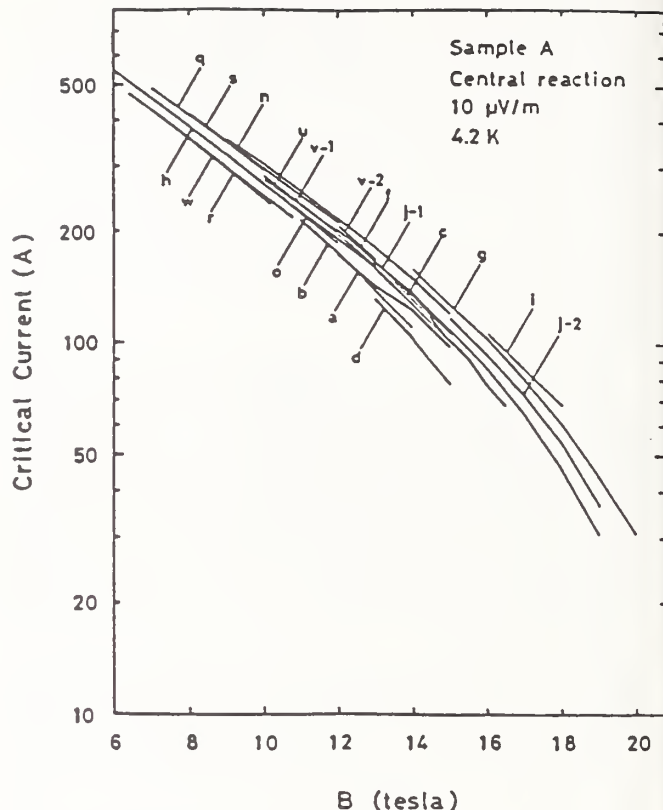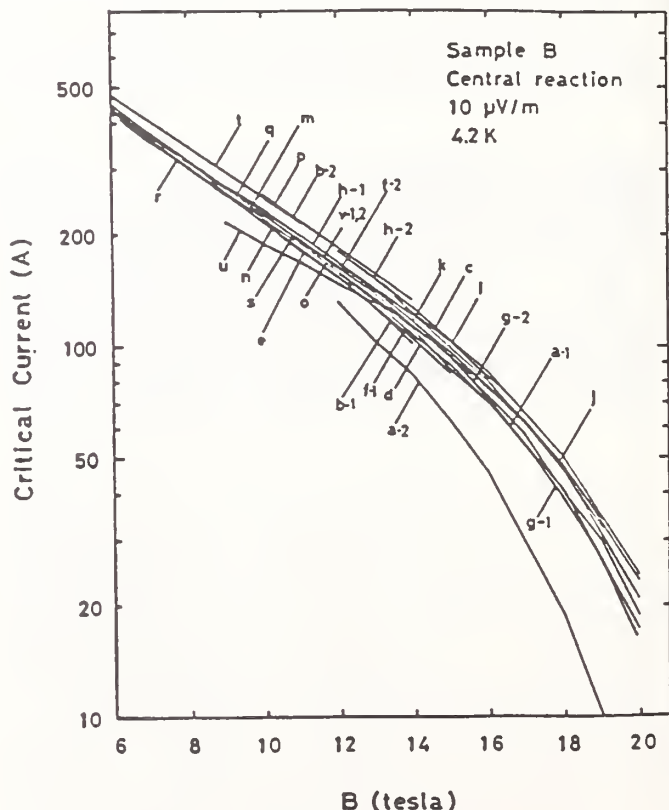Fig.2 I_c's at 10 μV/m as a function of field for sample A of central reaction; results of participant labs.

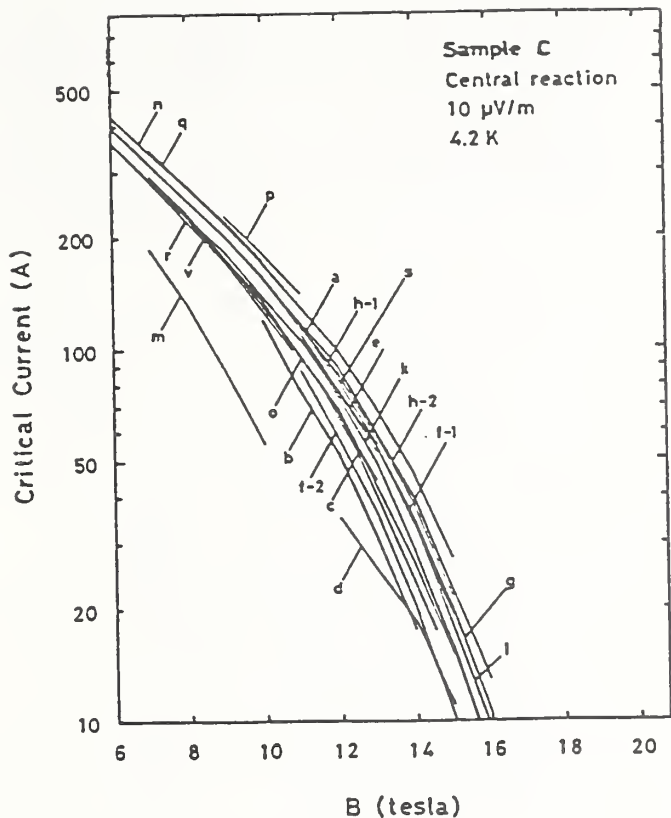Fig.3 I_c's at 10 μV/m as a function of field for sample B of central reaction ; results of participant labs.

Fig.4 I_c's at 10 μV/m as a function of field for sample C of central reaction ; results of participant labs.

Standard deviations are within 1.3% at all fields.

Based on these homogeneity studies, it may be concluded that the present test samples A and B are rather homogeneous in superconducting properties over the whole length of wire and adequate for the round robin test. The homogeneity study has not yet been carried out on sample C.

Results of the Round Robin Test

In Figs 2, 3 and 4 I_c's at 10 μV/m are shown as a function of applied field for samples A, B and C, respectively. The name of labs is coded like a, b, c in no special order. These results were obtained in the antiparallel self field except for those of labs q and s.

The semilogarithmic plots show that for samples A and B the logs of the I_c decreases almost linearly with increasing field up to about 15 Tesla, and then drops off more rapidly above this field. I_c's in sample C decrease in a similar way but with a steeper slope, and start to drop off above about 12 Tesla. The averaged n values generally decrease with increasing magnetic field and are much more scattered than the I_c's, especially for sample A.

In Tables IV and V are shown averages and standard deviations of I_c data and n values obtained at participant labs, respectively. Four extraordinarily outlying data sets were excluded in the calculations because these data sets were obtained in cases where the specimens stuck to the reaction holders and were likely damaged in removal or for other similar reasons. There was no single magnetic field where all labs reported data on any sample. A future publication comparing all data sets at a single magnetic field, by means of a Kramer extrapolation method, is planned. Coefficients of variation of I_c's at 10 μV/m and 12 Tesla are about 7, 6 and 21 % of the averages for samples A, B and C of central reaction, respectively, and become larger at higher magnetic fields. These values are appreciably larger than those obtained in the homogeneity studies which are 2.4 and 1.3 % for samples A and B, respectively.

Table IV. Averages and standard deviations of critical currents at 10 μV/m for samples A, B and C of central reaction.

Field (Tesla)	sample A			sample B			sample C		
	No.	Ave. (A)	σ (A)	σ /Ave (%)	No.	Ave. (A)	σ (A)	σ /Ave (%)	No.	Ave (A)	σ (A)	σ /Ave (%)
6	1	544.1	0.0	0.0	4	447.4	18.7	4.2	3	393.8	25.7	6.5
7	4	447.9	26.2	5.9	7	372.2	15.4	4.1	7	309.3	24.3	7.9
8	5	388.7	21.8	5.6	8	315.2	13.0	4.1	6	248.6	20.8	8.4
9	7	327.4	23.3	7.1	10	265.3	11.1	4.2	9	197.3	20.6	10.4
10	9	277.1	18.0	6.5	15	229.1	13.1	5.7	11	150.0	18.5	12.3
11	7	234.4	14.3	6.1	13	195.3	12.6	6.5	13	106.9	16.2	15.1
12	11	195.7	13.6	6.9	17	163.6	10.4	6.3	16	72.5	15.2	20.9
13	10	158.0	14.5	9.2	14	134.6	7.2	5.3	13	45.4	10.7	23.6
14	10	130.5	15.5	11.9	16	114.3	7.8	6.8	13	30.0	8.4	28.0
15	10	106.7	12.9	12.1	12	92.2	5.0	5.4	10	16.9	5.0	29.4
16	6	91.9	10.8	11.8	10	75.8	4.8	6.4	7	8.5	2.6	30.5
17	3	71.8	6.3	8.8	4	57.5	2.5	4.4	2	3.4	0.2	6.4
18	4	57.4	9.0	15.7	7	43.7	2.6	8.4	2	2.1	0.7	33.7
19	3	36.8	5.3	14.4	4	30.6	2.6	8.4	1	1.0	0.0	0.0
20	2	26.4	4.4	16.7	5	19.4	2.7	13.9				

No:number of data,   σ :standard deviation,   σ /Ave:coefficient of variation

In Fig. 5 I_c's at 10 μV/m and at 12 Tesla reported from labs are compared. In cases no I_c values were reported at 12 T, they were estimated by extrapolations not exceeding 2 T. In the figure, $\Delta I_c/\sigma$ denotes the difference in I_c between lab and average normalized to the standard deviation, σ. Labs are arranged in incremental order of mean laboratory value of $\Delta I_c/\sigma$. The arrows attached to some of the data symbols indicate that these data actually lie either above or below the vertical limits of the plot. The maximum to minimum spread in I_c at each lab is almost within 2 times of σ, rather small compared to the total maximum to minimum spread (6 times of σ). These results clearly indicate systematic differences among the labs in the measured I_c of each sample. These differences may be due to the

Table V. Averages and standard deviations of n values for samples A, B and C of central reaction.

Field (Tesla)	sample A				sample B				sample C			
	No.	Ave.	σ	σ/Ave (%)	No.	Ave.	σ	σ/Ave (%)	No.	Ave	σ	σ/Ave (%)
6					4	37.2	2.4	6.5	3	32.2	2.8	8.5
7					6	39.3	5.0	12.8	7	32.8	7.6	23.3
8	4	78.3	33.9	43.4	8	36.8	5.6	15.2	6	32.5	4.9	14.9
9	5	87.8	38.5	43.8	10	34.2	4.5	13.1	9	28.6	3.5	12.1
10	7	58.0	21.4	36.9	13	32.6	5.5	16.8	11	26.7	5.2	19.3
11	6	50.0	23.3	46.7	13	32.3	8.2	25.3	13	26.8	8.8	32.8
12	9	52.7	18.7	35.5	17	30.3	6.6	21.8	16	21.9	7.7	35.0
13	8	43.9	16.5	37.7	15	28.3	7.5	26.7	13	18.7	7.4	39.7
14	7	35.1	14.8	42.3	16	27.8	6.2	22.2	13	14.5	5.1	34.9
15	6	37.3	13.1	35.1	12	28.1	5.1	18.0	10	12.4	3.5	28.5
16	3	33.0	3.6	10.8	10	25.9	4.0	15.4	7	10.5	2.7	25.5
17					4	24.2	5.3	21.9	2	8.8	1.6	17.7
18	1	22	0.0	0.0	7	20.6	4.3	20.9	3	6.3	0.7	10.8
19					4	19.0	3.5	18.2	1	5.2	0.0	0.0
20					5	12.8	2.3	17.8				

No:number of data, σ:standard deviation σ/Ave:coefficient of variation
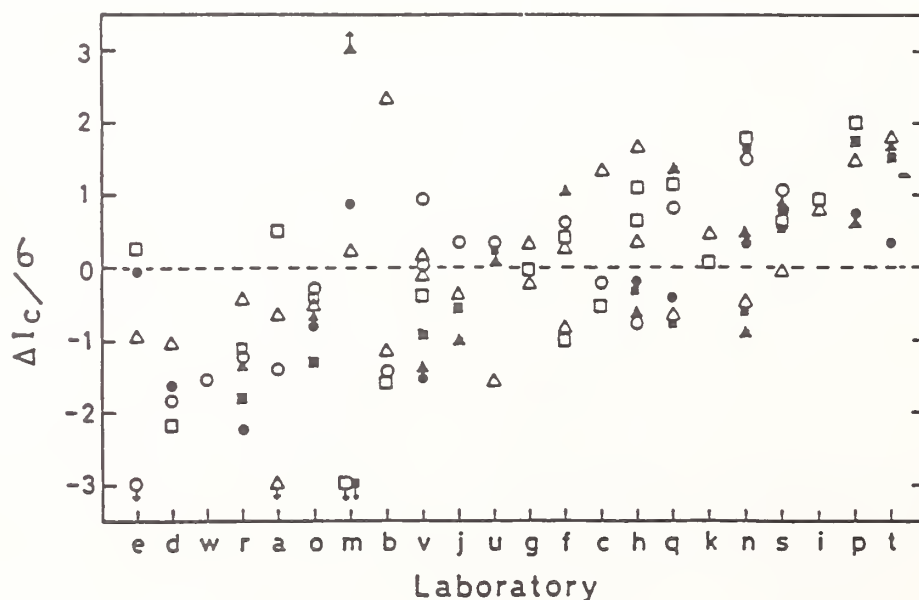
Fig. 5 Comparison of I_c's among participant labs at 12 T. Symbols (○, ●), (△, ▲) and (□, ■) refer to the samples A, B and C (central reaction, self reaction), respectively.

different sample holders, sample handling, the measurement method, and variations in instrument calibration. More detailed papers addressing these possible sources of systematic differences are planned for future publication.

The ratios of $I_c(\uparrow\uparrow)$ to $I_c(\uparrow\downarrow)$ are shown in Fig. 6 for sample B. $I_c(\uparrow\uparrow)$ and $I_c(\uparrow\downarrow)$ denote the I_c's for which the self and the applied fields are in parallel and antiparallel directions, respectively. If the specimen is tightly fixed on the holder, there should be no difference between $I_c(\uparrow\uparrow)$ and $I_c(\uparrow\downarrow)$, the ratio of $I_c(\uparrow\uparrow)$ to $I_c(\uparrow\downarrow)$ being unity. The tightness of the fixing depends on the bonding material and its amount. Epoxy resins such as 'stycast' seem to give better fixing than grease, as is apparently shown in Fig. 6. Some of the curves of the ratio $I_c(\uparrow\uparrow)/I_c(\uparrow\downarrow)$ drop below unity at higher fields in Fig. 6. If a specimen is uniformly deformed by concentric hoop stress, the ratio will approach unity as the field increases. Therefore, nonuniform deformation of specimen may result in the ratio less than unity.

In order to see if the 'self reaction' carried out at each lab was the exact copy of the 'central reaction', data of I_c's for two reactions were compared. This comparison between self and central reactions did not include all of the available data, but rather, it only included data from labs that measured both of their specimens on similar holders. Averaged I_c's of self reacted sample B are nearly the same as those of centrally reacted one. However, averaged I_c's of self reacted sample A are always smaller than those of centrally reacted one, while those of self reacted sample C are smaller at lower fields and larger at higher fields than those of centrally reacted one. These results indicate that I_c's of samples A and C are more sensitive to the heat treatment condition than those of sample B. The reaction time for sample C is the shortest of the three samples and, consequently, the sensitivity of sample C to both reaction time and temperature may be greater than for the other samples. Furthermore, sample C's apparent sensitivity to the reaction conditions may be due to an inadequate confinement of the internal tin at the specimen ends during the heat treatment. The coefficient of variation of I_c of self reacted samples, which may reflect the difference in reaction conditions among labs, correspond to 4-8 % of I_c almost independent of magnetic field and sample. The possibility of sample damage incurred during shipping is also a variable in the comparison between the self and central reactions.

Strain Effect

The tensile strain effect on I_c's were examined at NBS, Osaka Univ. and Rutherford Lab using the round robin test samples. Although the measurement details were different, there was good agreement among three sets of data. As examples, results for 14 Tesla at NBS and those for 15 Tesla at Osaka Univ. are compared in Fig. 7 where I_c's have been normalized to the maximum values. The I_c of Nb_3Sn conductor increases with increasing tensile strain up to 0.2-0.3% where the precompressive strain imposed on the Nb_3Sn compound is mostly released. As can be seen in this figure, the tensile stain sensitivity of I_c is largest for sample C and relatively small for sample B. This may be related partly to the H_{c2} of these samples; sample C has a relatively low H_{c2} of ~19 Tesla, while it is ~24 Tesla for samples A and B. A more complete comparison of the strain effect data will be the subject of a future paper.

Effects of the thickness of the FRP holder on the I_c were examined at NBS[2] using specimens of samples B and
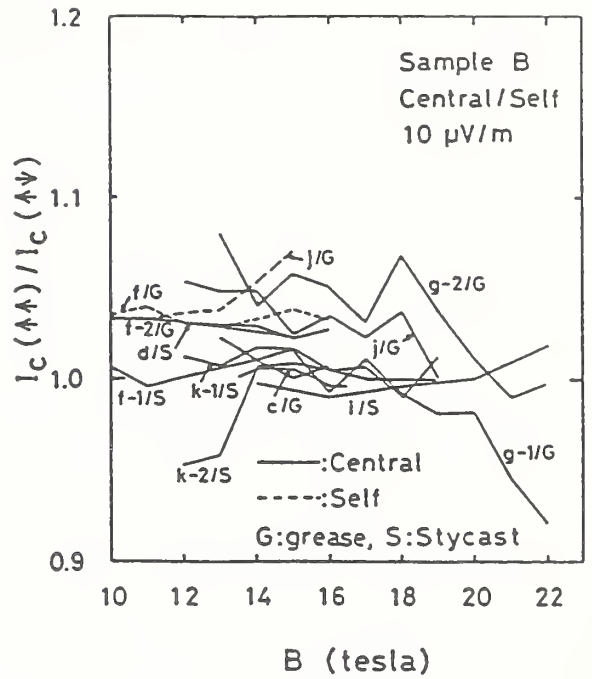

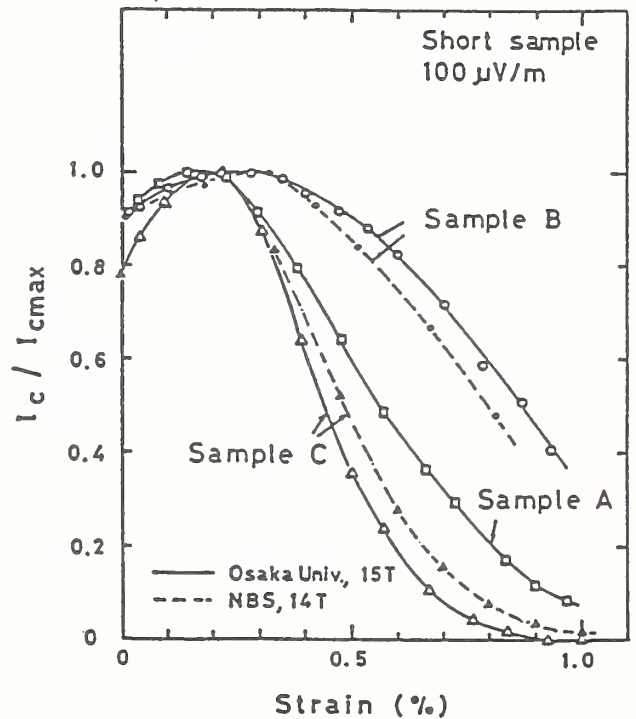Fig.6 Ratio, $I_c(\uparrow\uparrow)/I_c(\uparrow\downarrow)$ vs. field curves for sample B.

Fig.7 I_c vs. strain curves for samples A, B and C obtained at NBS and Osaka Univ. I_c is normalized to its maximum value.

C. Specimens were first mounted on thick walled FRP
holders. After the I_c measurement the holders were
bored so as to have thin walls. It was found that I_c's
for these bored holders with thin walls were slightly
enhanced. The thermal contractions of thick and thin
wall holders are different due to the textured struc-
ture of FRP, and estimated to be about 0.4% for thick
wall and about 0.25% for thin wall on cooling from room
temperature to 4.2K. It was concluded that the com-
pressive strain in the specimen resulting from the
thermal differential contraction between the FRP holder
and the specimen was responsible for the discrepancy in
I_c in those specimens mounted on thick and thin wall
holders.

The sample holder material and geometry, in conjunc-
tion with the specimen bonding method, can have an ef-
fect on the strain state of the specimen and this will
have a significant effect on the results of the I_c
measurements. Thus, this could be a major source of
the observed systematic variation in the measured I_c's.

Conclusions

Results of the present round robin test may be sum-
marized as follows.

a) Homogeneity test on the I_c showed the present
   samples were enough homogeneous along the whole
   length of wire to be used in the round robin test.

b) Coefficients of variation of I_c's were 7%, 6% and
   21% at 12 Tesla for samples A, B and C, respec-
   tively. They were largest for sample C which was
   most sensitive to strain and heat treatment condi-
   tions. Coefficient of variation increased at higher
   fields for all of samples.

c) n values showed larger coefficient of variation than
   I_c. n values were rather small in case the specimen
   was soldered on a metallic holder.

d) Strain effects on the I_c of three wires were ex-
   amined. It was pointed out that the strain in the
   specimen was a major origin for the scatter in I_c.

e) Materials of the specimen holder and tightness of
   fixing have significant effects on the I_c through
   the strain effect.

Several parameters influencing the I_c value of Nb_3Sn
wires have been extracted and analyzed through the
VAMAS round robin test. However, the present round
robin test was performed with few restrictions on the
measurement method, and more strict determination of
measurement conditions will be required to minimize the
scatter in I_c and to furnish a really effective stand-
ard method of the I_c measurement.

A more complete report on the present round robin
test will be submitted to the steering committee of
VAMAS from the Technical Working Party. A number of
papers addressing specific aspects of this round robin
test are planned for future publication.

Trade names are used in this document to specify the
measurement details. In no instance does this iden-
tification imply endorsement by the authors or their
institutions, nor does it imply that the particular
products are necessarily the best available.

The authors wish to thank all the scientists and
representatives who have been involved in the present
round robin test for their cooperation.

References

[1] H. Jones, "First Meeting of the VAMAS Technical
Working Party on Superconductors and Cryogenic
Structural Materials", Cryogenics, vol. 26, pp.
488-489, August (1986).

[2] L.F. Goodrich and S.L. Bray, "Critical-Current
Measurements of Nb_3Sn Superconductors: NBS Con-
tribution to the VAMAS Interlaboratory Comparison",
submitted for publication in Cryogenics.

VAMAS Interlaboratory Comparisons of
Critical Current vs. Strain in Nb$_3$Sn

J. W. Ekin
National Inst. of Standards and Technology
Electromagnetic Technology Division
Boulder, Colorado 80303

Abstract

A comparison is made of measurements of the effect of axial tensile strain on the critical current of multifilamentary Nb$_3$Sn superconductors by three different laboratories. Two of the laboratories used short sample testing apparatus wherein a straight section of conductor was cooled in a force-free state. One of the laboratories used a spring apparatus wherein a long sample was reacted in a coil shape and attached to a spring sample holder. The agreement between the results for the two laboratories that used the straight sample apparatus was quite good, within 15% for all three conductors at 15 T, except at very high strain for one conductor which had an upper critical field close to the measurement field. To make a comparison with the data obtained using the spring method, it was necessary to fit the data to the compressive prestrain determined using the straight-sample technique. With such a fit, the agreement was variable, between 15 and 25% depending on the conductor. Values of the prestrain and irreversible strain obtained from the straight sample data agreed within 0.06% and 0.05% respectively. Values of the maximum (strain-free) upper critical fields agreed within several tenths of a tesla.

During the course of the VAMAS interlaboratory testing of the critical current density J_c of Nb$_3$Sn multifilamentary superconductors, the effect of axial tensile strain on J_c was measured by three laboratories. This paper presents a brief comparison of those results.

Three conductors designated as A, B, and C were tested. Details of the wire characteristics are given in Ref. 1. Three laboratories participated in the testing. Laboratories I and II used a short-sample testing apparatus wherein a straight section of conductor was cooled in a force-free state, and then axial tensile strain was applied and measured using custom low-force strain extensometers. Laboratory III used a spring apparatus wherein a long sample was reacted in a coil shape and attached to a spring sample holder. The spring was then bent, tightening the sample against the spring, which would then applied tensile strain to the sample. The

advantages of the spring method are that the long sample length allows J_c to be measured directly at more sensitive criterion levels and permits sampling J_c over a longer sample length; the disadvantages are that the prestrain value cannot be measured because of differential thermal contaction between the spring material and superconductor, and variable bending strain can be introduced into the sample from the tightening of the sample onto the spring as it is initally bent.

The results from laboratory I were obtained at 15 T only, so this was chosen as the field for comparison of results. The results from laboratories II and III were measured as a function of magnetic field. However laboratory II's results were obtained at even values of the fields only, so the 14 T and 16 T results were used to interpolate the results at 15 T using the strain scaling law.[2]
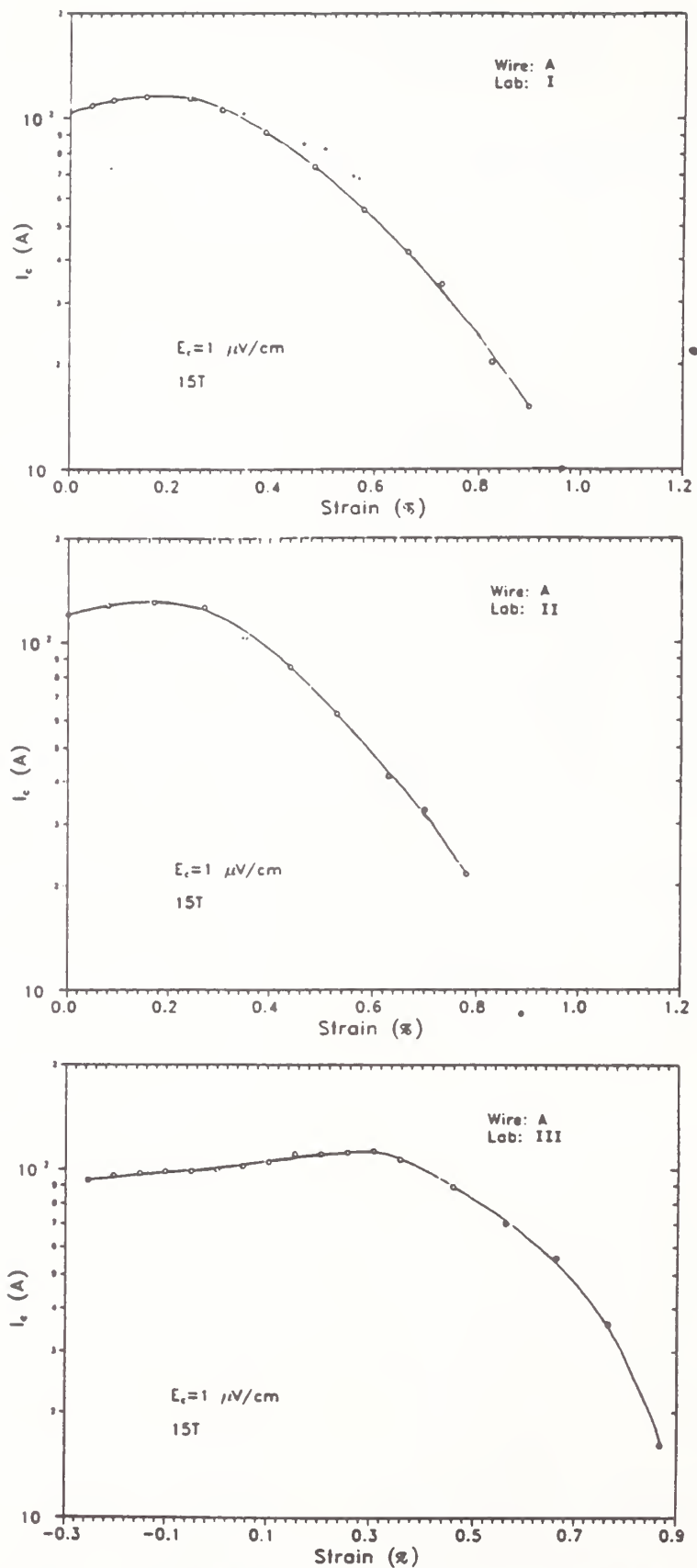
Fig. 1 J_c vs. strain characteristic for conductor A, as measured using short-sample apparatus with force free cooling (laboratories I & II) and long-sample spring method (laboratory III). Unloaded J_c data are denoted by the symbol x.
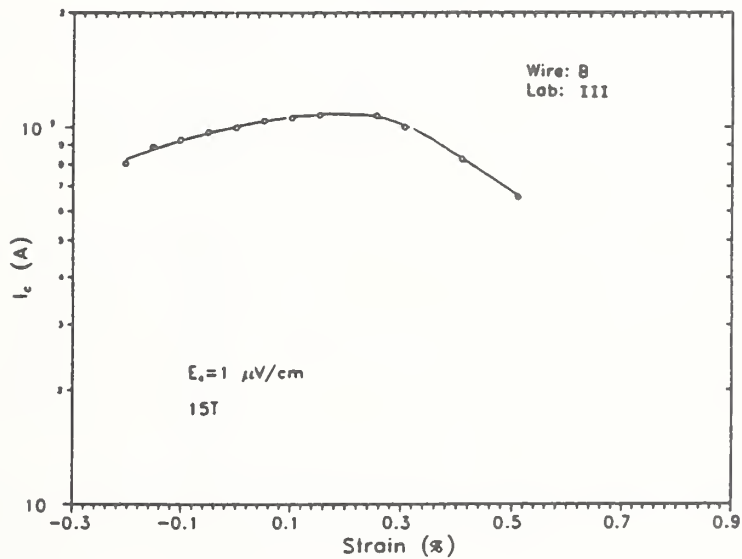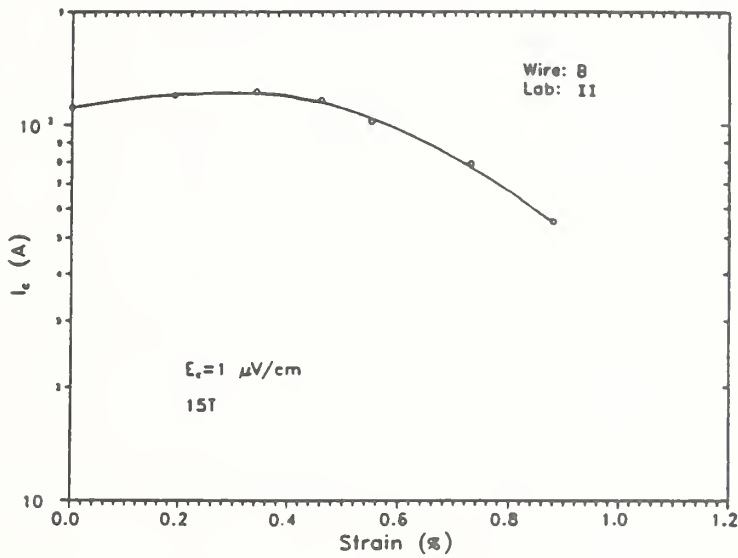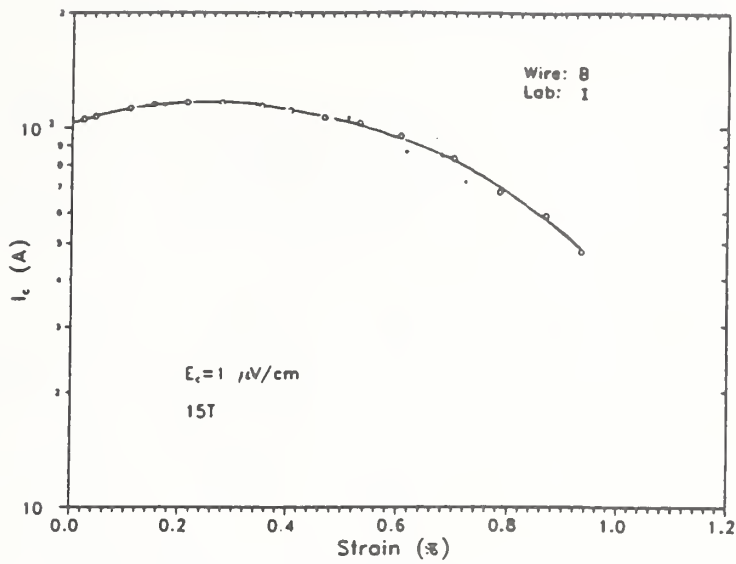
Fig. 2 J_c vs. strain characteristic for conductor B, as measured by laboratories I, II, & III.

Table I. Comparison of Electromechanical Parameters

Conductor	Meas. Lab.	ε_m	ε_{irrev}	$\varepsilon_{o,irrev}$	B^*_{c2m}
	I	0.18%	≥0.97%	≥0.79%	--
A	II	0.18%	≥0.80%	≥0.62%	24.6 T
	III	--	--	--	24.5 T
	I	0.25%	0.85	0.6%	--
B	II	0.31%	0.82%	0.51%	25.7 T
	III	--	--	--	26.2 T
	I	0.20%	≥1.08%	≥0.88%	--
C	II	0.21%	1.10%	0.89%	--
	III	--	--	--	--
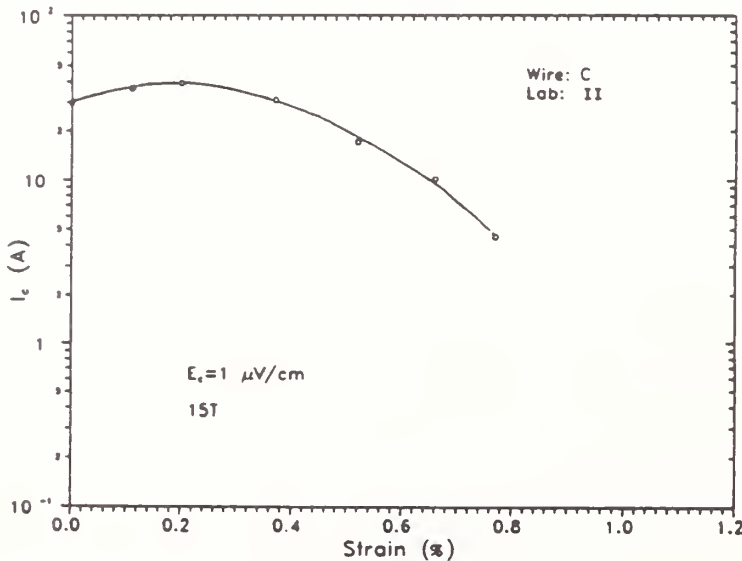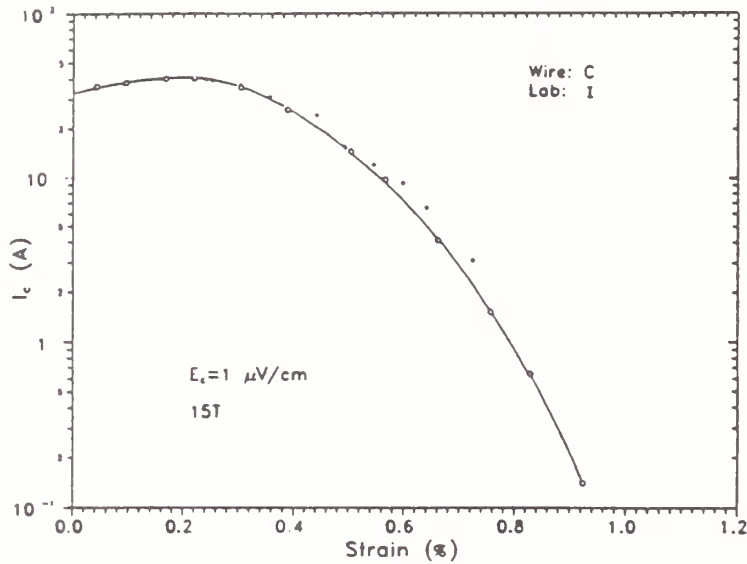
Fig. 3 J_c vs. strain characteristic for conductor C, as measured by laboratories I and II.

Figs. 1a-1c show the comparison of results for conductor A obtained by all three laboratories. Figs. 2a-2c compare the results for conductor B, and Figs. 3a-3b show the results for conductor C.

The agreement between laboratories I and II is quite good, within 15% for all three conductors at 15 T, except at very high strain for conductor C where the initially low value of B_{c2} resulted in B_{c2} being degraded to the point that it approached 15 T. In this case, the interpolation and measurement errors become extreme because of the rapid change of J_c near B_{c2}. Overall an agreement within 15% at such a high fields is considered to be fairly good considering the mechanical nature of the measurements, range of data, and types of conductor tested.

To make a comparison with the data from laboratory III, it was necessary to fit the data to the prestrain ϵ_m values determined by laboratories I and II, which used the force-free cooling technique. With such a fit, the data from laboratory III agreed within 15% for the conductor A and within 25% for conductor B.

The agreement of the strain sensitivity (slope of the J_c vs. strain curve) for laboratory III compared with I and II was variable, well matched for one conductor, Fig. 1, but not for the other, Fig. 2.

Values of the prestrain[3] ϵ_m, irreversible strain[4] ϵ_{irrev}, and intrinsic irreversible strain[5] $\epsilon_{o,irrev} = \epsilon_{irrev} - \epsilon_m$ were obtained from the data for laboratories I and II and are compared in Table I.

The prestrain values agreed within 0.06%. The comparison of irreversible strain values is more limited, but where directly measured (conductor B) the agreement was well within 0.05% (which is also consistent with the lower limit data available for conductors A and C).

Values of the maximum (strain-free) B_{c2m}^* for each sample are also shown in the last column of Table I for laboratories II and III. (A maximum B_{c2m}^* value for laboratory I could not be determined since data were available at only one field.) The maximum B_{c2m}^* values determined from the data of laboratories II and III agreed within several tenths of a tesla.

References

1. K. Tachikawa, K. Itoh, H. Wada, D. Gould, H. Jones, C. R. Walters, L. F. Goodrich, J. W. Ekin, and S. L. Bray, IEEE Trans. Mag. MAG-25(2), 2368 (1989).

2. J. W. Ekin, Cryogenics 20, 611 (1980).

3. G. Rupp, IEEE Trans. Mag. MAG-13, 1565 (1977).

4. J. W. Ekin, IEEE Trans. Mag. MAG-15, 197 (1979).

5. J. W. Ekin, Adv. in Cryo. Eng. 30, 823 (1984)

STRAIN EFFECTS IN VAMAS ROUND ROBIN TEST WIRES

K. Katagiri, K. Saito, M. Ohgami, T. Okada, A.Nagata+, K. Noto++,
K. Watanabe+++, K. Itoh*, H. Wada* K. Tachikawa**, J.W. Ekin†,
and C.R. Walters††,

ISIR, Osaka University, Ibaraki, Osaka 567, Japan

+Fac. Mining, Akita University, Akita 010, Japan

++Fac. Eng., Iwate University, Morioka, Iwate 020, Japan

+++IMR, Tohoku University, Sendai, Miyagi 980, Japan

*Nat. Res. Inst. Metals, Tsukuba, Ibaraki 305, Japan

**Fac. Eng., Tokai University, Hiratsuka, Kanagawa 259-12, Japan

†Nat. Inst. Stand. Tech., Boulder, CO 80303, USA

††Rutherford Appleton Lab., Didcot, OX11 0QX, UK

ABSTRACT

The strain characteristics of critical current, I_c, in three kinds of
VAMAS round robin test wires were evaluated. The multifilamentary Nb3Sn
samples measured are: bronze route Ta added and internally stabilized wire
A, Ti added and externally stabilized wire B and internal tin diffusion
processed wire C, respectively. The strain for I_c peak ranged 0.20-0.30 %
and the reversible strain limit 0.8-1.1 %. The results obtained at 15 T in
three institutes, NIST, Rutherford Lab. and Osaka/Tohoku Univ., are
compared. Fairly good agreement was obtained. The strain sensitivity was
higher in the order of C, A and B. This can be mainly attributed to the
effect of addition of the third element. The correlation between the
strain sensitivity and the scatter of critical currents measured in the
round robin test participant laboratories is briefly discussed.

INTRODUCTION

Interlaboratory comparison of the critical current, I_c, measurements
using common multifilamentary Nb3Sn sample superconducting wires (round
robin test) have been successfully carried out as an activity of VAMAS
(Versailles Project on Advanced Materials and Standards).[1-3]   The summary
report suggested that there exists a strong correlation between the scatter
of I_c values and strain effects associated with the measurements.   This
paper describes interlaboratory comparisons of the strain effects of VAMAS
wires measured in three laboratories and discusses how strain effects in the
conductor influence I_c measurements.

61

Table 1.   Specication of samples

	Wire A	Wire B	Wire C
Fabrication Method	Bronze	Bronze	Internal Sn
Wire Diameter (mm)	0.8	1.0	0.68
Structure	NbTa/CuSn	Nb/CuSnTi	Nb/Cu/Sn
Cu/non-Cu	0.22	1.68	0.88
Bronze/Cores	2.8	2.5	3.1
Filament Diam.(μm)	3.6	4.5	2.7
No. Filaments	10,000	5,047	5,550
Heat Treatment	973 K	943 K	973 K
	96h	200h	48h

EXPERIMENT

Samples

Three multifilamentary Nb_3Sn sample wires were tested. The first and the second, A and B, are bronze route wires with Nb_3Sn filaments containing the third additional elements of Ta or Ti, respectively. Wire A is stabilized by copper internally and B externally. The third, C, is an internal Sn processed wire with no third element addition. Brief sample specifications are given in Table 1. Further details have already been previously reported.[1]

Apparatus and Measurement

Three groups of laboratories participated in the strain effects evaluation tests using apparatus of their own. They are Inst. Sci. Ind. Res., Osaka Univ./Mater. Res. Inst., Tohoku Univ., National Inst. Standard Technology and Rutherford Appleton Lab.; these institutes are labeled disorderly as Laboratory I, II and III in this paper. Laboratories I and II used a short straight sample testing apparatus.[4,5] Axial tensile strain was applied in the magnet bore perpendicularly to the magnetic field; the I_c was measured using custom low-force clip-on gauge. The sample was cooled in a force-free state. Laboratory III used a long coil shape sample soldered on the outer periphery of a spring sample holder. Twisting the spring results in tensile or compressive strains in the sample.[6]

Only the data at magnetic fields of 15 T were provided by laboratory I, whereas more detailed results measured as a function of the magnetic field were presented by laboratories II and III. The results are compared based on the data at this field using an I_c criterion of 1 μV/cm. The data at 15 T of laboratory II are obtained through simple interpolation using points at 14 and 16 T.

RESULTS AND DISCUSSION

Strain Effect

As an example of results, the strain dependence of I_c in wire C is shown in Fig. 1. The I_c increases with strain to the peak, I_{cm}, at ε_m where compressive pre-strain in Nb_3Sn induced by the other constituents with different thermal contraction coefficients on cooling is released. It decreases on further straining. The irreversible strain limit ε_{irrev} is determined as a strain beyond which the I_c value on unloading does not fall

62
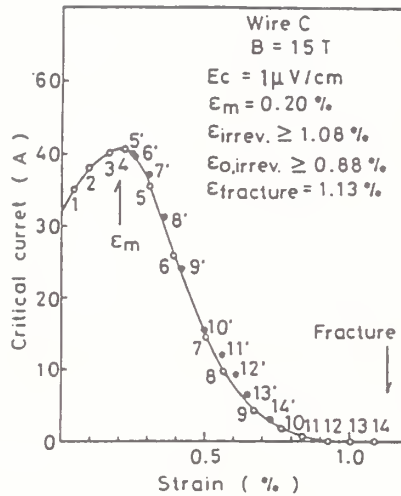
Fig. 1.   Ic vs. strain characteristic for wire C (laboratory I).
(Open circles are obtained on loading, solid unloading)
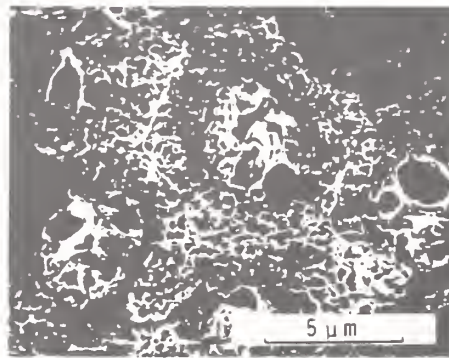
Fig. 2.   Fracture surface of wire C. (4.2 K, 15 T).

on the curve obtained by previous loading. Figure 1 indicates $\varepsilon_m = 0.2$ %
and I_c is reversible until the wire is nearly strained to fracture, ε_f.
The highly reversible characteristics of this wire is ascribed to the wire
construction: The fractograph of this wire at 4.2 K, 15 T indicated that the
size of voids observed in the distributed Sn core is small, which does not
induce a significant strain concentration (Fig.2). This is in contrast with
the large voids observed in internal tin diffusion processed wires with
larger core size, in which the ε_{irrev} is small and the strain sensitivity of
I_c is high.[7,8]

Comparison of Measurements Among Laboratories

Values of ε_m, ε_{irrev}, and fracture strain ε_f obtained in each
laboratory are compared in Table 2. The prestrain value ε_m agrees within
0.06 % for laboratories I and II. The ε_m values differ somewhat from the

63

102

Table-2.   Comparison of characteristic strain values

		$\varepsilon_m(\%)$	$\varepsilon_{irrev}(\%)$	$\varepsilon_f(\%)$
	lab.I	0.18	>0.97	1.02
Wire A	lab.II	0.18	>0.80	0.91
	lab.III	0.25	–	–
	lab.I	0.25	0.85	>3.5
Wire B	lab.II	0.31	0.82	>1.70
	lab.III	0.20	–	–
	lab.I	0.20	>1.08	1.13
Wire C	lab.II	0.21	>1.05	1.34
	lab.III	–	–	–
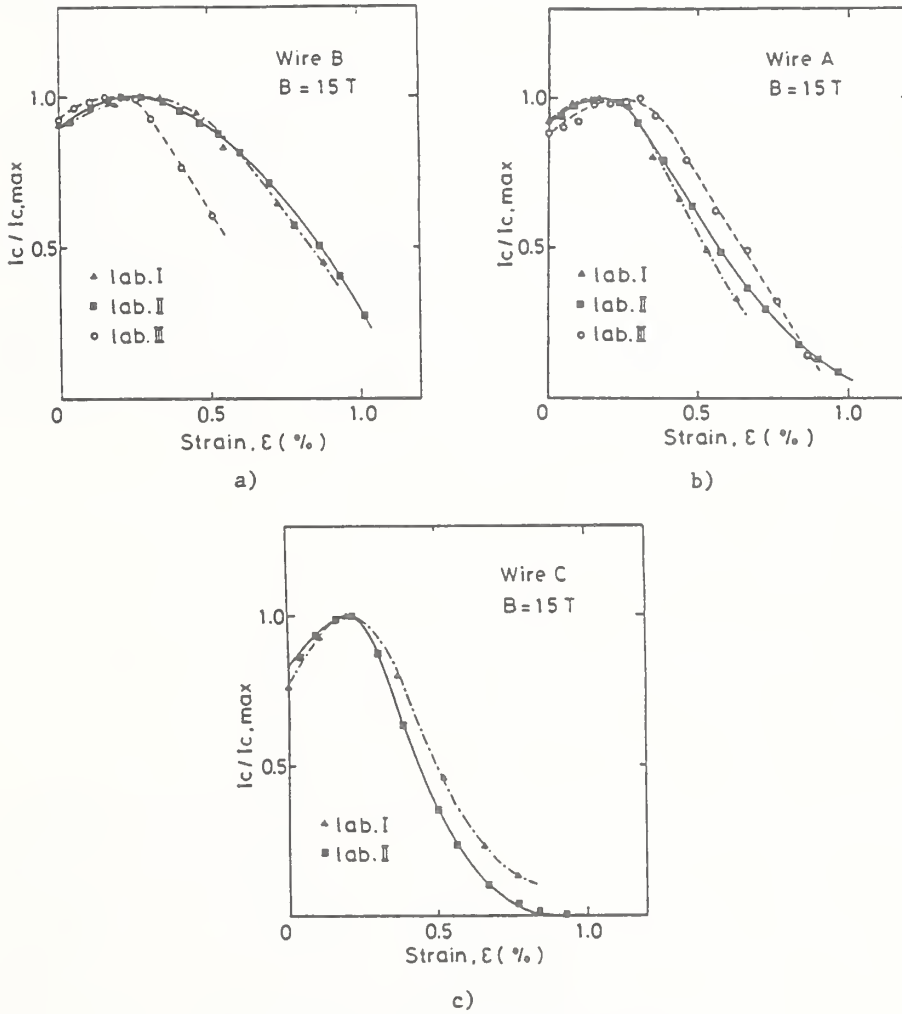
Fig. 3.   Strain dependence of I_c/I_{cm}.

results obtained by others for laboratory III. The irreversible strain limit values, or its lower limit values, agreed well, within 0.05 %, in wire B and are somewhat scattered in wires A and C. The reason for large scatter of ε_{irrev} is that the reversible strain limit coincides with the wire fracture strain at which I_c can be no longer determined. The fracture is controlled by the weakest defect in wires A and C, whereas the reversible strain limit in ductile wire B is determined by micro-fracture in the filaments prior to the final fracture.

The strain dependence of I_c for the three wires obtained by the three laboratory groups are shown in Fig. 3. The I_c is normalized to that at peak strain, I_{cm}. The agreement of ε_m, as mentioned above, as well as the strain sensitivity between laboratories I and II is quite good. To make a meaningful comparison with the data from laboratory III, in which the wire is soldered to a strip of copper firmly laid over the surface of the titanium spring, it appears necessary to fit the data to the prestrain values determined by laboratories I and II, which are obtained through force-free cooling.

The ε_m is largest in wire B in which both the bronze-to-core ratio, R, and the copper-to-non-copper ratio, S, are high. The smallest ε_m in wire A is presumed to be the consequences of low R and S and the position of the stabilizer.[9]

Strain Sensitivities and Scatter of I_c Measurements

Figure 4 shows comparison of tensile strain sensitivities for three wires obtained in laboratory I. The sensitivity is highest in the wire C and tends to decrease lower in the order of A and B. These are mainly controlled by their upper critical field, B_{c2}; 19 T, 24.5 T, and 26 T, respectively. The change in B_{c2} is attributed to the species and the amount of additional elements to Nb_3Sn; no addition, Ta, and Ti respectively. The strain sensitivity of I_c is known to be higher in the conductor with a higher R ratio and higher ε_m.[10] The ratio S is also supposed to contribute to it in the same direction. It seems worthy to note that I_c in the wires stabilized internally are more sensitive as compared with that in externally stabilized wires.[9] However, it appears that these effects are masked by the vast difference in B_{c2}.
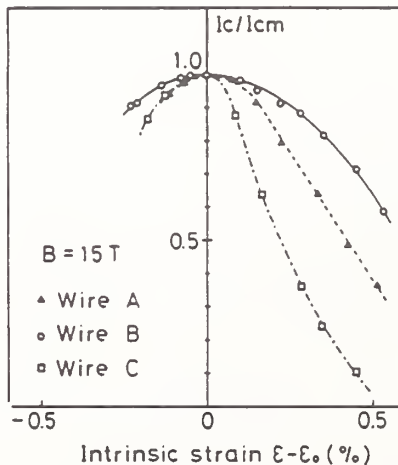
Fig. 4. Strain sensitivity of Ic (laboratory I).

65

104
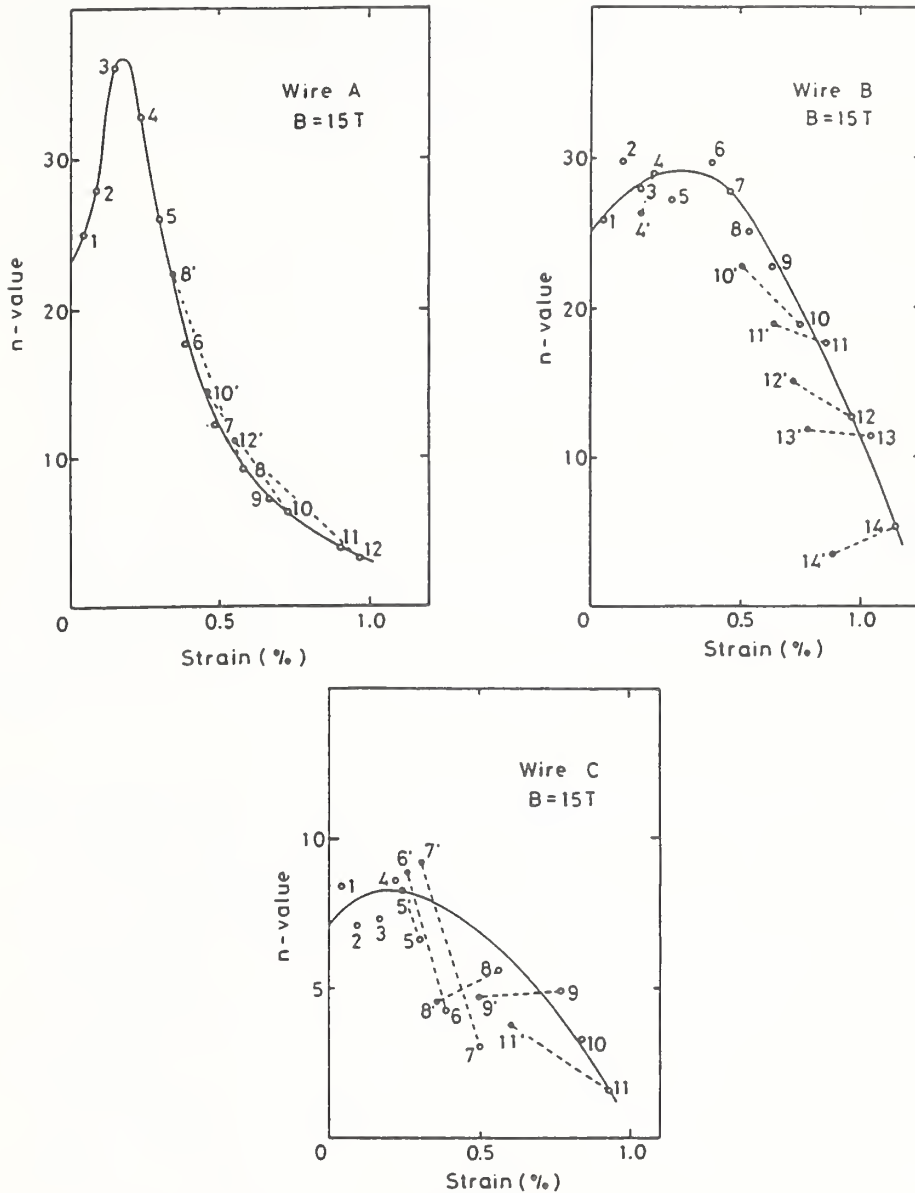
Fig. 5. Strain dependence of "n" value (laboratory I).
(Open circles are obtained on loading,
solid unloading)

According to a summary of the round robin test of I_c determined by the criterion of 10 μV/m, the coefficient of variation in I_c data, s/Ave where s is standard deviation and Ave is averaged value of I_c's, increases as the magnetic field is increased. Further, the variance is larger in the order of samples C, A, and B; s/Ave are 29.4, 12.1, and 5.4 % at 15 T, respectively. The order coincides with that of the strain sensitivity of I_c mentioned above. These facts indicate that the scatter in the I_c measurements is closely related to the strain characteristics of the wire; the intrinsic sensitivity of the conductor associated with the prestrain during handling and/or cooling down. The systematic differences among

Table 3. Comparison of Icm

		Icm, A
Wire A	lab.I	115
	lab.II	132
	lab.III	114
Wire B	lab.I	116
	lab.II	124
	lab.III	107
Wire C	lab.I	40
	lab.II	41
	lab.III	–

laboratories in the round robin test have also been mainly attributed to the strain effect associated with the sample holder (Fig. 5 in the reference 1).

So long as the value of the prestrain experienced before the I_c measurement is small, the importance of the magnitude of ε_m is to be emphasized. Because the extent of change in I_c is directly associated with the strain sensitivity around the zero applied strain, the value of ε_m, the deviation from the peak, has significant meaning not only for the I_c value itself but also the scatter of I_c measurement.

It must be noted, however, that the values of I_{cm}, the I_c free from strain are also different among the laboratories (Table 3). This indicates that factors other than strain still can exist in the measurements of each laboratory; variation of magnetic field, parameters specific to the apparatus (excluding strain effect), recording equipments, and variation of sample itself. The parameters excepting the last one can partly be responsible for the systematic differences among laboratories. Difference in heat treatment condition also leads to variation of B_{c2}, I_{cm} and, therefore, the strain effect. More significant variation is induced in the samples with shorter heat treatment time in the order of wire C, A, and B. The situation for wire C is particularly bad because there is another problem with inadequate confinement of internal tin in short sample during heat treatment. The filament diameter (increasing in the order of wire C, A and B) may in part be responsible for a variation in the longitudinal homogeneity of the wires. The results of a homogeneity check for wires has been reported, except wire C. The scatter in wires A and B is rather low .

Strain Sensitivity of "n" Value

In the course of I_c round robin tests, n values specifying the relationship between the voltage V and the transport current I in a empirical expression $V \propto I^n$ has been also evaluated. A larger n value corresponds to a sharper transition in the specimen and is an index of good homogeneity.[11] The dependence of I_c on criterion voltage is higher for conductors of smaller n values.[12] Changes in n values determined within the voltage range of 0.5 to 5 $\mu V/cm$ versus strain for three wires are shown in Fig. 5. Although the scatter of n is rather large, especially in wire C, n changes with strain as in the case of I_c. Because n reflects the homogeneity of the conductor, the irreversibility in n value is presumed to be caused by damage in the filaments. The change in n is larger in the wires C and A. The value of n near the peak I_{cm} is larger in wire A, but at strains other than the peak region it is rather small as compared to wire B.

67

The effect of the difference in position of stabilizer on the n value is not clear at present. The n values in wire C are erratic and small. A dull increase in voltage, i.e. smaller n value, will result in scatter of I_c if I_c criteria is of high accuracy, 1 μV/cm or smaller, or when the voltage base line in measurement has some fluctuation.

CONCLUSIONS

1. Interlaboratory comparisons of strain effects in three VAMAS sample superconductors showed fairly good agreement in prestrain ϵ_m, irreversible strain ϵ_{irrev}, and strain sensitivity of I_c.

2. Scatter of I_c measurement in the round robin test samples is mainly ascribed to strain effects; strain sensitivity and magnitude of prestrain.

ACKNOWLEDGMENTS

REFERENCES

1. K. Tachikawa, K. Itoh, H. Wada, D. Gould, H. Jones, C.R. Walters, L.F. Goodrich, J.W. Ekin and S.L. Bray, IEEE Trans. Magn., 25:2368 (1989).
2. K. Tachikawa, "Proc. 6th Japan-US Workshop for High Field Superconductors", Boulder, 1989, in press.
3. J.W. Ekin, ibid.
4. J.W. Ekin, Cryogenics, 20:611 (1980).
5. K. Katagiri, M. Fukumoto, K. Saito, M. Ohgami, T. Okada, A. Nagata, K. Noto, and K. Watanabe, Presented at the ICMC, Los ANGELES, CA, July 24-28, 1989.
6. C.R. Walters, I.M. Davidson, and G.E. Tuck, Cryogenics, 26:406 (1986).
7. M. Umeda, H. Yamazaki, M.Watanabe, Y. Kimura, Cryog. Eng., 22:110 (1987) (in Japanese).
8. K. Katagiri, K. Saito, M. Ohgami, T. Okada, A. Nagata, K. Noto, and K. Watanabe, in: "New Developments in Applied Superconductivity", p. 401 Y. Murakami ed., World Sci. Publ. (1989) SINGAPOLE.
9. K. Katagiri, M. Ohgami, T. Okada, T. Fukutsuka, K. Matsumoto, M. Hamada, K. Noto, K. Watanabe, and A. Nagata, Presented at the ICMC, Los ANGELES, CA, July 24-28, 1989.
10. T. Luhmann, M. Suenaga, D. O. Welch and K. kaiho, IEEE Trans. Magn. 15:699 (1979).
11. W.H. Warnes, D.C. Larbalestier, in: "Proc. Int. Symp. Flux Pinning Electromagn. Prop. Superconds.", T. Matsushita, K. Yamafuji and F. Irie, eds., P. 156, Matsukuma Press, Fukuoka (1985).
12. L.F. Goodrich and F.R. Fickett, Cryogenics, 225 (1982).

VAMAS Nb$_3$Sn Test Conductor

A bronze-process Nb$_3$Sn conductor was measured as part of the second VAMAS (Versailles Project on Advanced Materials and Standards) international critical-current round robin. The conductor specifications are given in Table 15. The critical current was measured as a function of magnetic field and axial tensile strain. The measured data are presented in Table 16 and in Figs. 23 and 24. The I_c and J_c values are based on an electric field criterion (E_c) of 1 μV/cm. In the first VAMAS round robin tests, differences in the test specimens' axial strain, caused by variations in the thermal contraction of different test fixtures, was a major source of interlaboratory variation in the critical-current data. Consequently, *electromechanical* characterization of the test specimen is important for data interpretation and error analysis. In the second round robin, the test apparatus and procedure were more rigidly specified. This increased experimental control reduced the critical-current variation by a factor of 3.5. The results of our measurements will be published in the final VAMAS report.

Table 15. VAMAS Nb$_3$Sn test conductor specifications.

Wire Diameter	1.0 mm
Cu:Non-Cu Ratio	1.68:1
Bronze:Core Ratio	2.5:1
Filament Dia.	4.5 μm
Filament No.	5047

Table 16. High-field critical current of VAMAS Nb$_3$Sn test conductor as a function of axial tensile strain applied at 4 K.

SP	E (%)	E0 (%)	FIELD (T)	Ic (A)	Jc (MA/m^2)	Ic/Icmax	N
0	0.045	-0.205	12	187.95	641.46	1.00	25.70
			14	134.76	459.92	0.94	34.54
			15	110.99	378.80	1.00	29.12
			16	91.18	311.20	0.92	30.22
			18	56.12	191.54	0.88	23.73
			20	28.81	98.32	0.81	16.17
			22	10.15	34.64	0.68	8.91
			24	1.36	4.63	0.48	3.57
			25	0.24	0.81	0.44	1.98
1	0.119	-0.131	14	140.08	478.10	0.97	34.39
			16	95.41	325.64	0.96	27.37
			18	59.61	203.45	0.94	22.22
			20	32.30	110.25	0.91	17.34
			22	12.73	43.45	0.85	11.62
			24	2.08	7.11	0.74	4.55
			25	0.35	1.18	0.65	2.08
2	0.219	-0.031	14	143.23	488.86	0.99	29.24
			16	99.27	338.82	1.00	30.59
			18	63.18	215.62	0.99	24.14
			20	35.39	120.78	1.00	19.49
			22	14.63	49.92	0.98	12.23
			24	2.81	9.59	1.00	5.42
			25	0.54	1.83	1.00	2.48
3	0.297	0.047	14	144.00	491.46	1.00	31.24
			16	98.91	337.58	1.00	27.22
			18	63.64	217.20	1.00	25.95
			20	35.52	121.24	1.00	18.68
			22	14.91	50.88	1.00	12.63
			24	2.63	8.97	0.94	4.91
			25	0.47	1.60	0.88	2.38
4	0.374	0.124	14	142.34	485.81	0.99	32.41
			16	97.83	333.88	0.99	32.09
			18	61.74	210.71	0.97	24.57
			20	33.42	114.06	0.94	15.96
			22	12.51	42.70	0.84	9.05
			24	1.91	6.53	0.68	3.89
			25	0.33	1.14	0.62	2.05
5	0.448	0.198	14	136.55	466.04	0.95	30.07

Table 16 cont'd

SP	E (%)	E0 (%)	FIELD (T)	Ic (A)	Jc (MA/m^2)	Ic/Icmax	N
			16	91.86	313.50	0.93	25.92
			18	56.54	192.98	0.89	20.93
			20	27.98	95.50	0.79	11.10
			22	17.72	60.47	1.19	5.62
			24	1.01	3.45	0.36	2.53
			25	0.15	0.51	0.28	1.49
6	0.521	0.271	14	127.88	436.46	0.89	24.21
			16	83.90	286.34	0.85	19.46
			18	49.14	167.71	0.77	14.87
			20	22.04	75.24	0.62	8.75
			22	5.79	19.76	0.39	4.65
			24	0.58	1.99	0.21	2.32
			25	0.07	0.23	0.13	1.28
6u	0.355	0.105	14	145.46	496.45	1.01	34.64
7	0.61	0.36	14	116.40	397.27	0.81	21.64
			16	74.10	252.91	0.75	16.18
			18	38.95	132.92	0.61	9.69
			20	15.99	54.56	0.45	7.32
			22	3.20	10.93	0.21	3.52
			24	0.20	0.67	0.07	1.46
			25	0.04	0.13	0.07	1.21
7u	0.401	0.151	14	142.41	486.05	0.99	31.80
8	0.688	0.438	14	107.25	366.04	0.74	23.17
			16	63.97	218.32	0.64	15.03
			18	31.35	106.98	0.49	8.88
			20	10.20	34.80	0.29	5.19
			22	1.63	5.56	0.11	2.72
			24	0.11	0.39	0.04	1.44
			25	0.03	0.09	0.05	1.18
8u	0.463	0.213	14	138.38	472.30	0.96	28.24
9	0.78	0.53	14	89.30	304.76	0.62	13.75
			16	52.00	151.47	0.45	7.80
			18	21.61	73.74	0.34	7.25
			20	5.39	18.40	0.15	3.92
			22	0.62	2.11	0.04	1.97
			24	0.04	0.15	0.02	1.28

Table 16 cont'd

| SP	E (%)	E0 (%)	FIELD (T)	Ic (A)	Jc (MA/m^2)	Ic/Icmax	N
9u	0.513	0.263	14	131.75	449.65	0.91	22.67
10	0.869	0.619	14	77.02	262.87	0.53	15.96
			16	39.59	135.13	0.40	10.60
			18	13.73	46.85	0.22	5.87
			20	2.54	8.66	0.07	3.12
			22	0.24	0.83	0.02	1.62
			24	0.03	0.11	0.01	1.19
10u	0.564	0.314	14	119.60	408.18	0.83	16.46
11	0.935	0.685	14	63.83	217.84	0.44	11.97
11u	0.602	0.352	14	104.09	355.24	0.72	10.79
12	1.001	0.751	14	48.52	165.60	0.34	8.19
12u	0.653	0.403	14	82.18	280.47	0.57	7.09
13	1.059	0.809	14	34.15	116.55	0.24	5.52
13u	0.688	0.438	14	56.92	194.25	0.40	4.42
14	1.113	0.863	14	21.26	72.56	0.15	3.81
14u	0.715	0.465	14	34.26	116.94	0.24	3.04
15	1.16	0.91	14	13.72	46.84	0.10	3.02
15u	0.742	0.492	14	21.71	74.09	0.15	2.48
16	1.21	0.96	14	8.25	28.15	0.06	2.37
16u	0.78	0.53	14	14.96	51.06	0.10	2.55
17	1.264	1.014	14	5.31	18.13	0.04	2.34
17u	0.819	0.569	14	10.57	36.08	0.07	2.58
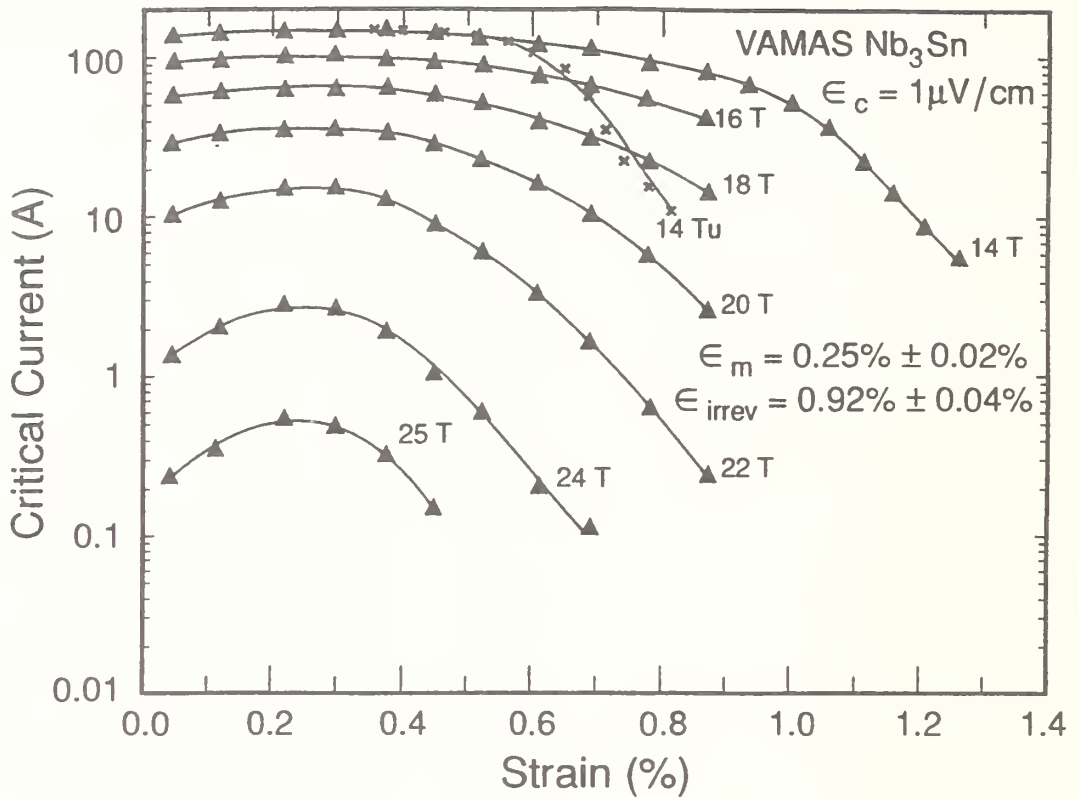
Figure 23. Effect of axial tensile strain on the critical current of the VAMAS Nb₃Sn test conductor at 4 k and several magnetic fields.
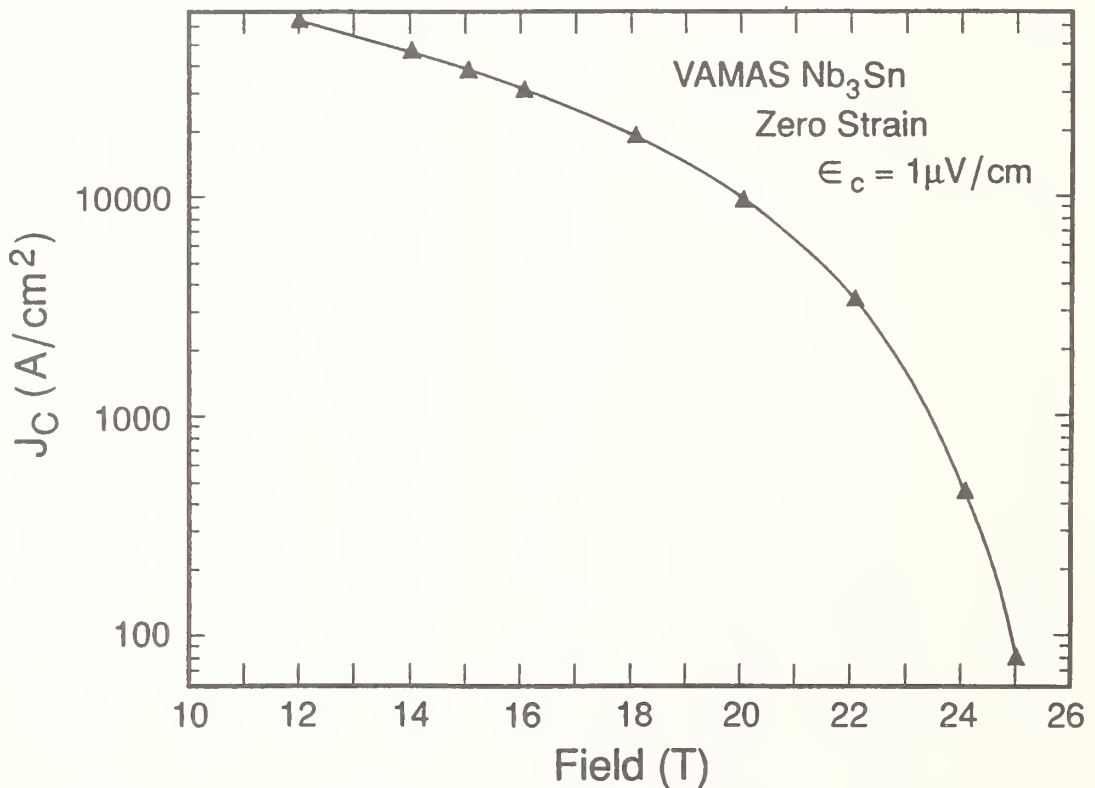

Figure 24. Effect of magnetic field on the critical current density of the VAMAS test conductor at 4 K.